Radial heat transfer studies in low tube to particle diameter ratio fixed bed reactors

BY

GUILLAUME LEISING

A THESIS

SUBMITTED TO THE FACULTY OF THE

WORCESTER POLYTECHNIC INSTITUE

IN PARTIAL FULFILLMENT OF THE REQUIREMENTS FOR THE DEGREE OF

MASTER OF SCIENCE

IN CHEMICAL ENGINEERING

APPROVED

_____

ANTHONY DIXON, ADVISOR
WORCESTER POLYTECHNIC INSTITUE

_____

DAVID DIBIASIO, DEPARTMENT HEAD
WORCESTER POLYTECHNIC INSTITUE

SPRING 2005

Table of Contents

List of Figures

List of Tables

Acknowledgments

In this section, I would like to thank all the people who were with me during my journey at Worcester Polytechnic Institute.

First of all, I would like to thank my advisor, Prof Anthony G. Dixon for his guidance, patience and enthusiasm concerning this work. I will always appreciate his continuous support and understanding throughout my stay at WPI.

Next I would like to thank all the faculty, staff and students from the Chemical Engineering Department at Worcester Polytechnic Institute.

I would also like to thank Prof. D. DiBiasio, W. Clark and A. G. Dixon for the financial supports: being for two years a Teaching Assistant for one of the most important courses for Chemical Engineering students taught me a lot, I gained a lot of valuable experience through this.

I would like to thank all my friends at WPI. They helped me through this journey and I had an enjoyable time in Worcester with them. Special thanks to the WPI water polo team for all the good times spent altogether.

Last but not least; I would like to thank my family: my parents, my brother, and my wife. They stood beside me for some of the big decisions that I had to make during my stay at WPI, and I really want to thank them for that.

I had to face educational challenges as well as important life decisions these last two years, so many thanks to all the persons who helped me to become the person who I am now.

Abstract

Fixed bed reactors are used in many different chemical processes, and are a very important part of chemical industry. To model fixed beds we must have a good qualitative understanding of heat transfer in them. Fixed bed models have been developed for high tube-to-particle ratio (N) beds. Modeling of low tube-to-particle beds ($3 \leq N \leq 8$), that are used in extremely exo- and endothermic processes in tube-and-shell type reactors, is complicated, due to the presence of wall effects across the entire radius of the bed. Heat transfer is one of the most important aspects. To obtain accurate models of heat transfer we need to study the physical mechanisms involved especially in the wall vicinity using CFD as a non intrusive tool to collect numerical data.

An extra heat transfer resistance is always present near the wall. This is caused by three mechanisms which happen in the wall vicinity. The change of porosity which leads to a change of bed conductivity, the damping of mixing due to the lateral displacement of fluid, the presence of a laminar (viscous) sublayer at the wall.

Many authors have been working on how to model the extra resistance near the wall. The main previous approach was to introduce a lumped parameter h_w (heat transfer coefficient) which idealizes these three contributions to the extra heat resistance to be at the wall.

Our approach will be to keep the parameter h_w which will now represent only the viscous boundary layer idealized at the wall, and we are going to incorporate velocity and porosity profiles in the energy equation. In this way we will able to get rid of artificial parameters using the true conductivity of the bed, and the real velocity profile. So we need to study separately each contribution of the different physical mechanisms to clearly understand what happens in the wall vicinity.

For this CFD will be a very powerful tool. How CFD models flow near the wall must be understood before starting simulations. Two main approaches for wall bounded flows

are available and will be studied: either solve all way down to the wall, or bridge numerical values from the core of the bed to the wall using semi-empirical formulas called wall functions. These methods will be studied and compared.

Also with CFD it is possible to run simulations without conduction in the bed, and so, study radial fluid displacement only and obtain reduced velocity profiles. Using the meshing it is also possible to get a very accurate porosity profile. These profiles will be combined in a simplified fixed bed model which will be used to predict temperature profiles. These may then be compared to the full CFD energy solution and to experiment to test the model.

1. INTRODUCTION

Fixed bed reactors are used in many different chemical processes, and are a very important part of the chemical industry. To model fixed beds we must have a good qualitative understanding of heat transfer in them. Computational Fluid Dynamics appears to be a powerful tool to help us model fixed beds.

1.1. BACKGROUND

Fixed beds are a major part of chemical industry. Usually the main feature which characterizes fixed beds is the ratio between the tube diameter and the particle diameter ratio (N). This number represents the average amount of catalyst particle on a cross section of the diameter.

Lots of packed bed reactors have a high tube to particle diameter ratio generally between 50 and 500. In these situations, the wall effects can be neglected, because the size of the region involved by these effects is very small compared to the reactor bulk. Reactions taking place in such kind of reactors are almost adiabatic or with a very small heat effect. Then there is no need to assure a high exchange of heat.

When heat transfer begins to be an essential part of the process, low tube to particle ratios reactors are used, generally between 3 and 8. To enhance heat transfer, smaller reactors are used to develop the exchange surface with reactants. These cases usually involve high reaction heat effects either highly exothermic or endothermic reactions such as ammonia synthesis, partial oxidation, steam reforming among others. The heat transfer rates are crucial in these situations. An uncontrolled heat transfer may lead to undesired products, yields, and sometimes reactor damage. So when a highly exo- or endothermic reaction is involved, the common way to achieve the reaction is to use multiple small reactors of very low tube to particle ratio instead of one large reactor. Thus heat transfer is enhanced.

But with such a low N, the wall effects are no more negligible. The influence of the wall is, for N = 3 to 8, across the entire bed.

To have a better understanding of what occurs in the fixed bed in terms of heat transfer, Computational Fluid Dynamics (CFD) appears to be an accurate and reliable tool to study both flow field in the bed and heat transfer mechanism. With a better accuracy and data, physical mechanisms of heat transfer especially in the near-wall region may be studied in more detail.

1.2. PROBLEM STATEMENT

Several studies have been made to model the radial temperature profile for various N reactors. When radial temperature profile is studied in these reactors, experimental data lead to a significant deviation in the near-wall region compared to models. This is mainly due to the drastic change in voidage responsible for a change in bed conductivity, the reduced radial dispersion and the viscous boundary layer. The common way to model them is to introduce an idealized temperature jump at the wall, h_w, the heat transfer coefficient. All phenomena which cause resistance in the wall vicinity are lumped into this one parameter. That is why the heat transfer coefficient h_w has no physical meaning but represents a convenient mathematical object to model experimental data for large N fixed bed reactors.

Because of its nature, it seems to be a good idea to get rid of h_w, and replace it, especially for low N fixed bed. To do so, one has to investigate further to understand these phenomena which happen close to the wall. At this point, CFD appears to be a good way to collect lots of various data without being intrusive and perturbing locally the ‘real’ flow.

Several studies have been done to try to correlate h_w with low N fixed bed reactors, or to investigate more deeply the relations between flow field, structure and heat transfer (Nijemeisland, 2003). For this, CFD has been used to collect extensive and accurate data to study the heat transfer in the near-wall region. Because of computer capacities in terms of hardware, only a wall segment has been used, composed of 2 layers of catalyst

particles only representing 120^o of the overall cross section of a N=4 fixed bed reactor. To compensate the removed part (240^o) a symmetric boundary condition has been set to the lateral surfaces. Several geometries have been meshed especially spheres, full cylinders and 1-hole cylinders in the same conditions as above. All have been studied (Nijemeisland, 2003) especially on the relation between flow and heat transfer. Results have not been so clear to conclude on specific relations or correlations.

One of the arising questions is to determine if the symmetric boundary condition has any influence on the previous results, if CFD is able to correctly solve it especially for non-spherical geometries.

Another major issue is how dependent are the results on wall functions and how well is the near-wall region modeled in CFD.

After that, what conclusion can be drawn and how is it possible to use results to understand and study physical mechanisms occurring in the wall vicinity.

To investigate these questions, CFD is used to compare and study different geometries and different CFD models, observe boundary condition effects on results. But models used in CFD have to be compared and analyzed to better understand heat transfer phenomena.

In this work, a comparative study will be made of the influence of symmetric boundary conditions on results, influence of different wall functions and wall approaches. Then a beginning of a new approach to model heat transfer will be presented.

1.3. COMPUTATIONAL FLUID DYNAMICS

CFD is a field perpetually growing these last decades, due to the incredible expansion of computer capabilities in terms of hardware and software also. First CFD has been introduced in Chemical Engineering quite late (1994) with the appearance of fluid mixing and chemical reaction codes (Bode, 1994; Harris et al., 1996; Ranade, 1995).

CFD is a variety of different codes which allows you to solve flow and chemical problem based on a given grid, composed of multiple cells in 2 or 3 dimensions (x-y-z). Each cell is connected between several others. Solutions are obtained by numerically

solving a number of balances over a large number of control volumes or elements forming the desired geometry. Balances are solved with given boundary conditions at the limits of the domain, with a guessed solution at the beginning and lots of iterations until convergence.

Balances are mainly fluid flow equation, based on Navier Stokes equations for conservation of mass and momentum. Depending on the model used, these equations are modified to solve specific problems.

1.3.1. Fluid Mechanics Fundamentals: Navier Stokes equations

CFD basis is to solve fluid flow equations for each iteration. Depending on the problem features, other equations may be added. Main equations are derived from Navier Stokes continuity and momentum conservation, solved for laminar fluid flow. Turbulence may be added, as well as heat transfer or mixing species.

Here is following the equation of Navier Stokes for conservation of mass (continuity):

$$\frac{\partial \rho}{\partial t} + \frac{\partial (\rho u_i)}{\partial x_i} = S_m \tag{1}$$

S_m is here defined as a source term of mass depending on the situation, like change of phase. This term is generally set to zero for our simulations, where no change of phase occurs.

For a fixed or non-accelerating reference, in a i direction, the conservation of momentum is derived as follows:

$$\frac{\partial (\rho u_i)}{\partial t} + \frac{\partial (\rho u_i u_j)}{\partial x_j} = -\frac{\partial p}{\partial x_i} + \frac{\partial \tau_{ij}}{\partial x_j} + \rho g_i + F_i \tag{2}$$

In this equation, p is the static pressure, τ_{ij} is the stress tensor, ρg_i is the gravitational body force and F_i an external body force term, always taken to zero in my simulations.

The stress tensor τ_{ij} for a Newtonian fluid is defined as:

$$\tau_{ij} = \mu\left(\frac{\partial u_i}{\partial x_j} + \frac{\partial u_j}{\partial x_i}\right) - \frac{2}{3}\mu\frac{\partial u_l}{\partial x_l}\delta_{ij} \quad (3)$$

Here μ is the molecular viscosity and the second term on the right hand side is the effect of volume dilation.

1.3.2. Turbulence Models

In most cases the main model used was Renormalization Group (RNG) κ-ε model. It has been proven that RNG κ-ε model is one of the best approaches available in the available CFD package (Nijemeisland 2000). The κ-ε model is a semi-empirical model based on model transport equations for the turbulence kinetic energy (κ) and its dissipation rate (ε). All equations are derived from Reynolds Averaged Navier Stokes equations. One of the major assumptions of this model is to consider the flow as fully turbulent, and consider the molecular viscosity negligible. The κ-ε model has been developed by Launder and Spalding in 1972

The Reynolds averaging process consists to decompose the velocity into the main component $\bar{u}_i$, and the fluctuating component u_i'. Following are the Navier Stokes equation for momentum conservation when the previous approach is used:

$$\frac{\partial(\rho u_i)}{\partial t} + \frac{\partial(\rho u_i u_j)}{\partial x_i} = -\frac{\partial p}{\partial x_i} + \frac{\partial}{\partial x_j}\left[\mu\left(\frac{\partial u_i}{\partial x_j} + \frac{\partial u_j}{\partial x_i}\right) - \left(\frac{2}{3}\mu\frac{\partial u_l}{\partial x_l}\right)\right] + \frac{\partial\left(-\rho\,\overline{u_i' u_j'}\right)}{\partial x_j} \quad (4)$$

All the solutions are now time averaged values. The turbulences are present in this equation in terms of 'Reynolds stresses' $-\rho\overline{u_i' u_j'}$, which are modeled by the Boussinesq hypothesis:

$$-\rho\overline{u_i' u_j'} = \mu_t\left(\frac{\partial u_i}{\partial x_j} + \frac{\partial u_j}{\partial x_i}\right) - \frac{2}{3}\left(\rho\kappa + \mu_t\frac{\partial u_i}{\partial x_i}\right)\delta_{ij} \quad (5)$$

The turbulent viscosity μ_t is a function of the turbulent kinetic energy κ, and the rate of dissipation ε:

$$\mu_t = \rho C_\mu \frac{\kappa^2}{\varepsilon} \tag{6}$$

Here are the adapted transport equations where the turbulent kinetic energy and dissipation rate are calculated:

$$\frac{\partial(\rho\kappa)}{\partial t} + \frac{\partial(\rho u_i \kappa)}{\partial x_i} = \frac{\partial}{\partial x_i}\left[\left(\mu + \frac{\mu_t}{\sigma_\kappa}\right)\frac{\partial \kappa}{\partial x_i}\right] + G_\kappa + G_b - \rho\varepsilon \tag{7}$$

and

$$\frac{\partial(\rho\varepsilon)}{\partial t} + \frac{\partial(\rho u_i \varepsilon)}{\partial x_i} = \frac{\partial}{\partial x_i}\left[\left(\mu + \frac{\mu_t}{\sigma_\varepsilon}\right)\frac{\partial \varepsilon}{\partial x_i}\right] + C_{l\varepsilon}\frac{\varepsilon}{\kappa}\left(G_\kappa + (1 - C_{3\varepsilon})G_b\right) - C_{2\varepsilon}\rho\frac{\varepsilon^2}{\kappa} \tag{8}$$

G_κ is here the generation of kinetic energy calculated using the turbulent stress described below:

$$G_\kappa = -\rho\,\overline{u_i' u_j'}\frac{\partial u_j}{\partial x_i} \tag{9}$$

G_b is the generation of turbulent kinetic energy due to buoyancy, calculated as shown below:

$$G_b = \beta g_i \frac{\mu_t}{Pr_t}\frac{\partial T}{\partial x_i} \tag{10}$$

Where Pr_t is the turbulent Prandtl number for energy and β is the thermal expansion coefficient defined as:

$$\beta = -\frac{1}{\rho}\left(\frac{\partial \rho}{\partial T}\right)_P \tag{11}$$

The other model constants are taken constant (default setting). Here are the following values:

$C_{1\varepsilon}$=1.44, $C_{2\varepsilon}$=1.92, C_{μ}=0.09, σ_{κ}=1.0, σ_{ε}=1.3, Pr_t=0.85.

These default values have been determined from experiments with air and water for fundamental turbulent shear flows. They have been found to work fairly well for a wide range of wall-bounded and free shear flows (Launder and Spalding, 1972). Most of the results showed in this study are solved using these constants as default values.

The other main model to solve turbulent flow is the standard and shear-stress transport (SST) κ-ω model. κ-ω model is an empirical model also based on model transport equations for turbulence kinetic energy κ, and the specific dissipation rate ω, which represent the ratio $\frac{\varepsilon}{\kappa}$. κ-ω model has been modified to accurately model free shear flows. One of the main difference remains also in the way to solve wall boundary conditions. The turbulence kinetic energy κ is treated the same way as κ-ε model but dissipation rate ω is calculated all down to the wall for sufficient fine mesh.

1.3.3. Energy equations

The energy equation involved in the RNG κ-ε model is based on an analogy concept of transport model for the static temperature. The enthalpy equation enables us to calculate the temperature. Here is the enthalpy equation from Fluent UNS:

$$\frac{\partial(\rho h)}{\partial t}+\frac{\partial(\rho u_i h)}{\partial x_i}=\frac{\partial}{\partial x_i}(k+k_t)\frac{\partial T}{\partial x_i}-\frac{\partial\sum_j h_j J_i}{\partial x_i}+\frac{Dp}{Dt}+(\tau_{ik})_{eff}\frac{\partial u_i}{\partial x_k}+S_h \qquad (12)$$

The term S_h here is a source term which accounts for heat of chemical reaction or inter-phase exchange of heat and any user defined volumetric heat sources. k_t is the conductivity due to turbulent transport, defined as:

$$k_t = \frac{c_p \mu_t}{Pr_t} \tag{13}$$

and the enthalpy h is :

$$h = \sum_j m_j h_j \tag{14}$$

where m_j is the mass of the species j and h_j is the enthalpy of the related species j defined as:

$$h_j = \int_{T_{ref}}^{T} c_p \, dT \tag{15}$$

$(\tau_{ij})_{eff}$ is the deviatoric stress tensor defined as:

$$\left(\tau_{ij}\right)_{eff} = \mu_{eff}\left(\frac{\partial u_j}{\partial x_i} + \frac{\partial u_i}{\partial x_j}\right) - \frac{2}{3}\mu_{eff}\frac{\partial u_i}{\partial x_i}\delta_{ij} \tag{16}$$

The terms in $(\tau_{ij})_{eff}$ account for the viscous heating.

One other important part of the heat transfer modeling is the conduction model through particles, which is crucial for our study of packed bed heat transfer. The equation involved is for solid parts, defined as shown below:

$$\frac{\partial(\rho h)}{\partial t} = \frac{\partial}{\partial x_i}\left(k\frac{\partial T}{\partial x_i}\right) + \dot{q} \tag{17}$$

The last term is a volumetric source term q. h is here the sensible enthalpy defined by the following equation:

$$h = \int_{T_{ref}}^{T} c_p \, dT \tag{18}$$

This appears to be consistent with the equation (14) since $c_p = \sum_j m_j c_{pj}$

For the κ-ω approach, energy equations are the same. The only difference is the way to treat wall boundary conditions.

1.3.4. Wall treatment approach

The presence of the wall significantly affects turbulent flows. The velocity field is affected by the no-slip condition present at the wall. Other effects due to wall presence may be involved like the viscous layer close to the wall reduces tangential velocities. The numerical solution depends significantly on how the near wall region is modeled. The variables in this area have the largest gradient especially for turbulent flow. Accurate representation of the near wall region determines successful predictions of wall-bounded turbulent flows.

The κ-ε models are valid for the core of turbulent flow, far from walls. Considerations have to be taken to model near wall regions. Wall functions are used to bridge the numerical variables of the flow core and the wall. In the case of κ-ω models, they have been designed to be valid just as well in the core and in the laminar viscous boundary layer. The only requirement is a sufficient fine mesh in the near-wall region.

The near-wall region can be separated into three main layers. The first one is the innermost layer also called the viscous sublayer, where the flow is almost laminar and the molecular viscosity plays a dominant role in momentum and heat and mass transfer. In

the outermost layer, called the fully-turbulent layer, the flow is fully turbulent. Between these two regions exists an intermediate one, where viscous effects and turbulence effects play an equally important role.

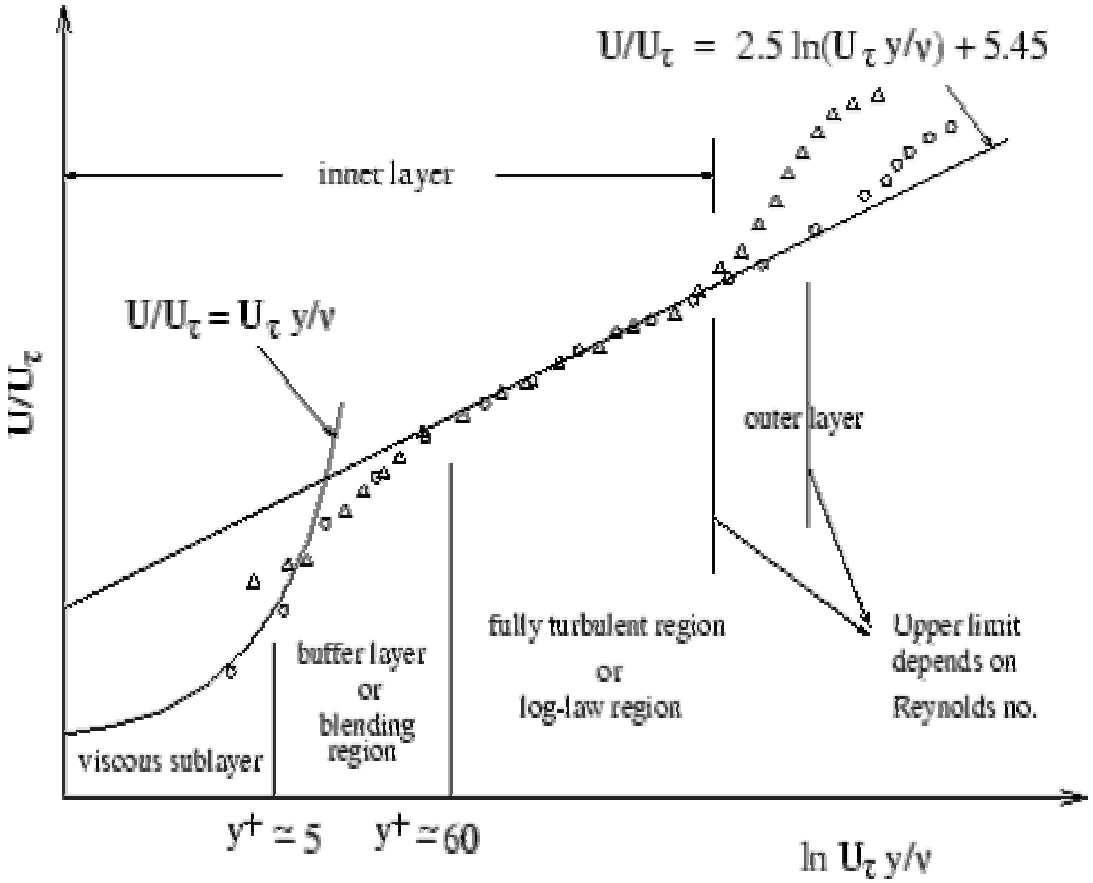

Figure 1.1: Subdivisions of the near-wall region in semi-log coordinates (from Fluent Manual, 1997)

Two main approaches are generally used to solve turbulent wall bounded flows. In the first approach, the viscous sublayer and the buffer layer are not solved. Semi empirical formulas called "wall functions" are used to bridge the turbulent flow to the wall region. Thus it is not necessary to modify the turbulence equations to account for the walls.

In the second approach, turbulence equations are modified to enable the model to solve viscous affected area all the way to the wall. The mesh has to be fine enough to give accurate results

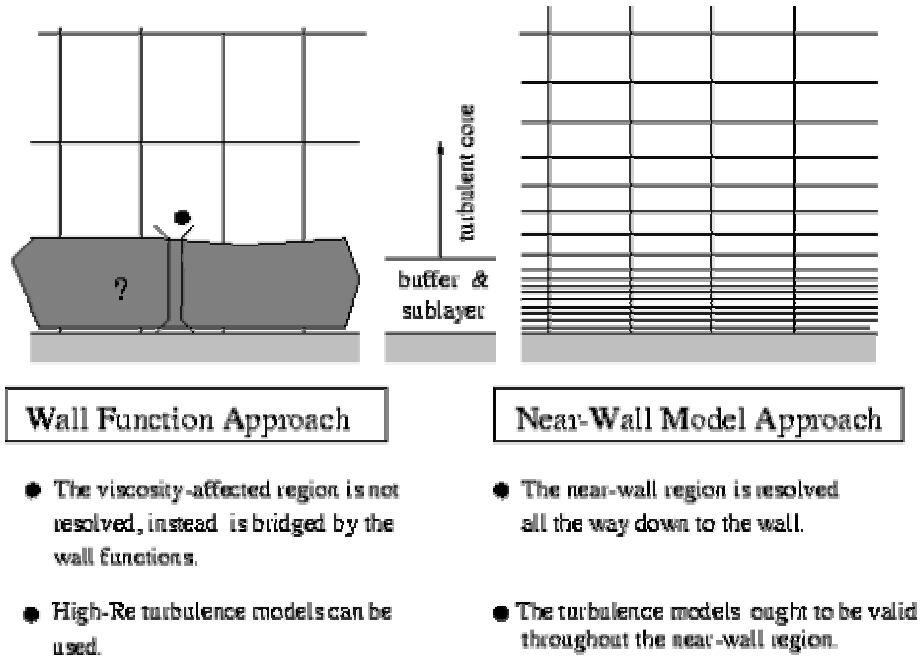

Figure 1.2: Near wall treatment in FLUENT (From Fluent Manual, 1997)

In the case of high Reynolds number flows, the wall functions give reasonably accurate results, and can save computational time because the viscous affected region is not solved but bridged. When the Reynolds number is relatively small, wall functions become inadequate to solve the near-wall region. In these cases, models able to solve all way to the wall are needed.

1.3.5. Wall functions

The standard wall function is based on a proposal in a publication by Launder and Spalding (1974). It gives relations between numerical values in the buffer and viscous layer and the turbulent core of the flow. It works pretty well with industrial flows especially high-Reynolds number flows. The equations are shown below:

$$U^* = \frac{1}{k}\ln\left(Ey^*\right) \tag{19}$$

with,

$$U^* \equiv \frac{U_P C_\mu^{0.25} \kappa_P^{0.5}}{\tau_w / \rho} \tag{20}$$

$$y^* \equiv \frac{\rho C_\mu^{0.25} \kappa_P^{0.5} y_P}{\mu} \tag{21}$$

Here are the constants used in the equation (19):

k = von Karman's constant (= 0.42)

E = empirical constant (= 9.81)

And for equation (20):

U_P = mean velocity at P

κ_P = turbulent kinetic energy at P

C_μ = model constant used in defining the turbulent viscosity

τ_w/ρ = related to friction velocity, $u_\tau \equiv \sqrt{\tau_w / \rho}$

In the equation (21):

y_P = distance of point P to the wall

When $y^*>11.225$, the equation 19 is used to calculate the mean velocity. When $y^*<11.225$ the laminar stress strain relationship is applied:

$$U^* = y^* \tag{22}$$

The parameter y^+, which is defined as $y^+ \equiv \rho u_\tau y/\mu$ is used to separate the different layers in the near-wall region. This parameter represents a dimensionless distance from the wall, modified by the friction velocity, u_τ, and the fluid viscosity. All Fluent calculations in the near wall region are based on y^*, instead of y^+, which is also a dimensionless parameter. There is almost no difference between y^* and y^+ values. They are pretty similar.

Because energy equations are also based on transport equations, a similar parameter as for momentum equations exists to determine whether a linear or logarithmic relation is used to calculate the profile over the cells of the near wall region. The nature of the fluid influences directly the size of the thermal conduction layer which is by the way different from the viscous sublayer. The parameter used to separate the different thermal layers is y_T^*. This value is computed using the calculation of the fluid molecular Prandtl number. Once this parameter is calculated, wall functions are used to calculate the temperature profile. The y_T^* is determined by the intersection between the linear and logarithmic areas. Here are following the equations used:

$$T^* \equiv \frac{(T_w - T_P)\rho C_\mu^{0.25} k_P^{0.5}}{\dot{q}''} \tag{23}$$

$$= \Pr y^* + \tfrac{1}{2}\rho \Pr \frac{C_\mu^{0.25} k_P^{0.5}}{\dot{q}''} U_P^2 \qquad \left(y^* < y_T^*\right) \tag{24}$$

$$= \Pr_t \left[\tfrac{1}{\kappa}\ln(Ey^*) + P\right] + \tfrac{1}{2}\rho \Pr \frac{C_\mu^{0.25} k_P^{0.5}}{\dot{q}''} \left\{\Pr_t U_P^2 + (\Pr - \Pr_t) U_c^2\right\} \qquad \left(y^* > y_T^*\right)$$

where P is computed using the Jayatilleke formula:

$$P = 9.24\left[\left(\frac{\Pr}{\Pr_t}\right)^{3/4} - 1\right]\left(1 + 0.28\, e^{-0.007\frac{\Pr_t}{\Pr}}\right) \tag{25}$$

using the following values:

T_P =temperature at the cell adjacent to the wall

T_w = temperature at the wall

Pr_t = turbulent Prandtl number (0.85 at the wall)

A = Van Driest constant (=26)

κ = von Karman's constant (=0.42)

E = wall function constant (=9.793)

U_c = mean velocity magnitude at $y^* = y_T^*$

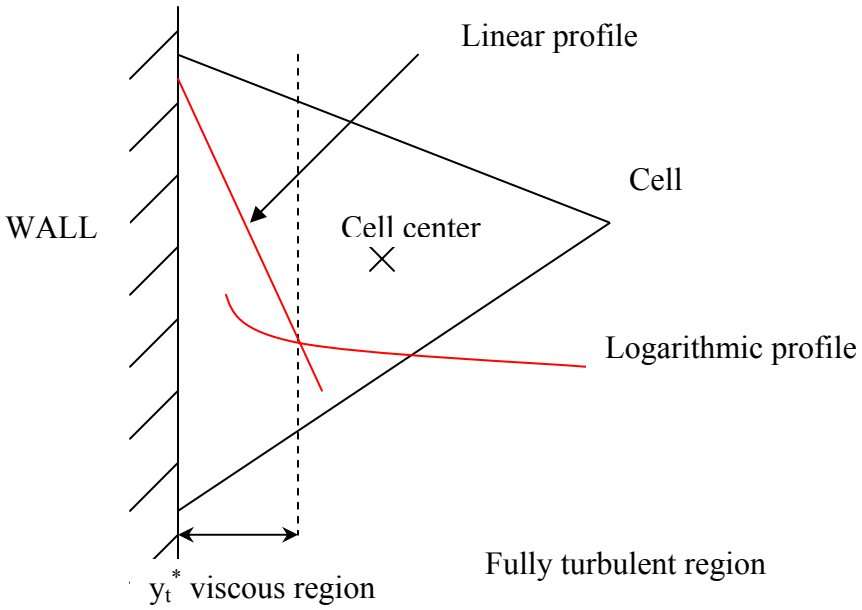

Figure 1.3: Picture of two layer approach model.

Now the thermal sublayer thickness, y_T^*, is calculated using the molecular Prandtl number and the intersection of the linear and logarithmic regions.

Depending on the wall boundary condition, one can either set the wall temperature or the heat flux at the wall, using the equation (23), depending on the y^*

value of the cell adjacent to the wall, the wall temperature, T_w, and the heat flux, $\dot{q}''$, are related.

The standard wall function gives reliable results for wall bounded flows especially for high Reynolds number simulations. But when the simulation conditions are too far from the wall functions assumptions, the model becomes to be less reliable. For example the constant shear stress and the local equilibrium assumptions restrict the universality of the standard wall functions. The local equilibrium assumption is a relation between the turbulence kinetic energy production and dissipation, which are equal in the wall bounded control volumes. In cases of a strong pressure gradient near the wall which means a high shear stress or the flow does not satisfy the local equilibrium condition an alternate model, the non-equilibrium model, is highly recommended to be used.

The non-equilibrium wall function is a derivate model from standard wall function which is more suitable for complex flows involving separation, reattachment, and impingement where the mean flow and turbulence are subjected to severe pressure gradients and change rapidly. Improvements can be obtained, especially in the wall shear and heat transfer prediction.

The equations shown below are the improvements from standard wall functions to account for higher pressure gradient. Non equilibrium wall functions change from standard wall functions in the definition of the velocity in equation (19) effectively replacing the definition in equation (20) with:

$$U^* \equiv \frac{C_\mu^{0.25} k^{0.5}}{\tau_w / \rho} \cdot \tilde{U} \tag{25}$$

$$\tilde{U} = U - \frac{1}{2}\frac{dp}{dx}\left[\frac{y_v}{\rho\kappa^* k^{0.5}}\ln\left(\frac{y}{y_v}\right) + \frac{y - y_v}{\rho\kappa^* k^{0.5}} + \frac{y_v^2}{\mu}\right] \tag{26}$$

where,

$$y_v \equiv \frac{\mu}{\rho C_\mu^{0.25} k_p^{0.5}} \cdot y_v^* \text{ and } y_v^* = 11.225$$

In the non-equilibrium wall function the equations for heat transfer calculation remain exactly the same. The mean velocity is more sensitive to pressure gradient effects. This does not seem to be crucial for our simulations.

Another wall function exists, called Enhanced Wall Treatment. This method combines a two-layer model with enhanced wall functions. If the mesh is fine enough in the near-wall region ($y^+=1$), then the enhanced wall treatment will be similar to a two-layer zonal model. But the mesh has to be fine enough everywhere close to the wall. This may impose too large a computational requirement. So this method can either have a near wall approach formulation when the mesh is fine enough or a wall function approach in case of coarser mesh.

In this approach, the near-wall region is divided into a viscous-affected region and a fully turbulent region. Here the limit between these two zones is delimited by a wall distance based criterion: the turbulent Reynolds number Re_y defined as below:

$$Re_y \equiv \frac{\rho y \sqrt{\kappa}}{\mu} \tag{27}$$

y is here the normal distance from the wall to the cell centers.

The fully turbulent region is defined as $Re_y > Re_y^*$ with $Re_y^* = 200$. In this region the κ-ε model is used. In the viscous affected region, the one-equation model of Wolfstein is used. The equations employed are the same as the κ-ε model except the turbulent viscosity which is computed as follows:

$$\mu_{t,2layer} = \rho C_\mu l_\mu \sqrt{\kappa} \tag{28}$$

Where the length scale in equation (28) is defined as:

$$l_\mu = yc_l\left(1 - e^{-\mathrm{Re}_y / A_\mu}\right) \tag{29}$$

The two layer viscosity for Enhanced wall treatment is smoothly blended with the High Reynolds Number μ_t definition using the formula:

$$\mu_{t,enh} = \lambda_\varepsilon\, \mu_t + (1-\varepsilon)\mu_{t,2layer} \tag{30}$$

Here μ_t is the same as the κ-ε model described above. The blending function is comprised between 0 (at the wall) and 1 (far from the wall):

$$\lambda_\varepsilon = \frac{1}{2}\left[1 + \tanh\left(\frac{\mathrm{Re}_y - \mathrm{Re}_y^*}{A}\right)\right] \tag{31}$$

with A defined as a width of the blending function, computed as:

$$\mathrm{A} = \frac{\left|\Delta \mathrm{Re}_y\right|}{\tanh(0.98)} \tag{32}$$

The ε is computed from the equation:

$$\varepsilon = \frac{\kappa^{3/2}}{l_\varepsilon} \tag{33}$$

With l_ε defined as a length scale computed as:

$$l_\varepsilon = yc_l\left(1 - e^{-\mathrm{Re}_y / A_\varepsilon}\right) \tag{34}$$

Using the following constants: $c_l = \kappa C_\mu^{-3/4}, \quad A_\mu = 70, \quad A_\varepsilon = 2c_l$

The Enhanced wall functions have to be valid throughout the near-wall region. To achieve it, the law for the wall has to be accurate whatever the layer involved. The same idea of using a blending function was kept. For our studies, the temperature and energy

equation treatment are very important. Equations for the near-wall temperature are derived below:

$$T^+ = e^{\Gamma} T^+_{lam} + e^{\frac{1}{\Gamma}} T^+_{turb} \tag{35}$$

Where the blending function Γ is computed using the following equation:

$$\Gamma = -\frac{a\left(Pr\, y^+\right)^4}{1 + bPr^3\, y^+} \tag{36}$$

In this equation Pr is the molecular Prandtl number, and $a=0.01c$, $b = \frac{5}{c}$, $c = \exp\left(f_r - 1.0\right)$ and f_r being the friction function, used in the control panel (taken as 0.5 by default).

1.3.6. Mesh topology

For CFD, mesh creation is one of the crucial steps to get accurate results. The mesh density directly influences the accuracy of the solution.

In our study of packed bed reactor, a 3D 120^o segment of tubular reactor has been used. The segments are composed of 2 layers of particles catalyst, in a tube-to-particle diameter ratio of N=4 which is relatively small.

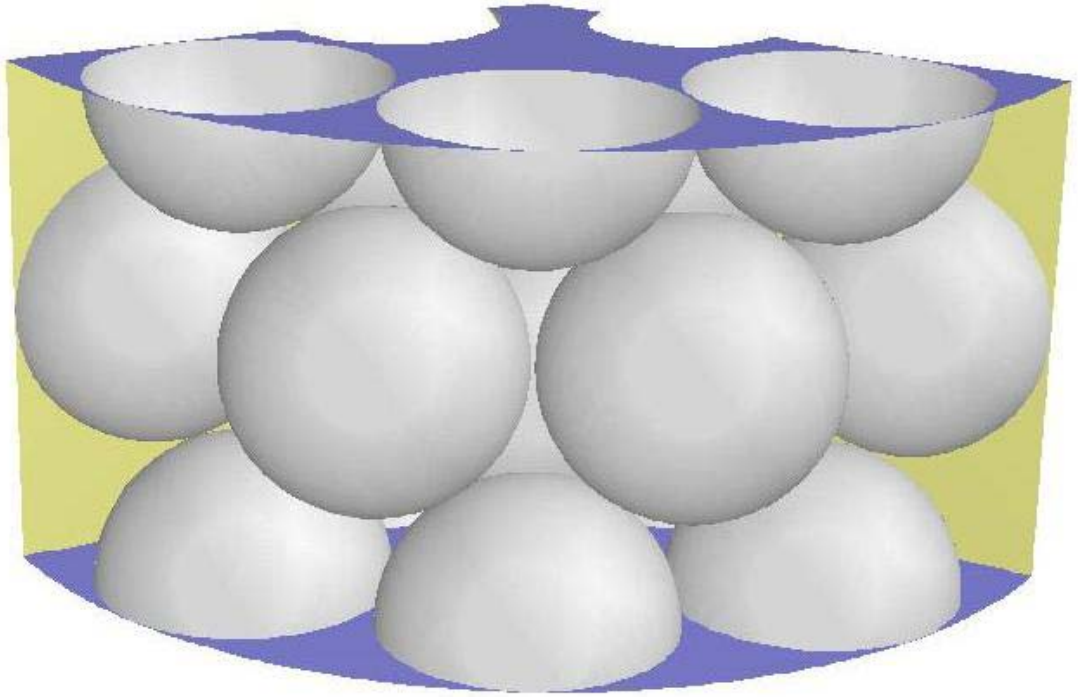

Figure 1.4: Mesh geometry for 3D 120o segment N=4, for spheres

Also some very similar meshes have been studied. The only difference remained in the shape of catalyst particle. Either spherical, full-cylindrical, or 1-hole-cylindrical catalyst particles were studied.

In another part of our study, a complete segment of 6 layers of spherical catalyst particles has been studied

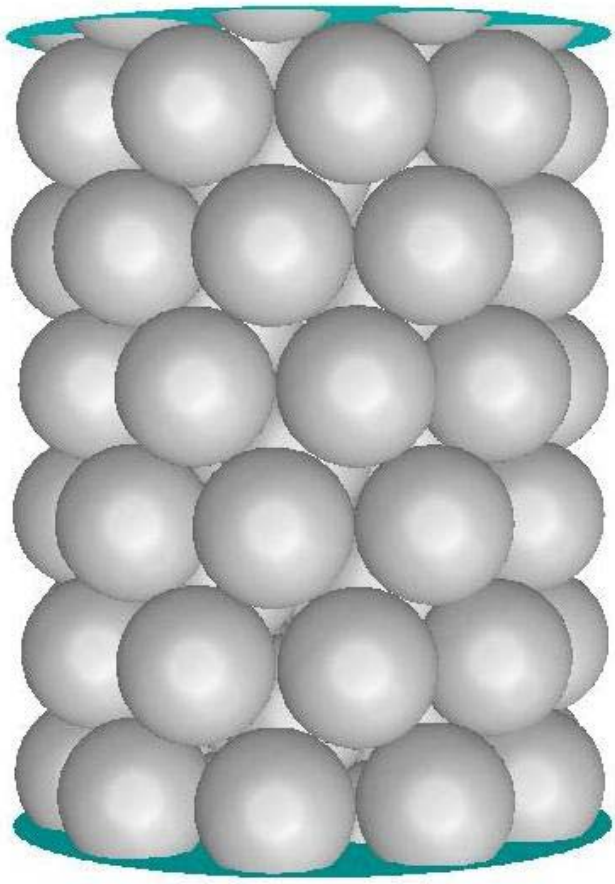

Figure 1.5: N=4, 6 layers of spherical catalyst particles bed

All meshes have been created by M. Nijemeisland for the present purpose using Gambit. Gambit is software specially designed to create meshes. They have been created in sake of optimization in terms of computational time versus accuracy. Depending on the mesh density, the solution will be more accurate but computationally expensive. An optimum has been found in terms of coarseness of the mesh. Most of the boundary conditions have been set before. Walls, catalyst particles have been set as wall boundary condition, interior of the bed is set as fluid, one face as flow inlet and another one to flow outlet. Other boundary conditions such as mass flowrate or wall temperature will be set in CFD package itself, not in the mesh creation software.

1.4. VALIDATION

Several experiments have been conducted by the former student (M. Nijemeisland) to study the accuracy of the mesh compared to laboratory experiments. During laboratory experiences, single tube, heated wall and packed bed were used. The tube-to-particle-diameter ratio N was set to either two or four. Thermocouples were used to acquire temperature profiles as a function of axial or radial position.

Also CFD package has been studied, by setting a simple model and comparing to energy balance theoretical models.

Data were collected either for laboratory simulations and CFD results and compared. Data collection method has been developed by O.R. Derkx, and is available in his Thesis (Derkx, 1995).

It seems that CFD is a reliable tool to get multiple numerical data all over the bed without any intrusive experimental errors. All the details of this study are available in the M. Nijemeisland MS thesis (2000).

2. PHYSICAL MECHANISMS IN WALL REGION

Thin tubular packed bed reactors are widely used in the industry. The way to model it has been developed especially for high N numbers (>10). But when models are applied to low N packed bed, a strong deviation appears, especially in the near-wall region. To understand why this deviation occurs, one has to understand the physical mechanisms involved in the wall vicinity heat transfer. Due to the specific geometry of the bed (low N) and the flow conditions (Reynolds number, Prandtl number) some heat transfer mechanisms become more effective than other mechanisms.

2.1. HEAT TRANSFER RESISTANCE

The main issue of packed bed reactor is the radial temperature drop observed close to the wall. Considering a turbulent flow in the core of the packed bed, heat transfer in this region is pretty well modeled, and various correlations have been studied. In the wall vicinity three heat transfer mechanisms take place: a heat transfer resistance due to the presence of a viscous boundary layer, a reduction of the bed conductivity, and a damping of mixing. These mechanisms are well understood for a long time. But the way to quantify them in the wall vicinity remains uncertain.

2.1.1. Viscous boundary layer

A viscous boundary layer is present at the wall. This is due to the no-slip condition at the wall. The flow in the wall vicinity is viscous. The size of this layer depends on the

Reynolds number of the flow. This layer acts as a resistance to momentum and mixing. So a similar thermal boundary layer exists in the near-wall region. Its thickness is determined by the molecular Prandtl number of the fluid. The heat transfer resistance due to that mechanism is in part responsible for the temperature drop.

2.1.2. Change in bed conductivity

The N value in our study is 4, which means that 4 catalyst particles may be placed in the radial position across the fixed bed. Because of that, drastic changes in porosity profile are noticed across the bed. On an ideal point of view the porosity idealized at the wall is one, which means only pure fluid is present. So, in a small range, from the wall to the half particle size region, the porosity profile changes from 0.4 to 1. This is not without consequences on heat transfer. The presence of solid catalyst particles increases the bed conductivity. As a consequence, the bed conductivity decreases a lot in the wall vicinity due to the high voidage. So the heat transfer by conduction is less important in the near-wall region than in the core of the fixed bed. This adds to the laminar viscous boundary layer.

2.1.3. Damping of mixing

As mentioned above, drastic changes on the bed porosity occur. So in the near wall region, large voids are present. In these large voids between catalyst particles, fluid flows with higher velocity and less turbulence. This is called channeling effect. So the mixing due to turbulence which takes place in the core of the fixed bed is damped in the near wall region. The flow becomes more parallel to the wall and there is less radial displaced

flow, which is probably responsible for better heat transfer. So the heat transfer by convection is less promoted in the voids of the wall vicinity.

A picture of radial porosity profile is available and will be discussed later in the section 4.1.

2.2. PREVIOUS LITERATURE

An extra heat transfer resistance is present in the wall vicinity of packed bed reactors. Lots of correlations have been found which model pretty well the heat transfer in the wall vicinity especially for high tube to particle ratio (N>10).

Yagi and Kunii (1961) have already highlighted the 3 mechanisms responsible for the heat transfer resistances which have been cited above.

The most common way to model the radial temperature profile in packed bed reactor is to lump all three contribution into one heat transfer resistance idealized at the wall.

Coberly and Marshall (1951) have been the first to introduce the heat transfer coefficient h_w in order to model the extra heat transfer resistance. This can be expressed in the form of a boundary condition at the wall. The mathematical formula associated is shown below:

$$h_w\left(T - T_w\right) = -k_r \frac{\partial T}{\partial r} \quad \text{at } r = R \tag{37}$$

But no consensus in the literature concerning heat transfer behavior in fixed can be obtained (Li and Finlayson, 1997; Tsotsas and Sclünder, 1990; Vortmeyer and Haidegger, 1991; Freiwald and Patterson, 1992; Gunn Ahmad and Sabri, 1987).

This approach may be convenient for high Reynolds number flows, and high tube-to-particle diameter ratio (N>10), because the size of the region affected by the wall is very

small and may be idealized directly at the wall. But this approach seems to be too simple when the value of N is low (N<10) and deviation is noticed when this approach is followed in thin packed bad reactors.

The change in void fraction close to the wall directly depends on the porosity profile. Drastic changes in porosity profile may be found for 0.5 to 1 particle diameter, which for low N, cannot be idealized at the wall. 1 particle represents 1/N of the total diameter in terms of size in the radial position.

Along the same lines, for the damping of mixing, the range of this phenomenon is also 0.5 to 1 particle diameter. Channeling effects occur directly in voids in the wall vicinity so directly depend on porosity profile. Lots of studies have been done to evaluate radial inhomogenities in the overall flow profiles (Kalthoff and Vortmeyer, 1980; Haidegger et al., 1989; Lerou and Froment, 1977; Froment and Bischoff, 1979; Papageorgiou and Froment, 1995). Many groups have tried to measure the radial distribution of the axial flow inside the bed (Morales et al., 1951; Price, 1968; Schuster and Vortmeyer, 1981; Ziolkowska and Ziolkowski, 1993; Daszkowski, 1991).

But for the laminar viscous boundary layer, the size of this region affected is very thin and just adjacent to the wall. The thickness of this region mainly depends on the Reynolds number, fluid characteristics and bed geometry.

For low tube to particle diameter ratio, lumping all three mechanisms into only one heat transfer resistance seems to be too rough as an approach. Tsotsas and Schlünder (1990) were the first to point this very important issue: “What is exactly the meaning of h_w? Does it make sense in a physical point of view?”

Their idea is based on flow characteristics: when the flow begins to be semi turbulent or laminar, then the main mechanism responsible for heat transfer is conduction, then the h_w parameter has not really any physical sense, because the viscous boundary layer does not exist any more.

To have a better understanding of what occurs in the wall vicinity, all three mechanisms need to be studied separately.

Tobis and Ziòlkowski (1988) tried to isolate the contribution of the laminar boundary layer. In their study, they tried to model and predict the thickness of the viscous boundary layer. This contribution is crucial in the heat transfer resistance modeling in the wall vicinity. For this, they tried to find a correlation to predict the Nusselt number close to the wall.

$$Nu_w = Nu_0 + \frac{1}{\frac{1}{Nu_m} + \frac{1}{Nu^*}} \tag{38}$$

Three contributions are present here. With:

Nu_0 the bed conductivity contribution

Nu_m the reduction of turbulent conductivity

Nu^* the contribution of the viscous boundary layer

They focused their research on Nu^* to find the thickness of the viscous boundary layer. They used a balance of the stresses acting on fluid in the near-wall region, coupled with Ergun's formula about pressure drop. Here is the resulting formula:

$$\frac{1}{r^*} = \frac{1}{d}\sqrt{\left[\frac{(1-\varepsilon_s)^2\,\varepsilon_m}{{\varepsilon_s}^2}\right]\left[\frac{(1+\theta)\ln(1+\theta)}{\theta^2} - \frac{1}{\theta}\right](150 + 1.75\,\mathrm{Re}')} \tag{39}$$

With:

$\varepsilon_m = 0.26$ (minimal contribution of area occupied by fluid at distance d/2 from tube wall, u_s/U'_s ratio)

$\varepsilon_s = 0.52$ (porosity of ring-shaped layer adjacent to tube wall)

$\theta = (\mu_0/\mu)\ \mathrm{Re}'$

$\mu_0 = 5.10^{-7}\ \mathrm{Ns/m^2}$

$\mu = 2.267.10^{-7}\ \mathrm{Ns/m^2}$ for air at 400K

Re'=Re/0.3 (in lab condition Re=1000)

d = 1 inch = 0.0254 m (or 0.029 m for cylinders)

Now the heat transfer coefficient is deduced accounting only for the viscous boundary layer contribution:

$$h_w^* = \frac{\lambda}{r^*} \frac{\theta \,\mathrm{Pr}}{\ln(1+\theta \,\mathrm{Pr})} \tag{40}$$

With

λ = 0.0333 W/mK (thermal conductivity for air at 400K)

Pr = 0.697 (Prandlt number for air at 400K)

Another approach for predicting the size of the viscous boundary has been studied, the Tsotsas and Schlünder (1990) approach. According to them, the size of the unmixed sublayer δ_u may be found using the following equation derived from the Ergun equation:

$$\delta_u = \left(\frac{\mu_f}{f_2 \overline{u_0}} \right)^{1/2} \tag{41}$$

With:

$$f_2 = \frac{A \rho_f}{d_p} \tag{42}$$

and $$A = \frac{1.75(1-\Psi)}{\Psi^3} \tag{43}$$

d_p: particle diameter (0.0254m for spheres, 0.029 for cylinders)

ρ_f: density of the fluid (0.875 kg/m^3 for air at 400K)

ψ: porosity of the bed (Taken as 0.4)

μ_f: viscosity of the fluid (2.267*10-5 kg/ms for air at 400K)

$\bar{u}_0$: mean superficial velocity (0.891 m/s for cylinders and 1.02 m/s for spheres).

2.3. COMPARISON WITH FLUENT SIMULATIONS

Now considering that the CFD package gives accurate numerical data all over the fixed bed, it is possible to compare the previously cited literature with simulation results. The aim here is to compare the size of the viscous boundary layer, and measure the contribution in a heat transfer point of view. Simulations have been conducted in the 120^o wall segment of 2 layers, either for spheres, full cylinders and 1-hole cylinders catalyst particle shapes. The material used was air to simulate laboratory conditions. For accuracy purposes, air properties have been taken at 400K (127^{o}C). The values are shown below:

$\mu = 2.267 \cdot 10^{-5}$ Ns/m^2
$k = 3.33 \cdot 10^{-2}$ W/mK
$\rho = 0.875$ kg/m^3
$C_p = 1.013$ kJ/kgK

The mass flowrate has been fixed to 0.0019 kg/s and 0.00166 kg/s for spheres and cylinders respectively. The corresponding Reynolds numbers are 788.4 and 789.2 for spheres and cylinders.

Using the equations expressed in the CFD equations part, especially equations (23) and (24), it is possible to calculate the cut off of the viscous boundary layer with given numerical values extracted from CFD simulations. This will be compared to Tobis and Ziolkowski and Tsotsas and Schlünder approaches of the boundary layer thickness at the wall.

	Thickness of boundary layer (m)		
Catalyst particle shape	**CFD**	**Tobis and Ziolkowsky**	**Tsotsas and Schlünder**
Spheres	$1.19 * 10^{-3}$	$2.77*10^{-3}$	$2.64 * 10^{-4}$
Cylinders	$1.64 * 10^{-3}$	$2.42*10^{-3}$	$3.02 * 10^{-4}$

Table 1.1: comparison of the viscous boundary layer thickness depending on the method used and shape of catalyst particles.

It seems that both methods are in good agreement with the CFD results. But Tsotsas and Schlünder formula accounts only for the true viscous boundary layer unlike CFD which calculates the viscous boundary layer plus a part of the buffer layer. Tobis and Ziolkowsky formula is calculated such that the limit of the viscous boundary layer is defined as a maximum of velocity in that region which does not necessarily correspond to the viscous sublayer. That is why Tsotsas and Schlünder formula gives a smaller prediction than CFD or Tobis and Ziolkowsky.

This viscous boundary layer is in a millimeter order of magnitude. Assuming that there is not a significant amount of catalyst particles in that region, it seems possible to idealize the heat transfer resistance due to this viscous boundary layer at the wall.

3. WALL MODELING IN CFD

One of the keys to CFD accurate modeling is the boundary conditions, and especially for wall-bounded turbulent flows. As mentioned above, several approaches are available in CFD to model walls; either fully solve the boundary layer all way down to the wall or bridge it with wall functions.

3.1. BOUNDARY CONDITIONS: THE SYMMETRIC CONDITION PROBLEM

But for sake of computational cost, 120^{o} segment of a tubular fixed bed of two layers of catalyst particles has been meshed, which corresponds to 1/3 of the complete section of the reactor. To compensate the two other thirds, symmetric conditions at the radial plane have been set, so that 2 other thirds are simulated also the same way as the meshed one.

Part of the study is to evaluate the deviation generated by this approach. The way to proceed was to define four quarters of 30^{o} each on the existing meshed segment. Then the task was to study the radial temperature profile in each region, and analyze differences.

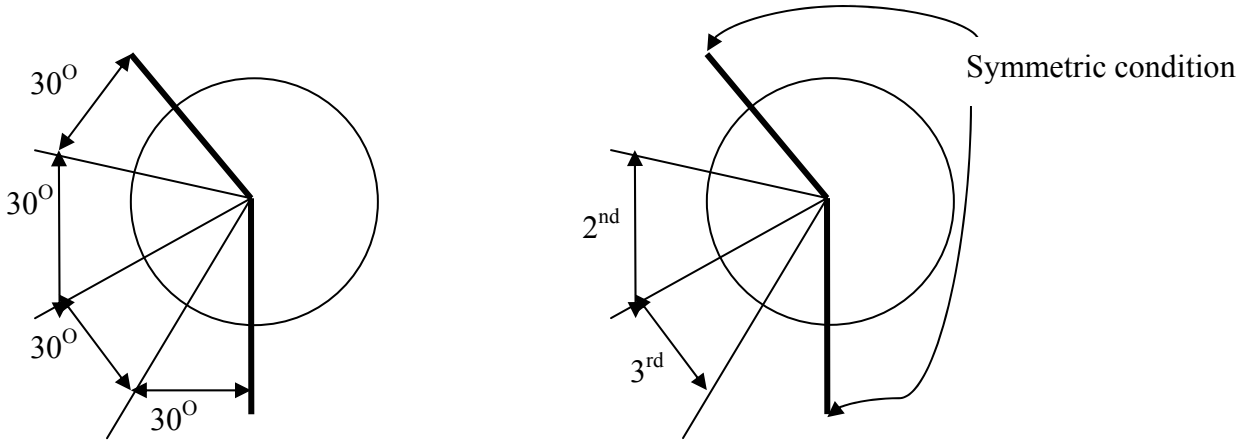

Figure 3.1: symmetric condition problem: geometry of the packed bed tubular reactor segment

Radial temperature profiles have been compared, just considering an average of the second and third section, and the other profile was an average of all four quarters. Here are presented below the plots:

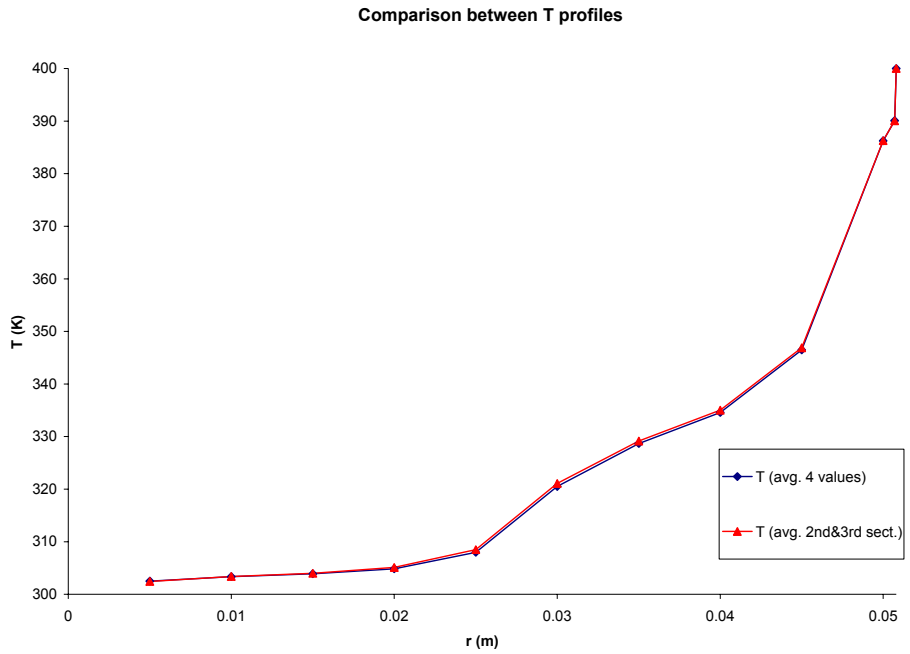

Figure 3.2: Temperature profile for second and third section compared to overall section. Catalyst pellets are Spheres.

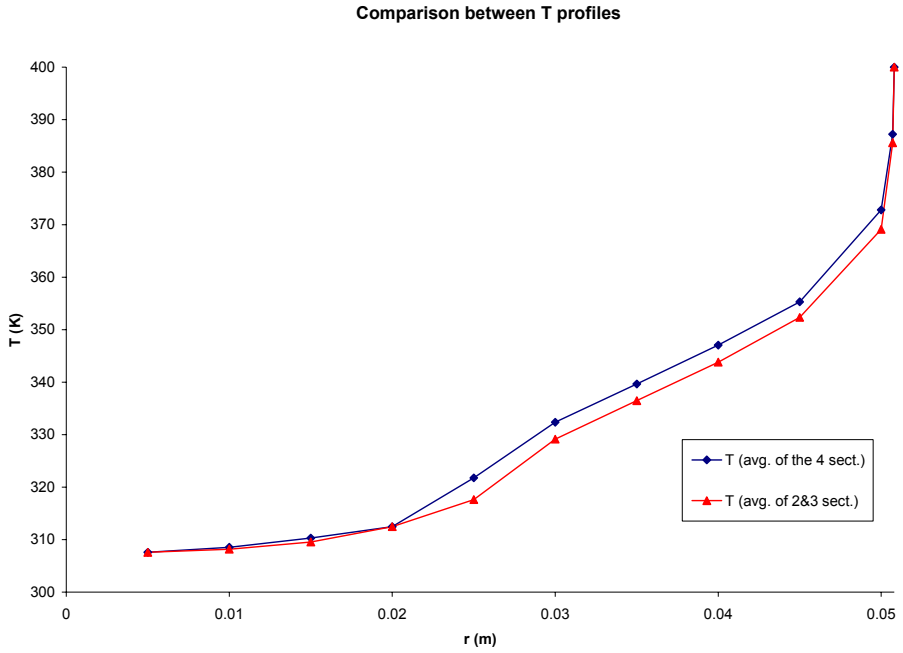

Figure 3.3: Temperature profile for second and third section compared to overall section. Catalyst pellets are Full Cylinders.

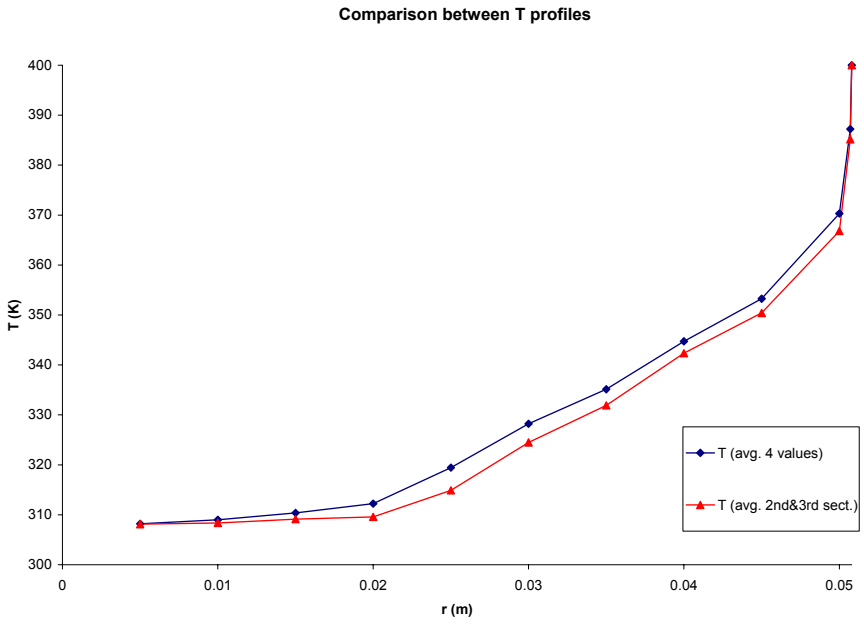

Figure 3.4: Temperature profile for second and third section compared to overall section. Catalyst pellets are 1-hole-Cylinders.

All simulations here have been run with a κ-ε model, with Enhanced Wall Treatment enabled. The temperature at the wall has been set to 400K for a corresponding Reynolds number of respectively 788.4 and 789.2 for spheres and cylinders geometries. Temperatures profiles have been extracted using planes of constant radius.

A difference can be observed for 1-hole and full cylinders catalyst particles, and especially in the core of the bed. This may be explained by the arrangement of catalyst particles which was in fact not really symmetric. So errors are propagated through all iterations, resulting in a $5^{o}C$ deviation in the core of the bed.

A much less deviation is observed in the bed center, due to the smallness of the region. The core region is so small that any deviation influences all four sections. So all differences are small and may be in this case neglected.

In the near wall region, also deviation is less than in the core of the bed. This is due to the fact that the main source of heat is generated by the 400K wall itself. Fluxes coming from the symmetric condition plane are negligible compared to the wall heat flux. That is why temperature profiles are very similar in the core and in the wall vicinity of the bed.

For the spheres, the problem is different. Due to the quasi perfect arrangement of spheres, the symmetric condition is more valid than for cylinders arrangement. The deviation wherever the radial position in the bed is never greater than $1^{o}C$. So in this case, symmetric condition is justified and valid.

Presented in appendix B, plots for the three same geometries but for different wall functions, like κ-ε model with standard wall functions or using κ-ω approach which has no need for any wall function. Results are pretty similar. Same conclusions may be drawn for these plots also.

3.2. WALL REGION MODELING USING CFD

As described in sections 1.3.4 and 1.3.5, several approaches are available in the CFD package for both turbulent model and wall treatment. In certain cases deviation may be detected for the same mesh, using the same boundary conditions, but just using a different approach to run the simulation. All models have assumptions, and have specifications to be as accurate as possible depending on the requirements of the simulation. These specifications have to be studied for obtaining the best results.

Our simulations are, in this work, a heat transfer study for turbulent flow through a fixed catalytic bed under laboratory conditions. In other terms, laboratory conditions mean 'low' turbulent particle Reynolds number (see Appendix A), usually between 500 and 1500, and a wall heated at 400K at constant temperature. Because of the low N ratio (4 in our cases) the tubular reactors are very thin. Presence of wall cannot be neglected and represent a crucial approach in CFD accuracy for turbulent flows. As specified in section 1.3.4, two main approaches are available: either bridge numerical variables from the core of the turbulent flow to the wall or fully solve the viscous boundary layer all way down to the wall. The first approach gives the choice between three wall functions explained in section 1.3.5.

In order to clearly choose the best wall approach, one needs to focus on the grid considerations. Because of the importance of turbulence effects, accuracy is here a matter of grid generation. The main criterion to choose the accurate model is y^+, which represents a dimensionless distance from the center of the nearest cell to the wall. y^+ is solution dependent, which means that the flow characteristics have an influence on y^+ value. y^+ is defined as above:

$$y^+ \equiv \frac{\rho u_s y}{\mu} \tag{44}$$

The table below describes the range of values of y^+ depending on the wall function approach.

Approach:	**WALL FUNCTIONS**		
	Standard wall functions	Non equilibrium wall functions	Enhanced wall treatment
y^+ value	between 30 and 60	between 30 and 60	< 5

Table 3.1: y^+ requirements for wall functions

Approach:	**Near wall approach κ-ω**	
	With transitional flow option	Without transitional flow option
y^+ value	< 5	between 30 and 60

Table 3.2: average y^+ requirements for near- wall approach

Model, wall approach		**Re_p**	**y***	**y^+**
sphere 99.5%	standard	788.4	1.41	1.5
	ewt	788.4	1.5	1.53
	k-ω	788.4	1.49	1.5
Full cylinders	standard	789.2	2.66	2.43
	ewt	789.2	2.66	2.74
	k-ω	789.2	2.66	2.71
1 hole cylinders	standard	789.2	2.48	2.27
	ewt	789.2	2.43	2.5
	k-ω	789.2	2.46	2.43

Table 3.2: y^+ values for different geometries and different wall approach

The y^+ values shown above correspond to the cells adjacent to the inner wall.

According to the last table, it is clear that all meshes and geometries, in our laboratory conditions, are fine enough to enable the CFD package to use the κ-ω with transitional

flow option methods or the κ-ε enhanced wall treatment model. According to the other two first tables, y^+ requirement for other methods are not met.

All three methods have been compared to study the influence of the way to solve the wall vicinity. The meshing is completely identical, for the same Reynolds number. Radial temperature profile is plotted. Only the second and third quarters have been used to calculate the mean temperature for each radial position.

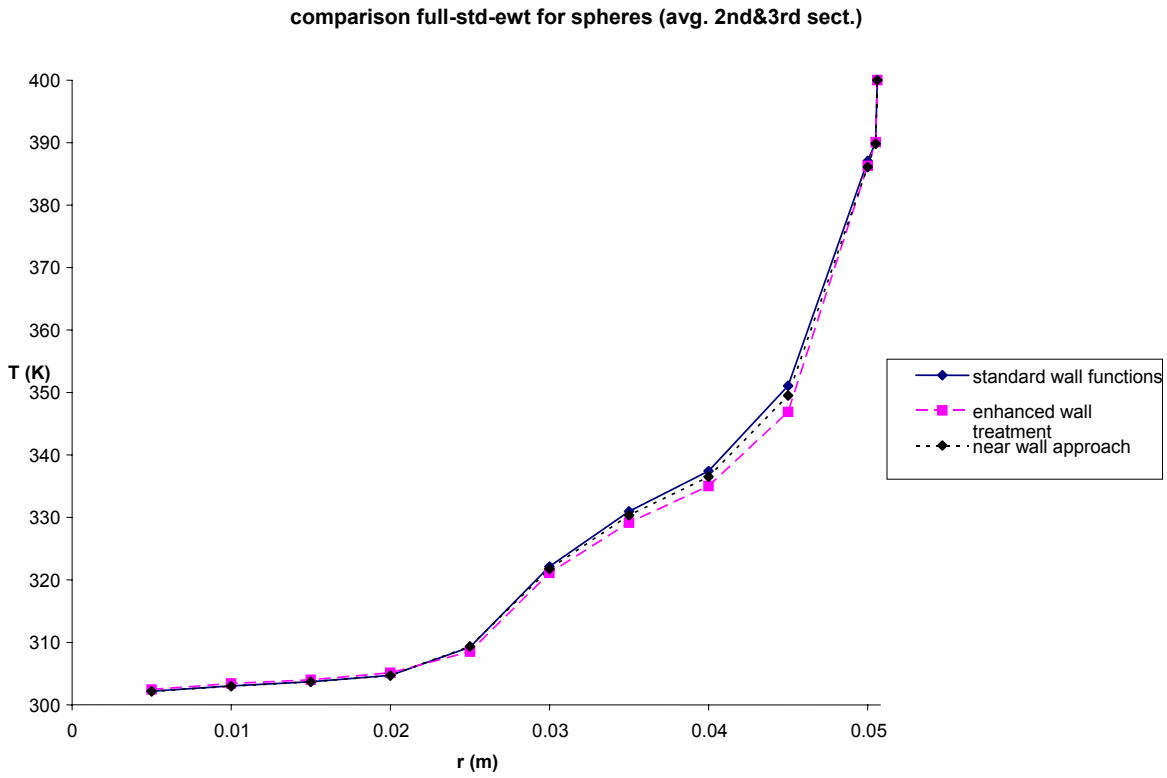

Figure 3.5: comparison between standard, enhanced wall functions and κ-ω approach for spheres catalyst particle geometry.

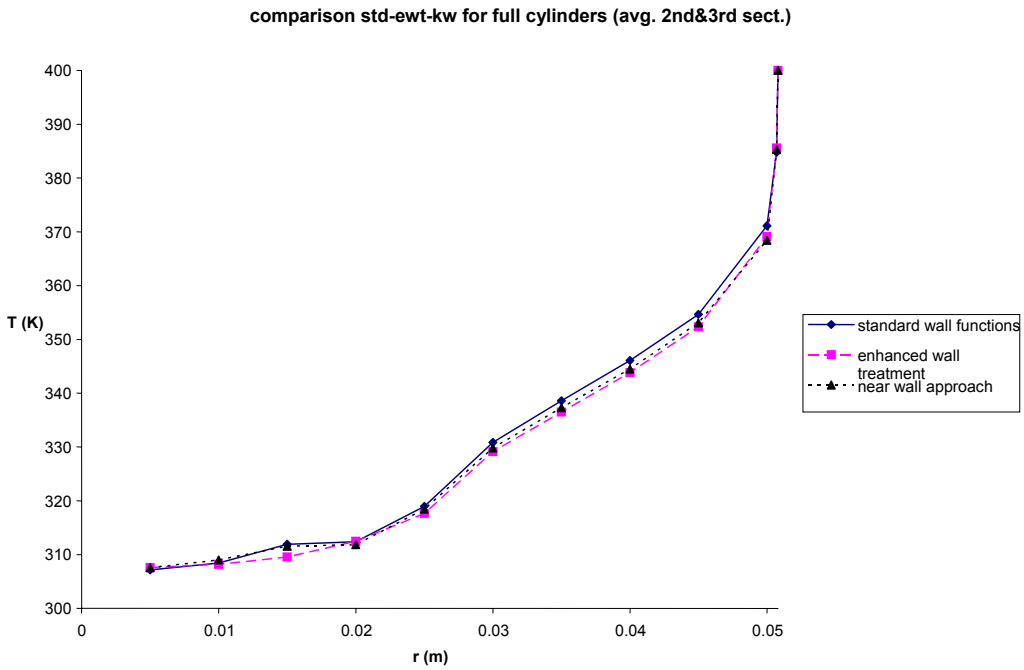

Figure 3.6: comparison between standard, enhanced wall functions and κ-ω approach for full cylinders catalyst particle geometry.

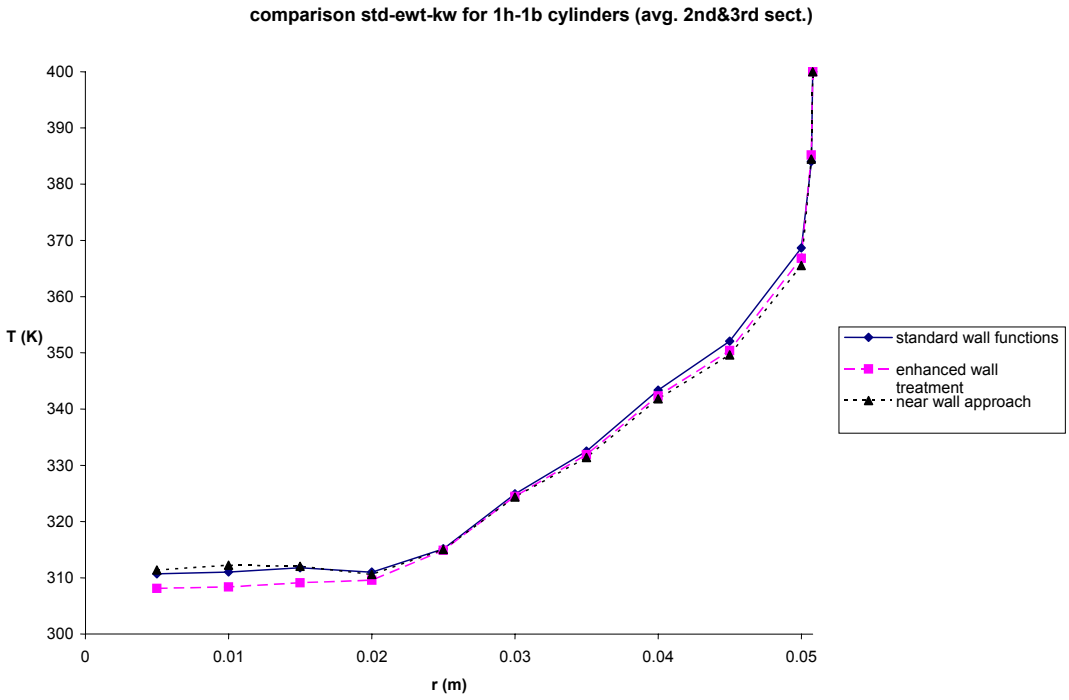

Figure 3.7: comparison between standard, enhanced wall functions and κ-ω approach for 1-hole cylinders catalyst particle geometry.

At first glance, there is no huge difference between all three profiles for three different geometries. There are some small deviations in the core of the bed. But our region of interest is the wall vicinity, and near wall region temperature profile. There is almost no difference between these three methods because all of them were set to wall temperature at 400K.

Now heat flux through the wall is compared since the temperature at the wall is set constant at 400K. By this way, we can more clearly see the difference in modeling depending on the methods employed:

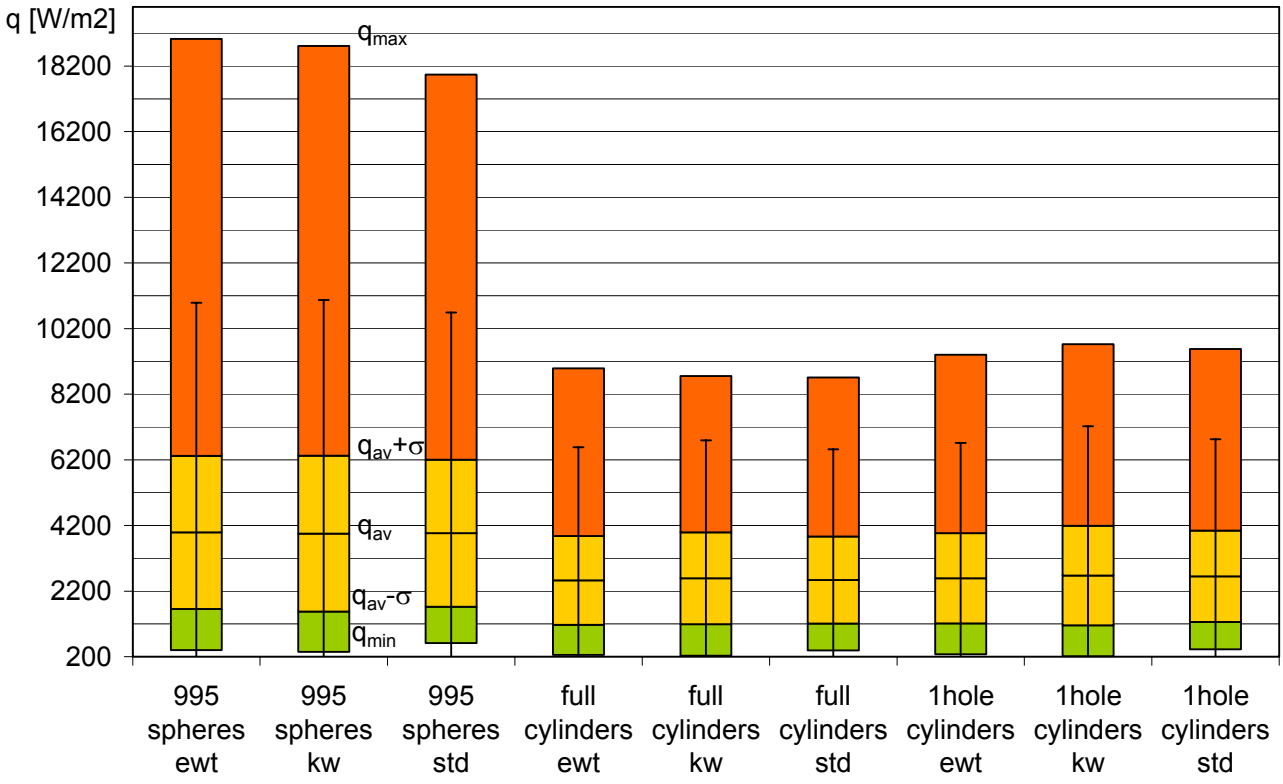

Figure 3.8: Comparison of wall heat flux depending on the different geometries and wall models

We can see that all models are almost identical in the way to model the near-wall region. The difference between cylindrical particles and spheres is due to many reasons. The voidage of the sphere arrangement is less than cylindrical shape voidage. So the bed conductivity is higher in the spheres arrangement. For spheres arrangement, a very thin

layer of fluid is present between the external layer of catalyst particles and the wall. This way of meshing is due to the fact that CFD convergence cannot be obtained with contact points directly against the wall. Simulation using a 10-sphere model with contact points at the wall have been studied by Logtenberg (Logtenberg et al., 1999).

For the cylindrical arrangement, the phenomenon is emphasized due to the much higher complexity of the arrangement. So the contribution of heat resistance due to the laminar viscous sublayer is greater in the cylindrical meshing than the spherical one. That explains the difference between spherical and cylindrical catalyst particles for heat fluxes at the wall.

It seems that even if the standard wall function approach is not accurate in terms of assumptions, it works pretty well and gives similar results to Enhanced Wall Treatment and κ-ω model. Another explanation may be that even if the geometry seems to be complex, the flow patterns are not so complicated. There is not drastic change in axial fluid velocity, so there is not huge pressure drop along the tubular reactor which makes it easier for the CFD package to solve accurately the runs.

Knowing the fact that the κ-ε model uses a linear law for the values of y^+, this appears to say it was not a bad decision. Results are very similar and comparable.

4. NEW APPROACH FOR RADIAL HEAT TRANSFER

Lumping all the physical mechanisms into only one parameter idealized at the wall seems to be a too simple approach for low tube to particle diameter ratio (N). After having studied the effect of the viscous laminar boundary layer, the two other mechanisms have to be studied separately. At this point CFD is an excellent tool to provide experimental results.

4.1. MODEL PROPOSED

Since the viscous boundary layer has been successfully isolated, the idea is to figure out the contribution either from conduction with bed porosity variation, and convection with flow characteristics.

According to previous paragraph 2.2, the problem of the conduction and convection phenomena are taking place in 0.5 to 1 diameter particle which represent in a N=4 bed up to a annular layer of ¼ of the total bed. According to this, it is not comparable to the size of the viscous boundary layer, which is only in the order of magnitude of a millimeter.

Tsotsas and Schlünder (1990) brought the idea that for low Peclet number flows, the standard model using the heat transfer resistance at the wall h_w is only an mathematical object which only accounts for maldistribution of fluid velocity, axial dispersion of heat and some systematical errors in the measurement. This is true because for low Peclet number, the main mechanism for heat transfer in the near wall region is conduction. According to them, for high Peclet flows, the use of h_w is justified because now the main mechanism of heat transfer is convection.

But all these statements do not account for the low N reactors. The way to reconcile low N tubes and the Tsotsas and Schlünder conclusion would be to keep the h_w approach but only to account for the viscous boundary layer. Whatever the turbulent flow, the thickness of this layer is always thin compared to half or one diameter of a catalyst particle. In that way, we can surely assume that a very small amount of catalyst surface is present in the viscous boundary layer, especially when catalytic reactions have to be modeled. Then the change in conduction and convection have to be modeled in another manner than using a lump parameter h_w. But as the Reynolds number decreases, the thickness of the boundary layer increases. So this approach would have a limit which directly depends on Reynolds number.

Then, to account for the change in conduction in the bed, the true bed conductivity has to be introduced using an accurate porosity profile assuming that the porosity is only a function of the radial position:

$$k_{bed} = k_f \, \Psi(r) + k_p (1 - \Psi(r)) \tag{45}$$

with k_{bed} is the bed conductivity

k_f is the conductivity of the fluid

k_p is the conductivity of the catalyst particles

$\psi(r)$ is the porosity profile

The way to extract porosity profile is explained in Appendix C.

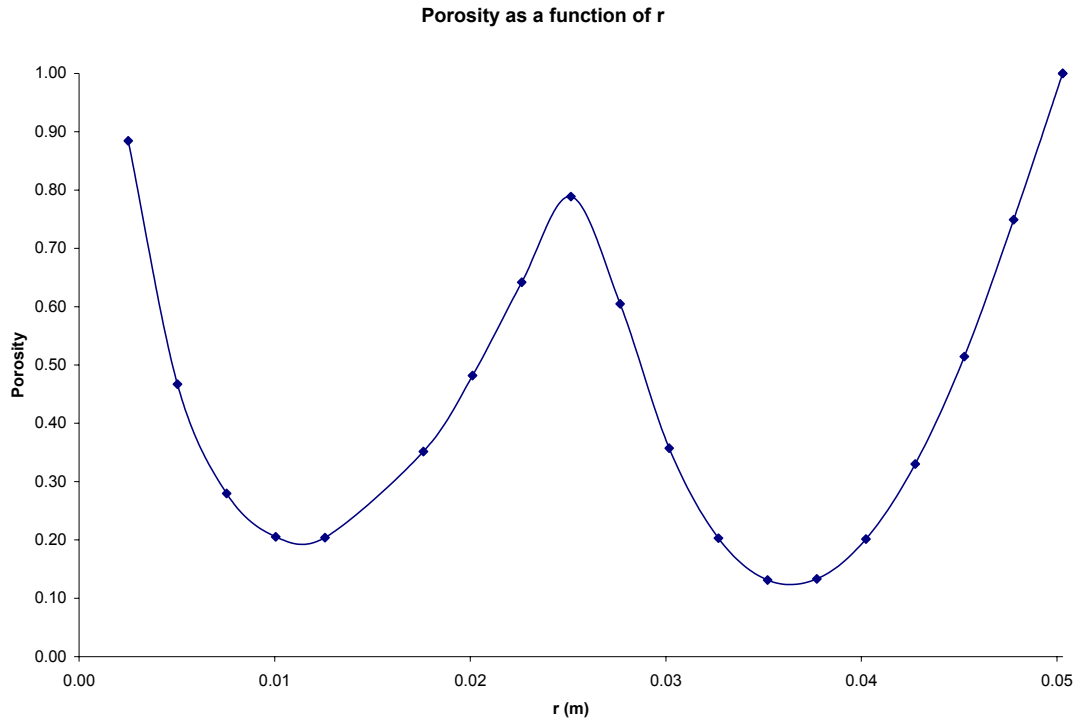

Figure 4.1: porosity profile as a function of radial position for spheres arrangement

The porosity profile for an N=4 tubular reactor is very sharp. Because of the low N, it is not possible to average the porosity profile in the core of the bed. The features are clear here: there are two gaps in the curve, corresponding to the two different layers of spheres on the radial position. Because of the way it has been extracted (average on 360^o of the fixed bed at constant radius position) the profile is strictly symmetrical to the axis x = 0. Two minima are observed, one at $\psi(r = 0.011m) = 0.2$,and the other one $\psi(r = 0.036m) = 0.15$, which correspond to the radial position of the center of the spheres layers. An average of the bed porosity leads to $\overline{\Psi} = 0.46$.

The model which assumes a constant porosity profile along the radial position may be a good assumption for N>10 but certainly not for low N tubular reactors. Introducing this 'true' porosity profile into the energy equations will surely increase the accuracy of the solutions. Then the true bed conductivity will be introduced, minimizing the error on it and getting rid of artificial or effective radial conductivity usually employed in standard models. Extensive work about fixed bed conductivity has been done (Bauer, 1993). This approach is to account for the drastic change in conductivity in the bed depending on the

radial position. Borkink, J. G. H. and Westerterp, K. R. (1993) have worked on the porosity profile influence on radial heat transfer.

The other physical mechanism responsible for radial heat transfer in the bed is convection. To improve the standard model about convection, true velocities along the bed need to be introduced. For that CFD appears to be a non intrusive and accurate tool. The idea is to replace the mean velocity in the energy equation by local velocities in the bed. The equation will become as followed below:

$$\rho \cdot Cp \cdot \left(u_r(r,z)\frac{\partial T}{\partial r} + u_z(r)\frac{\partial T}{\partial z} \right) \quad \text{instead of } \rho \cdot Cp \cdot \bar{u}\frac{\partial T}{\partial z} \tag{46}$$

This can only be done using CFD, due to the availability of numerous numerical variables wherever the location in the bed.

So the new equation (pseudo homogeneous) model will be:

$$\rho_f \, Cp_f \left(u_r(r,z)\frac{\partial T}{\partial r} + u_z(r)\frac{\partial T}{\partial z} \right) = \frac{1}{r}\frac{\partial}{\partial r}\left(r\left(k_f \, \Psi(r) + k_p(1-\Psi(r))\right)\frac{\partial T}{\partial r} \right) + k_a \frac{\partial^2 T}{\partial z^2} \tag{47}$$

To verify if this approach is accurate, many experiments have to be conducted. CFD is going to be used. The main idea is to first confirm the rate of radial heat transfer only by convection.

Using a Fortran program written by A. G. Dixon (code available in Appendix D) it is possible to solve equation (47) only accounting for convection by setting k_p to zero. A set of velocities has to be extracted from experiments. To compare the program results to the experiment, CFD is used, and identically, we set k_p to zero.

The most awkward part of this study is to extract the velocities from the core of the bed.

4.2. VELOCITIES EXTRACTION PROCESS

Velocities extractions might seem easy at glance, but a wrong way to extract them can directly lead to large deviation between CFD results and energy equation solving. Also due to the pseudo homogeneous nature of the energy equation involved, one has to be careful on how to account for spheres volumes corresponding to no velocities (fixed bed).

The first assumption is to assume that axial velocities are only a function of radial position: $u_z = u_z(r)$. The flow here is periodic, due to the symmetric structure of the fixed bed. The same flow characteristics are noticed through 3 stacks of 2 layers of catalyst particles, corresponding to the 6 layers of spherical catalyst pellets composing the fixed bed. So the assumption of axial velocities only depending on radial position seems to be justified.

The second assumption is to assume that radial velocities are function of radial position and axial position: $u_r = u_r(r,z)$. Because the radial component of velocity is mainly considered responsible of the turbulences and mixing, we considered that it was important to keep radial velocities as functions of radial and axial positions.

Third, tangential velocities have been also extracted. The values of them are very small, around 0.1 m/s as an order of magnitude, which can be neglected compared to axial velocities and radial velocities which are much higher (at least 10 times).

Now we have to deal with both radial position and axial position. The way we extracted velocities is similar to porosity profile. First I defined 13 planes of constant radius corresponding to cylinders all through the fixed bed. For each plane, thanks to CFD, numerous numerical variables have been extracted especially radial and axial velocities. All results are provided in a table with the coordinates of the cell and

associated numerical values. So we had to deal with a way to map numerical values such that we can find a logical way to extract them.

For axial velocities, there are no problems for extraction. A simple averaging over all the velocities available has been done for each plane of constant radius. Here is the following plot for axial velocities:

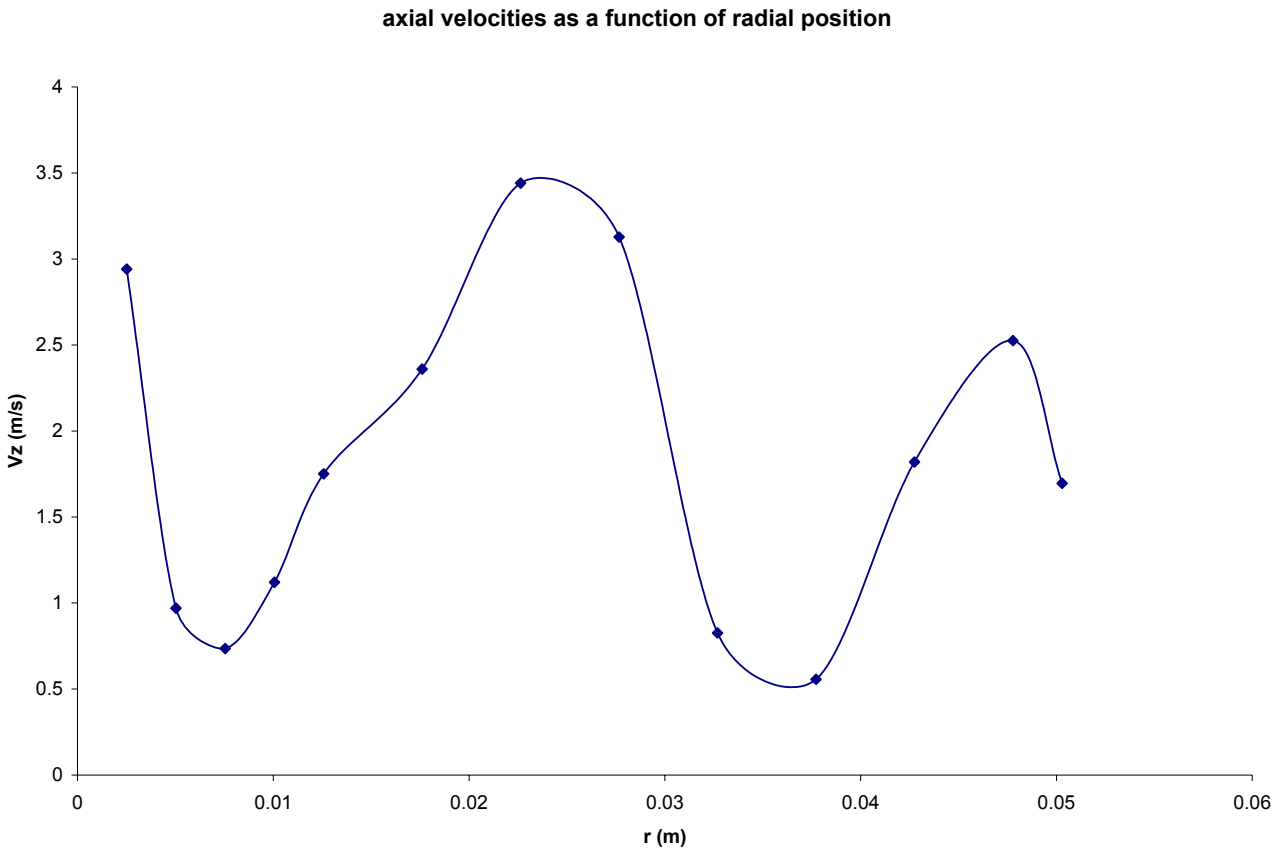

Figure 4.2: axial velocities as a function of radial position

The axial velocity profile is also very disparate. It advocates the idea to get rid of any averaged velocity. Values are spread between 0.7 and 3.5 m/s. Also two gaps are noticed corresponding to the two layers of spheres in the radial direction. According to a profile like this, no averaging is allowed for accuracy sake.

As expected, axial velocity profile is very similar to porosity profile, except near the wall. So high flowrates are located in high-porosity regions, but in the wall vicinity, axial velocity drops due to the no-slip condition at the wall.

For radial velocities, we had to map radial velocities depending on the current location of the cell. Depending on coordinates for each cell, true radial distance has been calculated. Then depending on the angle, also calculated thanks to cells coordinates, maps of radial velocities have been plotted:

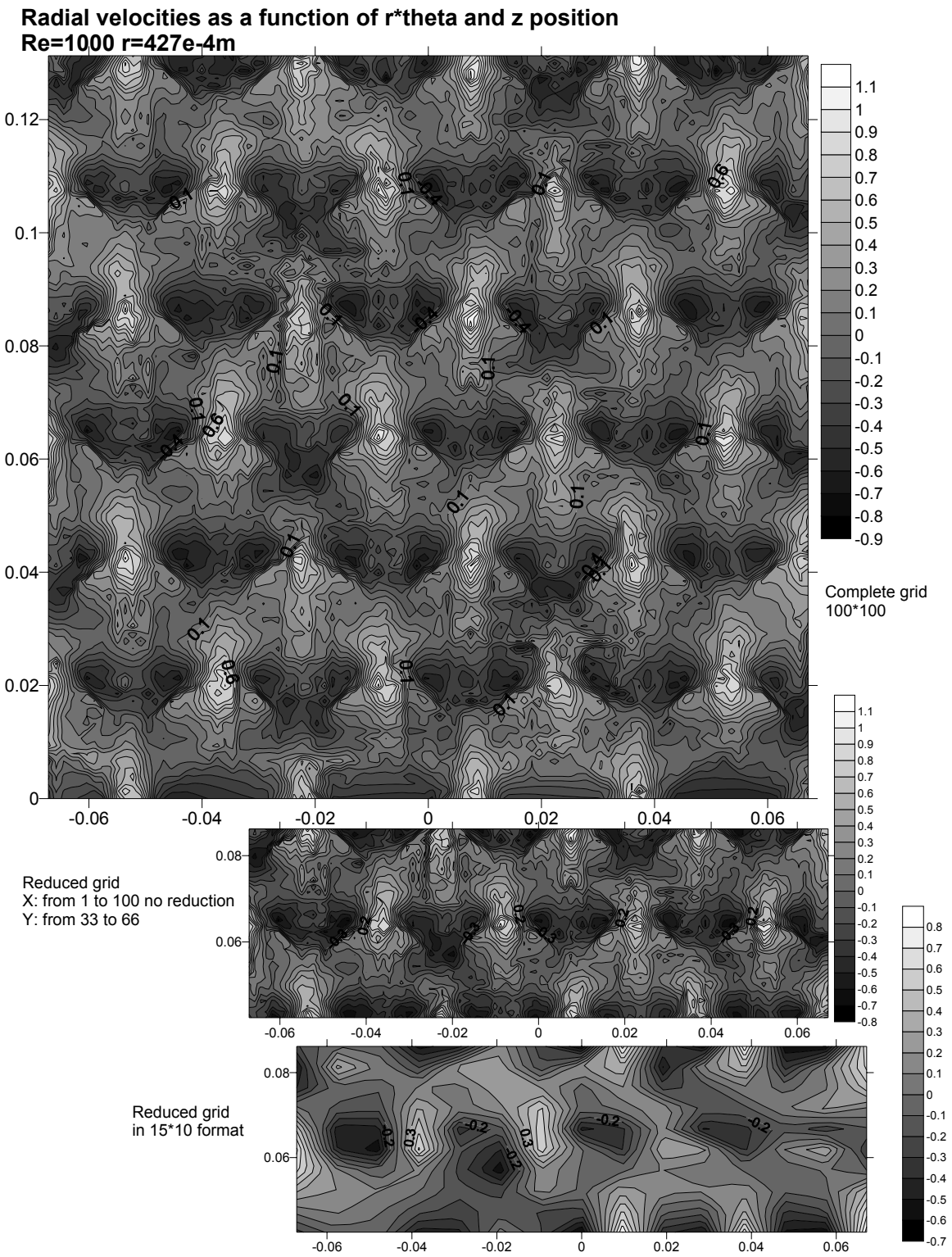

Figure 4.3: Map of radial velocities for a r=426e-4m plane

Maps have been plotted using Surfer Software.

When the complete map has been plotted, we divided into three parallel layers. Each layer corresponds to 2 layers of spheres. It can be done due to the periodicity of the flow through the fixed bed.

Then to reduce the number of points, we used a method included in the program to transform the grid into a coarser one. The interpolation method used is called 'Kriging method'. This method calculates numbers for the new grid in a linear approximation. This is acceptable considering the large amount of data available thanks to CFD (sometimes as huge as 300,000 point for one plane). Then the final number of points in the grid is deduced by 'trial and error' method to keep the same features of the complete grid. The aim of this is to get grids with a reasonable number of points to be easily exploitable.

In Appendix E, a procedure is available explaining all details to transform data into maps of acceptable size. In the same Appendix are also all 13 maps available like the one presented above.

Below are shown an example of radial velocities as a function of radial position for different axial positions.

The plots are directly the results of points extracted from the reduced maps. All the values shown below are in absolute value. Some of them are in reality negative. But for clarity sake, it has been chosen to plot them in absolute value. 4 profiles have been plotted corresponding to 4 different axial positions which are extracted in the first 2 layers of spherical catalyst particles. It is relevant to plot only that region because of the flow periodicity.

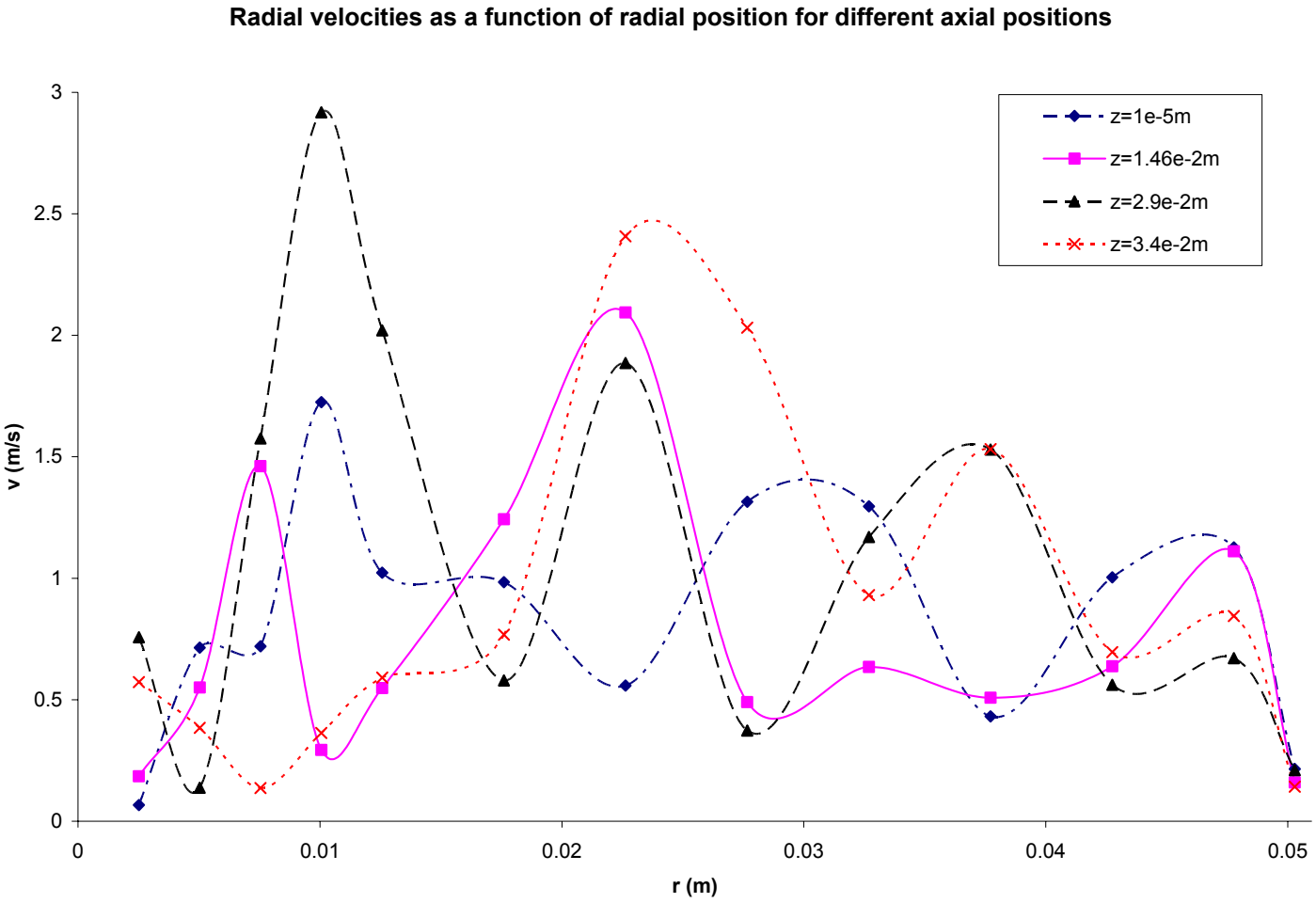

Figure 4.4: Radial velocity profile as a function of radial position for different axial positions

Some of the plots present the same features in terms of maxima and minima. A large range of velocities is observed. It clearly depends on the porosity at a specific axial position and the spheres packing. In some cases some low radial velocities correspond to presence of spheres, and maxima correspond to voidage in the spheres arrangement. Same as axial velocities, there is a drop near the wall due to the no-slip condition.

4.3. RESULTS

The first and logical way to extract velocities was to average all of them. For each given plane, extract all velocities at a same height and average them to give a value for a specific z at a constant radial position. This process is repeated for all planes of constant radius. Reduced planes have been used to extract averaged velocities.

Then a set of radial, axial velocities plus porosity profile is introduced into the Fortran program to solve the energy balance. Also one has to specify some constants in the program. For our case, the catalyst pellet conductivity is set to 0. The Biot number, defined here as:

$$Bi = Nu_w^* \frac{d_t / d_p}{2} \tag{48}$$

In our case, Nu_w^* is taken as 128.072 so

Bi=256.65

We also set that axial Peclet number is set to 2 so that

$$\frac{\mathrm{Re}\,\mathrm{Pr}}{k_a / k_f} = 2 \tag{49}$$

So in our conditions because Pr = 0.689 then we have

k_a/k_f is 344.815, and

the Reynolds number is set to Re = 1000.

With all these data the program can be correctly set.

Remark: the program has been modified from its original version. Matrices dimensions have been increased, so that we can insert up to 30 velocities for each radial position. It is also possible to have up to 30 radial positions. To improve the accuracy, the number of radial points has been increased. Otherwise some stability problem occurred during the calculations.

Then a set of radial temperature profiles are obtained depending on the axial position. So to account for heat transfer over the total length of the bed, an average of all radial profile is done. This is possible because all temperature profiles are evenly extracted along the bed.

Temperature profile is also extracted from the fixed bed corresponding to the same condition in Fluent.

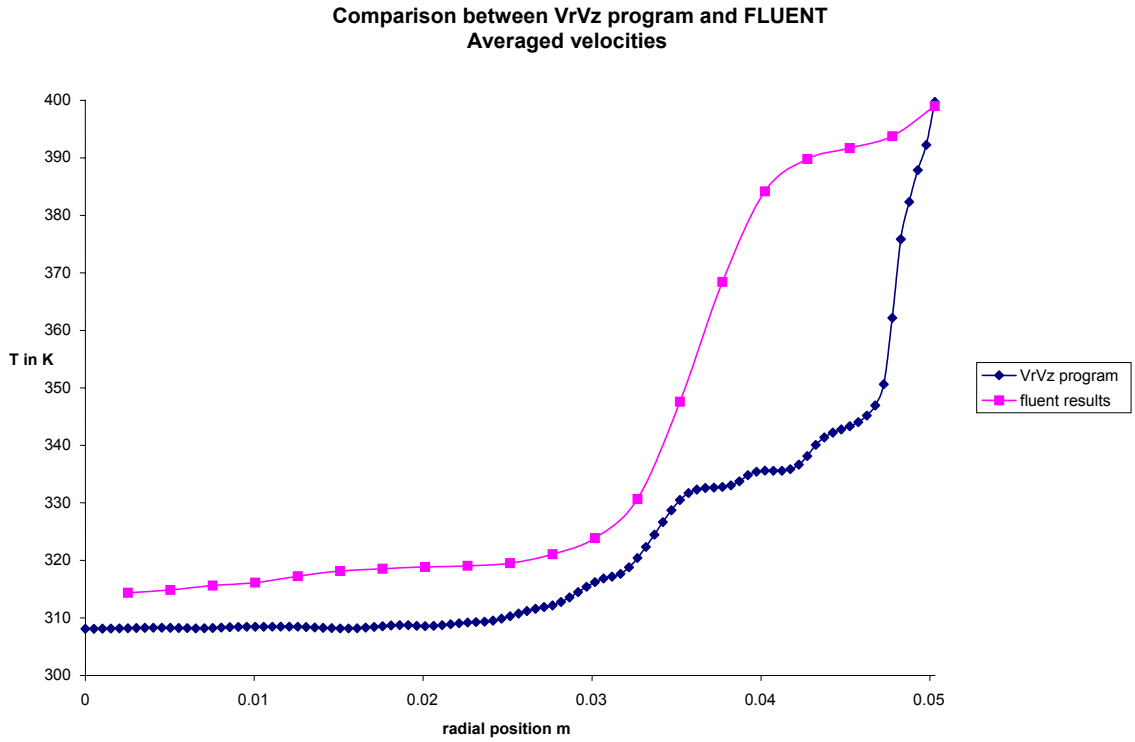

Figure 4.5: comparison between CFD temperature profile and VrVz program

As you can see, temperature profile calculated using the program is underestimated compared to CFD radial temperature profile. That may be explained by the fact that the velocities are averaged on the whole width of the map. Particle pellets are also present, which correspond to no velocities, turbulent convection is underestimated because of the spheres catalyst particles.

Another way to extract the velocities is to do it manually. Velocities maps are reduced to exploitable size. The idea is to scan for each map at the same axial positions all the values. Then only the highest absolute value is selected to be placed in the velocities table. Whatever the position, only the highest, either positive or negative is kept.

This method leads us to the following profile:

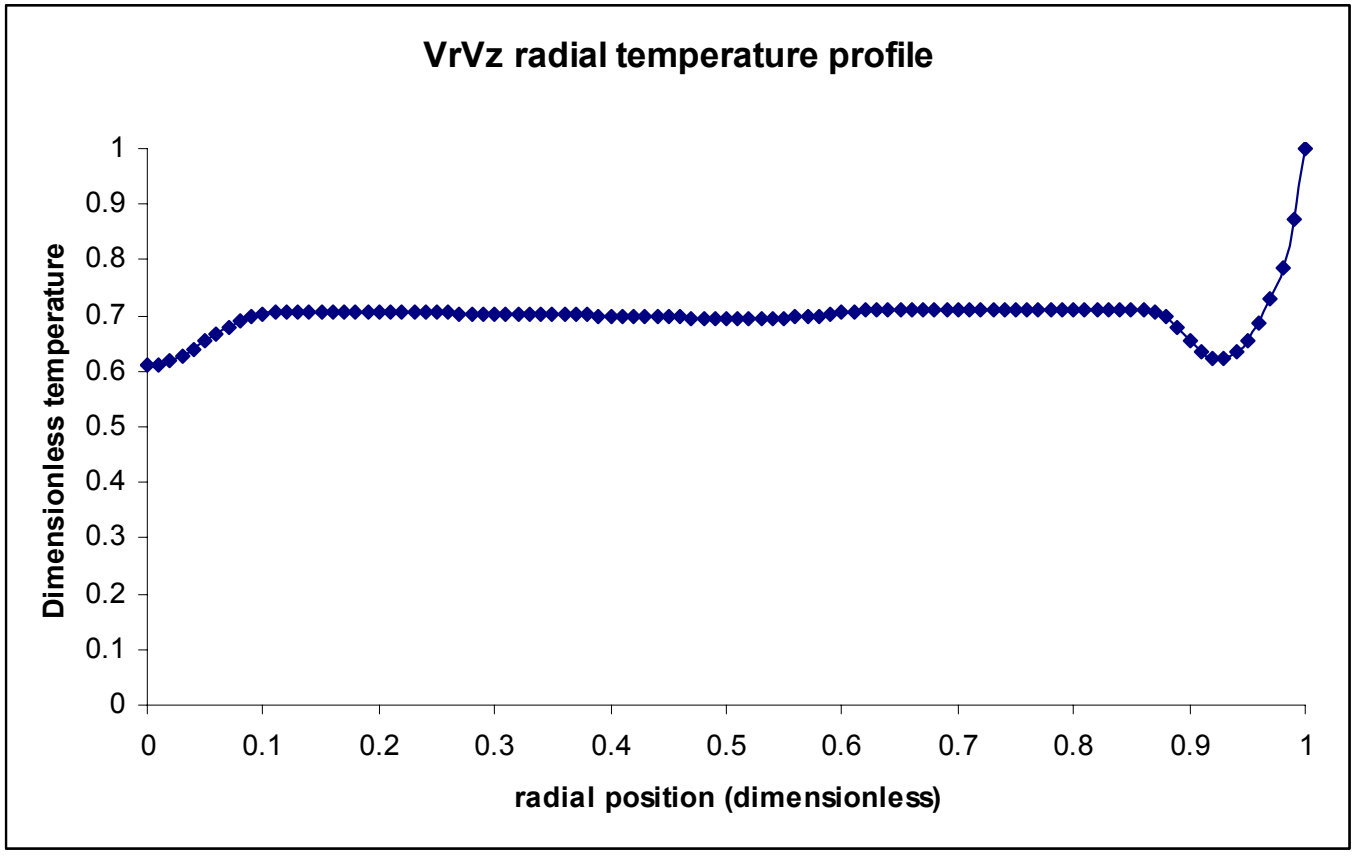

Figure 4.6: radial temperature profile using highest velocity-value method

Is it clear in that case that contrary to the first method, velocities seem to be overestimated. The temperature profile is flat and a clear gap is visible close to the wall. One of the quick fixes we tried is to use exactly the same velocity set, except the fact that all numerical values have been taken positive. Not drastic changes have been noticed for the radial temperature results.

The third idea was to smooth the profile a little bit. Velocities maps have special features: there are some 'holes' were the velocities are zero corresponding to the presence of spheres. Then the idea was to try to extract velocities around them, in the axial direction. The other idea is to capture velocities along a path where a fluid particle may probably go through. Then continuity is kept and velocities are extracted and then radial temperature profile is computed. The corresponding profile is given:

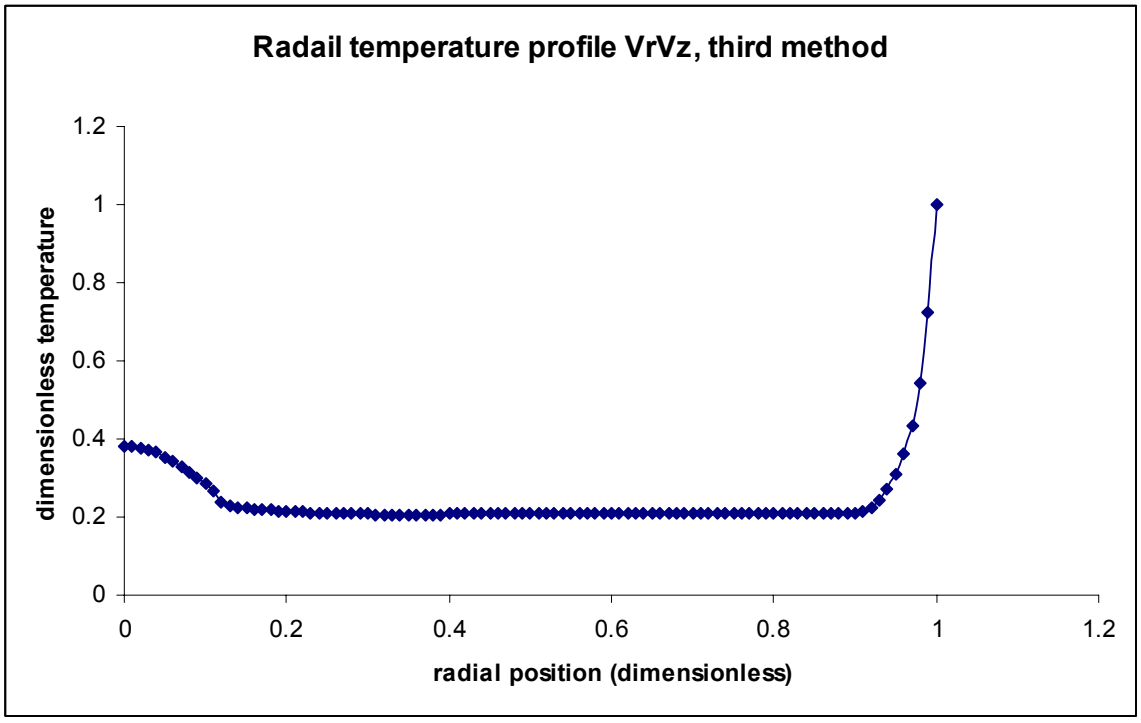

Figure 4.7: radial temperature profile using continuity method

This profile fits better the expectations. Similarly a temperature jump is present at the wall, phenomenon increased by the fact that there is no conduction, so no heat flux into catalyst particles. The temperature profile in the core of the bed is flat.

This continuity method seems to work pretty well.

One of the arising problems is the Fluent Post-Processing. For the Fluent radial temperature profile, there is no gap at the wall, which is clearly a problem. This phenomenon is mainly due to the fact that the mesh is very fine at the wall. So during the extraction, average facet temperature has been selected. Due to the fine meshing, hot cells close to the wall are much numerous than cold cells. Then the averaging is not well justified.

One of the points which can be improved is to select in the post processing: area-weighted-average. This may get rid of cell numbers problem because all cells are weighted depending on the surface of each one. It seems that our computers are not enough powerful to handle such option.

5. CONCLUSION

The CFD simulation is a perfect tool to investigate radial heat transfer in the near wall region. One of the crucial points is the near-wall region modeling. One part lies on the mesh density for accuracy reason. If a very fine mesh is used then accuracy will be guaranteed. But it is going to be computationally very expensive. So once an optimum mesh is defined, the other accuracy problem is in choosing the right method, especially a good one to solve wall bounded flow.

Two main methods are available; either to completely solve the viscous boundary layer using equation which are valid all way down to the wall: the near-wall approach. Or numerical variables may be bridged from the core of the bed to the wall, using semi-empirical equations, they are called wall functions. Three different wall functions are available. It seems that all methods give almost the same profile, depending on the geometries of beds.

The boundary conditions are one of the key to accuracy in CFD. It seems that the symmetric boundary condition may be powerful when the mesh is really symmetric. Otherwise deviations are noticed. The other important boundary condition is the viscous laminar layer at the wall. It seems that good agreements are found to model this layer. Especially all models take care of this heat transfer resistance, which corresponds pretty well to the available literature.

CFD helped us to understand physical heat transfer mechanisms in the fixed bed low N reactors. CFD enable us to conduct some simulations where there is no conduction through solid particles, which cannot be done in real experiments. Then convection may be isolated and studied separately. In that way it is possible to precisely measure the contributions of all physical mechanisms in the wall vicinity.

6. RECOMMENDATIONS

An immediate extension of the research presented could be to investigate the post processing for the CFD and get a more accurate radial temperature profile. Then it has to be compared to the results of the VrVz Fortran program results with the last set of velocities, obtained by continuity method. That will confirm the contribution due to convection in the bed.

Ideally, this has to be done for various Reynolds number to make sure that results are reliable for all kind of turbulent flow. It would means that we clearly defined the contribution of convection in low N fixed beds.

The next following step would be to rerun CFD simulation but this time with particles modeled, in other terms with conduction added to the bed. Then it will be possible to keep the same velocity set rerun the VrVz program with also conduction in it and compare CFD results to energy equations results.

This future work I hope would lead to a new way of model radial heat transfer in fixed beds: keeping h_w accounting for only the true viscous boundary layer, and model true convection and conduction as the same time.

Nomenclature

c_p = fluid heat capacity	[J/kgK]
d_t = tube diameter	[m]
d_p = particle diameter	[m]
G = mass flow rate	[kg/m2s]
h = heat transfer coefficient	[W/m2K]
h_w = wall heat transfer coefficient	[W/m2K]
k_f = fluid conductivity	[W/mK]
k_r = radial conductivity	[W/mK]
k_p = conductivity of the catalyst particles	[W/mK]
L = length of the heated bed	[m]
N = tube to particle ratio (d_t/d_p)	[-]
Nu_w = Nusselt number at the wall	[-]
P, p = static pressure	[Pa]
q = heat flux	[W/m2]
r = radial coordinate	[m]
R = tube radius	[m]
T = temperature	[K]
u = gas velocity	[m/s]

v = superficial gas velocity [m/s]

x = coordinate [m]

y = coordinate [m]

z = axial coordinate [m]

Greek Symbols

β = thermal expansion coefficient [K^{-1}]

ε = turbulence dissipation rate [J/s]

κ = turbulent kinetic energy [J]

μ = fluid viscosity [Ns/m^2]

θ = dimensionless temperature $(T-T_{in})/(T_{wall}-T_{in})$ [-]

ρ = fluid density [kg/m^3]

ψ = porosity profile [-]

Dimensionless flow numbers

Biot number $$Bi = Nu_w^* \frac{d_t / d_p}{2}$$

wall Nusselt number $$Nu_w = \frac{h_w d_p}{k_f}$$

Péclet number $$Pe = \frac{G c_p d_p}{k_f}$$

Prandtl number $$\mathrm{Pr} = \frac{c_p \mu}{k_f}$$

Reynolds number $$\mathrm{Re} = \frac{\rho v d_p}{\mu}$$

References

Bauer, R. (1983) Stagnant packed beds

Hemisphere Publishing Corporation, 2.8.1-1

Bauer, R. (1983) Packed bed with a gas flowing through.

Hemisphere Publishing Corporation, 2.8.2-1

Bode, J. (1994) Computational fluid dynamics applications in the chemical industry.

Computers & Chemical Engineering **18** SUPPL, S247-S251

Borkink, J. G. H. and Westerterp, K. R. (1993) Significance of the radial porosity profile for the description of Heat transport in Wall-cooled packed beds.

Chemical Engineering Science **49**, 863-876.

Coberly, C. A. and Marshall, W. R. JR. (1951) Temperature gradients in gas streams Flowing through fixed granular beds.

Chemical Engineering Progress **47** No. 3, 141-150

Derkx, O.R. (1995) Wall heat transfer coefficient in a fixed bed reactor. *M.S. Thesis* Worcester Polytechnic Institute.

Derkx, O.R. and Dixon, A.G. (1996) Determination of the fixed bed wall heat transfer coefficient using computational fluid dynamics. *Numerical Heat Transfer Part A* **29**, 777-794.

Freiwald, M.G. and Paterson, W.R. (1992) Accuracy of model predictions and reliability of experimental data for heat transfer in packed beds. *Chemical Engineering Science* **47**, 1545-1560.

Froment, G. and Bisschoff, K. (1979) *Chemical Reactor Analysis and Design.* Wiley, New York.

Gunn, D. J. Ahmad, N. M. and Sabri, M. N. (1987) Radial heat transfer to fixed bed of Particles *Chemical Engineering Science* **42**, 2163-2171

Kunii, D. and Suzuki, M. (1966) Heat transfer between wall surface and packed solid. *AIChE Journal* , 344-352.

Kunii, D. and Suzuki, M. (1968) Heat and mass transfer from wall surface to packed beds.
Journal of the faculty of Engineering, University of Tokyo(B) , Vol XXX, No. 1.

Launder, B. E. and Spalding D.B. (1974) The numerical computation of turbulent flow *Applied Mechanics Eng., **3**,269*

Lerou, J.J. and Froment, G.F. (1977) Velocity, temperature and conversion profiles in fixed bed catalytic reactors. *Chemical Engineering Science* **32**, 853-861.

Li, C.H. and Finlayson, B.A. (1977) Heat transfer in packed beds - a reevaluation. *Chemical Engineering Science* **32**, 1055-1066.

Logtenberg, S.A. (1997) Computational fluid dynamics studies of fixed bed heat transfer. *M.S. Thesis*, Worcester Polytechnic Institute.

Logtenberg, S.A. and Dixon, A.G. (1998a) Computational fluid dynamics studies of fixed bed heat transfer. *Chemical Engineering and Processing* **37**, 7-21.

Logtenberg, S.A. and Dixon, A.G. (1998b) Computational fluid dynamics studies of the effects of temperature-dependent physical properties on fixed-bed heat transfer. *Industrial and Engineering Chemistry Research* **37**, 739-747.

Logtenberg, S.A., Nijemeisland, M. and Dixon, A.G. (1999) Computational fluid dynamics simulations of fluid flow and heat transfer at the wall-particle contact points in a fixed bed reactor. *Chemical Engineering Science* **54**, 2433-2439.

Melanson, M.M. (1984) Solid phase radial heat transfer in stagnant packed beds for low tube to particle diameter ratios. *M.S. Thesis,* Worcester Polytechnic Institute.

Morales, M., Spinn, C.W. and Smith, J.M. (1951) Velocities and effective thermal conductivities in packed beds. *Industrial and Engineering Chemistry Research* **43**, 225-231.

Nijemeisland, M. (2000) Verification studies of computational fluid dynamics in fixed bed heat transfer. *M.S. Thesis* Worcester Polytechnic Institute.

Nijemeisland, M. (2003) Influences of catalyst particle geometry on fixed bed reactor near-wall heat transfer using CFD. *Ph.D. Thesis* Worcester Polytechnic Institute.

Papageorgiou, J.N. and Froment, G.F. (1995) Simulation models accounting for radial voidage profiles in fixed-bed reactors. *Chemical Engineering Science* **50**, 3043-3056.

Price, J. (1968) The distribution of fluid velocities for randomly packed beds of spheres. *Mech. Chem. Engng Trans.* **7**, 14.

Ranade, V.V. (1995) Computational fluid dynamics for reactor engineering. *Reviews in Chemical Engineering* **11**, 229.

Smirnov, E.I. Muzykantov, A.V. Kuzmin, V. A. Kronberg, I.A. Zolotarskii, I.. A. Radial heat transfer in packed beds of spheres, cylinders and Rashig rings. Verification Of model with a linear variation of λ_{er} in the vicinity of the wall
Chemical Engineering **91**, 243-248.

Thompson, K.E. and Fogler, H.S. (1997) Modeling flow in disordered packed beds from pore-scale fluid mechanics. *AIChE Journal* **43**, 1377-1389.

Tobis, J. and Ziòlkowski, D. (1988) Modelling of heat transfer at the wall of a packed Bed apparatus.
Chemical Engineering Science **43**, 3031-3036.

Tsotsas, E. and Schlünder, E.-U. (1990) Heat transfer in packed beds with fluid flow: remarks on the meaning and the calculation of a heat transfer coefficient at the wall. *Chemical Engineering Science* **45**, 819-837.

Vortmeyer, D. and Haidegger, E. (1991) Discrimination of three approaches to evaluate heat fluxes for wall-cooled fixed bed chemical reactors. *Chemical Engineering Science* **46**, 2651-2660.

Winterberg, M. Tsotsas, E. Krischke, A. and Vortmeyer, D. (1999) A simple and Coherent set of coefficients for modeling of heat and mass transport with and without Chemical reaction in tubes filled with spheres.
Chemical Engineering Science **55**, 967-979.

Yagi, S. Kunii, D. (1961) Studies on heat transfer in Packed Beds
AICHE Journal 750-759

Ziòlkowska, I. and Ziòlkowski, D. (1993) Modeling of gas interstitial velocity radial distribution over a cross-section of a tube packed with a granular catalyst bed.
Chemical Engineering Science **48**, 3283-3292.

Appendices

APPENDIX A

Reynolds number calculation

General calculation

Consider: R = radius of the tube (m)

Re_p = particle Reynolds number (dimensionless)

u_s = superficial mean velocity of the fluid (m/s)

d_p = particle diameter (m)

μ = viscosity of the fluid (Ns/m^2)

ρ = density of the fluid (kg/m^3)

m_s = superficial mean mass flowrate (kg/s)

A_s = superficial area of the cross section of the tube

By definition, Reynolds number is defined as:

$$Re_p = \frac{\rho u_s d_p}{\mu} \tag{50}$$

Fluent usually needs to set the flow the mean velocity of the fluid. But here the periodic condition applies, which means that Fluent needs the mean mass velocity to set the flow. From (1) it is easy to deduce the mean velocity knowing the Reynolds number:

$$u_s = \frac{Re_p \mu}{\rho d_p} \tag{51}$$

The mean mass flowrate is defined as:

$$m_s = \rho u_s A_s \tag{52}$$

where

$$A_s = \pi R^2 \tag{53}$$

so

$$m_s = \frac{\mathrm{Re}_p \mu \pi R^2}{d_p} \tag{54}$$

The fluid considered here is air. The properties of air are assumed constant in the simulation. For accuracy purpose, air properties have been taken at 400K (127°C). the values are shown below:

$\mu = 2.267 \cdot 10^{-5}$ Ns/m^2
$k = 3.33 \cdot 10^{-2}$ W/mK
$\rho = 0.875$ kg/m^3
$C_p = 1.013$ kJ/kgK

The tube radius is very close to 2inches (0.050292m). The meshing was done such as the tube-to-particle diameter ratio was close to N = 4. Spheres are 0.025135m diameter.

To calculate the cylinder 'diameter', one has to consider a virtual sphere of the same volume as the cylinders: for pellets of 1inch diameter and 1inch length:

The corresponding volume is:

$$V_c = \frac{\pi d_p^2}{4} \cdot L \tag{55}$$

So $V_c = 1.287 * 10^{-5}$ m^3

Considering now the virtual sphere of the same volume:

$$V_c = \frac{4}{3}\pi R^3 \tag{56}$$

The corresponding diameter is :

$R = 1.454*10^{-2}m$
$d_p = 2.907*10^{-2}m$

This leads to the following values for spheres ($d_p = 2.5135*10^{-2}m$):

Reynolds number	u_s (m/s)	m_s (kg/s)
1349	1.391E+00	9.668E-03
1117	1.151E+00	8.005E-03
1000	1.031E+00	7.167E-03
872	8.988E-01	6.249E-03
589	6.071E-01	4.221E-03
359	3.700E-01	2.573E-03
100	1.031E-01	7.167E-04
10	1.031E-02	7.167E-05
1	1.031E-03	7.167E-06

Table of Reynolds number using air properties at 400K

For cylinders ($d_p = 2.907*10^{-2}$m):

Reynolds number	u_s (m/s)	m_s (kg/s)
1349	1.202E+00	8.359E-03
1117	9.955E-01	6.922E-03
1000	8.912E-01	6.197E-03
872	7.772E-01	5.403E-03
589	5.249E-01	3.650E-03
359	3.200E-01	2.225E-03
100	8.912E-02	6.197E-04
10	8.912E-03	6.197E-05
1	8.912E-04	6.197E-06

Table of Reynolds number using air properties at 400K

APPENDIX B

Plots of the radial temperature profile difference between whole segment average and second and third quarters average.

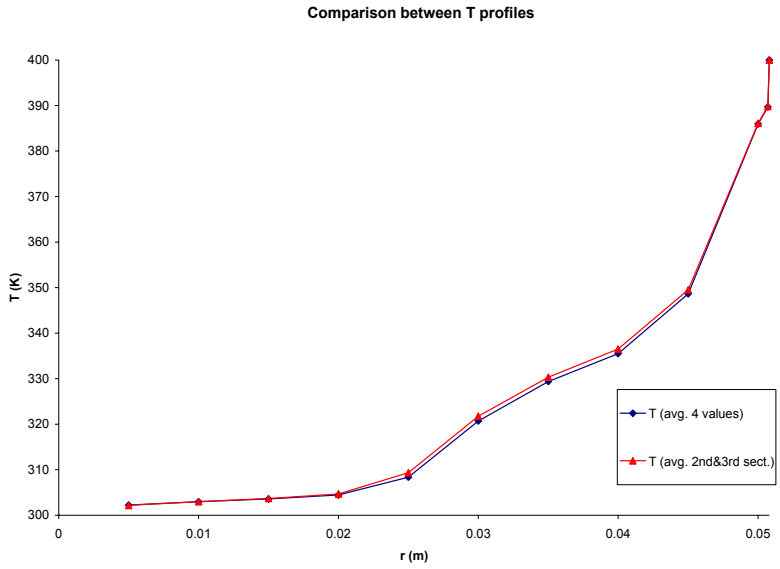

Figure B.1: Radial temperature profile for spheres, κ-ω approach, Re = 788.4

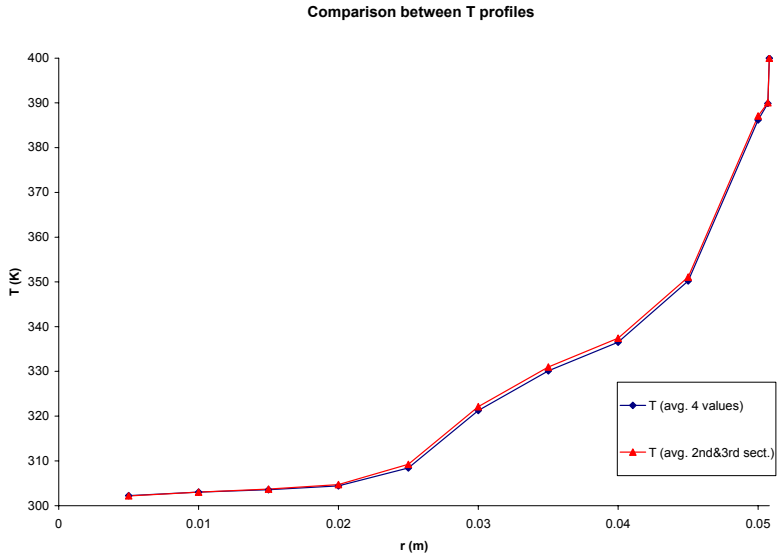

Figure B.2: Radial temperature profile for spheres, κ-ε approach, standard wall functions Re = 788.4

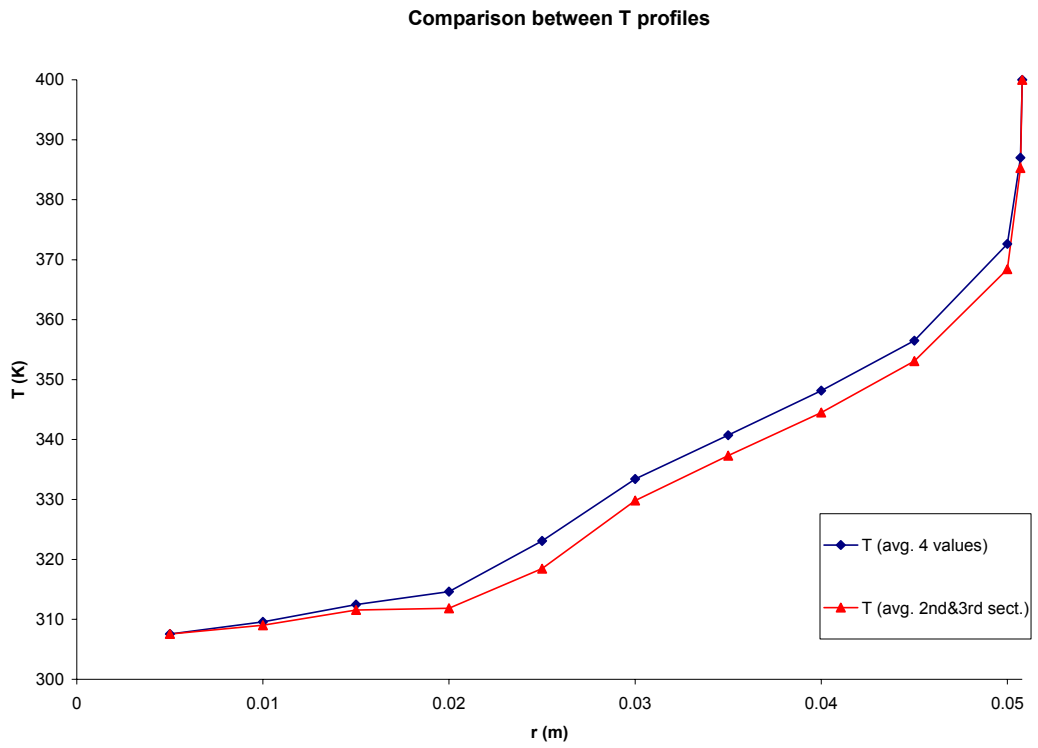

Figure B.3: Radial temperature profile for full cylinders, κ-ω approach, Re = 789.2

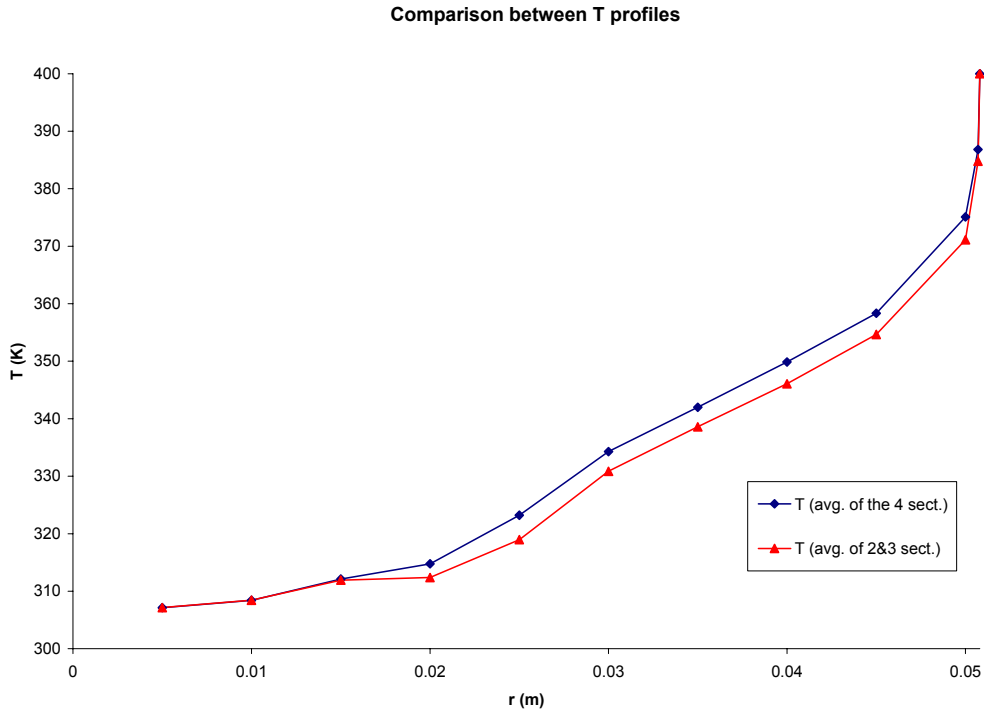

Figure B.4: Radial temperature profile for full cylinders, κ-ε approach, standard wall functions Re = 789.2

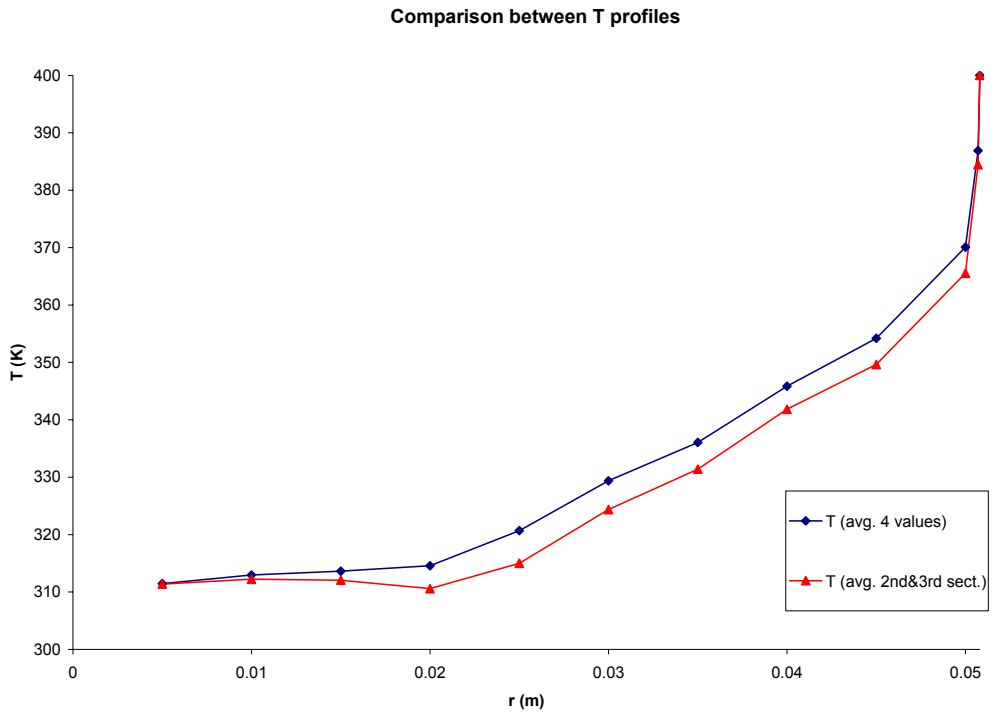

Figure B.5: Radial temperature profile for 1-hole cylinders, κ-ω approach, Re = 789.2

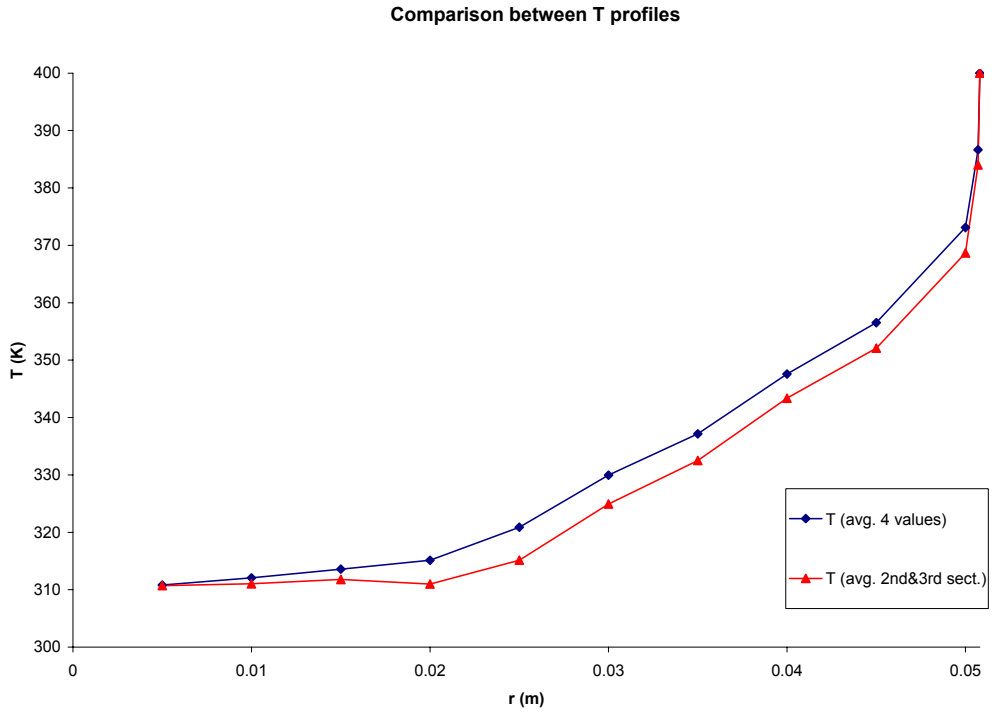

Figure B.6: Radial temperature profile for 1-hole cylinders, κ-ε approach, standard wall functions Re = 789.2

APPENDIX C

Porosity profile calculation

Porosity profile is extracted using CFD as follows:

20 planes of constant radius are defined all into the bed, at a constant distance. The surface of the fluid is then extracted from the Surface integrals menu, and these values are divided by the overall surface of each plane calculated easily knowing the radius and the height of the fixed bed. So the porosity profile is extracted as a function of the radius, average over the entire length of the bed (z = 0.13m) corresponding to 6 layers of spheres.

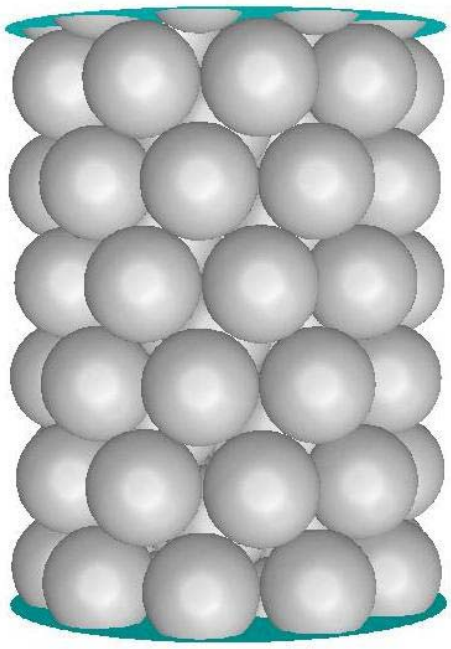

N=4, 6 layers of spheres

Here are the data extracted from Fluent:

plan #	R=cst (m)	Total Surface (m^2)	Fluid surface (m^2)	Porosity
1	9.8502E-05	8.1248E-05	NA	NA
2	2.5146E-03	2.0741E-03	0.001834551	0.88
3	5.0292E-03	4.1483E-03	0.001937815	0.47
4	7.5438E-03	6.2224E-03	0.001740963	0.28
5	1.0058E-02	8.2966E-03	0.001703966	0.21
6	1.2573E-02	1.0371E-02	0.002117124	0.20
7	1.5088E-02	1.2445E-02	NA	NA
8	1.7602E-02	1.4519E-02	0.005105611	0.35
9	2.0117E-02	1.6593E-02	0.007994453	0.48
10	2.2631E-02	1.8667E-02	0.011981621	0.64
11	2.5146E-02	2.0741E-02	0.016362028	0.79
12	2.7661E-02	2.2816E-02	0.013799095	0.60
13	3.0175E-02	2.4890E-02	0.008893156	0.36
14	3.2690E-02	2.6964E-02	0.005475677	0.20
15	3.5204E-02	2.9038E-02	0.003813656	0.13
16	3.7719E-02	3.1112E-02	0.004145071	0.13
17	4.0234E-02	3.3186E-02	0.006690094	0.20
18	4.2748E-02	3.5260E-02	0.011645934	0.33
19	4.5263E-02	3.7335E-02	0.019203814	0.51

20	4.7777E-02	3.9409E-02	0.029521005	0.75
21	5.0292E-02	4.1483E-02	0.001812764	1.00

Table C.1: porosity data as a function of radial position

The corresponding profile is shown below, for a radius value of 0.052:

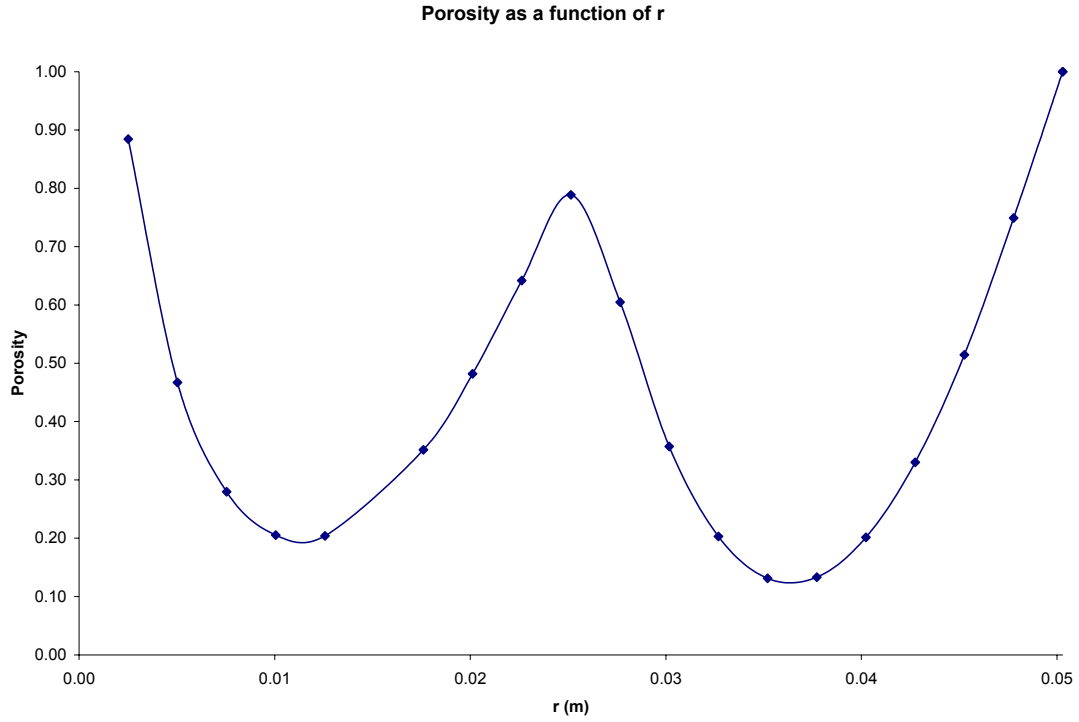

Figure C.1: porosity profile as a function of radial position

APPENDIX D

Copy of the Fortran code used to solve the energy equation (chapter 4).

```
C     ************************************************************************
C     ***************************** VRVZ.FOR *********************************
C     ************************************************************************
C     * MODEL WITH VELOCITIES FROM CFD. SOLVED USING CUBIC HERMITE SPLINE    *
C     * COLLOCATION. DATA ARRAYS INTERPOLATED BY B-SPLINES                   *
C     ************************************************************************

      USE MSIMSLMS

C     NDAT IS THE MAXIMUM NUMBER OF DATA POINTS IN THE DATA FILE. IF MORE
C       ARE NEEDED IT MUST BE INCREASED. NNDAT IS NDAT^2.
      PARAMETER (NDAT=30,NNDAT=900)

      REAL(4) KSKF,KAKF
      CHARACTER*11 FNAME

C     ARRAYS TO HOLD THE DATA AND DIMENSIONLESS DATA
      DIMENSION EDAT(NDAT),VTDAT(NDAT),VYDAT(NDAT,NDAT)
      DIMENSION ERDAT(NDAT),ZDAT(NDAT),RDAT(NDAT),VZDAT(NDAT),
     &          VRDAT(NDAT,NDAT)

C     BREAKPOINT ARRAYS FOR NUMERICAL METHOD
      DIMENSION YB(101),TB(21)

C     ARRAYS FOR THE DIMENSIONLESS TEMPERATURE SOLUTION AND ITS LOCATION
      DIMENSION U(200,10),Y(200),T(10)

      COMMON/DAT/NYDAT,NTDAT,YDAT(NDAT),TDAT(NDAT),ECOEFF(NDAT),
     &          VTCOEFF(NDAT),VYCOEFF(NNDAT),YKNOT(35),TKNOT(35)
      COMMON/PARAMS/RE,PR,DTDP,KSKF,KAKF,BIOT

      DATA TB /-1.0,-0.1,-0.05,-0.025,0.0,0.025,0.05,0.075,0.1,0.125,
     &         0.15,0.175,0.2,0.25,0.3,0.35,0.4,0.5,0.6,0.8,1.0/

      WRITE(6,*) 'GIVE DATA FILE NAME:'
```

```
      READ(5,100) FNAME
100   FORMAT(A11)

      OPEN(UNIT=20,FILE=FNAME,STATUS='UNKNOWN')

        READ(20,*) NRDAT,NZDAT
      READ(20,*) DT,DP,VZAV
      DTDP=DT/DP

      READ(20,*) (ZDAT(I),I=1,NZDAT)
      DO I=1,NRDAT
       READ(20,*) RDAT(I),ERDAT(I),VZDAT(I),(VRDAT(I,J),J=1,NZDAT)
      END DO

        CLOSE(20)
      SCALE=5.375

C     SET CONSTANTS FOR THESE RUNS
      RE=1000.0
      PR=0.6896
C     ks/kf IS THE TRUE SOLID/FLUID THERMAL CONDUCTIVITY RATIO
      KSKF=0.0
C     ka/kf IS THE EXPERIMENTALLY-DETERMINED VALUE
      KAKF=344.815
C     NEED A CORRELATION FOR BIOT NUMBER
        BIOT=256.65

C     MAKE INPUT QUANTITIES DIMENSIONLESS & SET UP FOR INTERPOLATION
      NYDAT=NRDAT+2
      NTDAT=NZDAT+1
      YDAT(NRDAT+2)=1.0
      EDAT(NRDAT+2)=1.0
      VTDAT(NRDAT+2)=0.0
      DO I=2,NRDAT+1
       EDAT(I)=ERDAT(I-1)
       YDAT(I)=RDAT(I-1)/DT*2
       VTDAT(I)=VZDAT(I-1)/VZAV
      END DO
      YDAT(1)=0.0
      EDAT(1)=EDAT(2)
      VTDAT(1)=VTDAT(2)
```

```
      DO J=2,NZDAT+1
       TDAT(J)=TANH(ZDAT(J-1)/DT*2/SCALE)
       DO I=2,NRDAT+1
        VYDAT(I,J)=VRDAT(I-1,J-1)/VZAV
         END DO
        END DO
      TDAT(1)=0.0
      DO I=2,NRDAT+1
       VYDAT(I,1)=VYDAT(I,NZDAT+1)
        END DO
      DO J=1,NZDAT+1
       VYDAT(1,J)=VYDAT(2,J)
       VYDAT(NRDAT+2,J)=0.0
      END DO

C       INTERPOLATE DATA
      CALL BSNAK(NYDAT,YDAT,3,YKNOT)
      CALL BSNAK(NTDAT,TDAT,3,TKNOT)
      CALL BS2IN(NYDAT,YDAT,NTDAT,TDAT,VYDAT,NDAT,3,3,
     1          YKNOT,TKNOT,VYCOEFF)
      CALL BSINT(NYDAT,YDAT,EDAT,3,YKNOT,ECOEFF)
      CALL BSINT(NYDAT,YDAT,VTDAT,3,YKNOT,VTCOEFF)

C     PLACEMENT OF RADIAL BREAKPOINTS          initials: 1 to 13 -> 0.93 and 13 to 21 -> 1
      YB(1)=0.0
      YB(101)=1.0
      YB(51)=0.85
      DO I=1,49
       YB(I+51)=YB(51)+(YB(101)-YB(51))/50.0*FLOAT(I)
        END DO
      DO I=1,49
       YB(I+1)=YB(51)*FLOAT(I)/50.0
        END DO


C     SPECIFY DESIRED RADIAL OUTPUT POINTS
      NY=101
      DO I=1,NY
       Y(I)=FLOAT(I-1)/(NY-1)
      END DO
```

```
C     AXIAL OUTPUTS AT L = 2", 4", 6", 8", 10"
C     X=L/R WHERE R = 1.388" FOR OUR EXPERIMENTAL COLUMN
C       Here L is in cm => I modified the units of R so X dimensionless
      NT=10
      DO I=1,NT
C         X=(FLOAT(I)*2.0)/1.388
          X=(FLOAT(I)*1.3)/5.03
         T(I)=TANH(X/SCALE)
          END DO

C     MAIN SUBROUTINE CALL before: (20,20,....)
      CALL E5SCO(100,20,YB,TB,SCALE,NY,Y,NT,T,U)

C     PRINT RESULTS IN DIMENSIONLESS FORM (ACCESS='APPEND' removed)
      OPEN(UNIT=20,FILE='RESULTS.DAT',STATUS='UNKNOWN')
          DO J=1,NT
         DO I=1,NY
          WRITE(20,102) Y(I),U(I,J)
            END DO
          END DO
          CLOSE(20)

102   FORMAT(8F10.4)
      END



C     ******************************************************************
C     ************* MAIN EQUATION SOLVER *******************************
C     ******************************************************************
      SUBROUTINE E5SCO(N,M,YB,TB,SCALE,NY,Y,NTT,T,U)
      REAL KSKF,KAKF
C       DIMENSION A(1764,95),XM(1764,46),IP(1764),B(1764)
      DIMENSION A(8484,415),XM(8484,208),IP(8484),B(8484)
      DIMENSION YB(101),TB(101),G(2),Y(NY),U(200,10),T(NTT)
      DIMENSION VI1(2,4),VI2(2,4),VI3(2,4),VY(4,16),VYY(4,16),VT(4,16)
      DIMENSION VA(4),VB(4),VC(16),VJ1(2,4),VJ2(2,4),VJ3(2,4)
      DIMENSION VTT(4,16)
      COMMON/PARAMS/RE,PR,DTDP,KSKF,KAKF,BIOT

      ND=8484
      MD=415
```

```
      M1D=208
      G(1)=(1-1/SQRT(3.0))/2
      G(2)=1-G(1)
      N1=N+1
      NT=4*N1*(M+1)
      MT=4*N+15
      M1=2*N+6
      MP=M1+1
      NV2=2*N

C     INITIALIZE MATRIX TO ZERO
      DO I=1,NT
       B(I)=0.0
       DO J=1,MT
        A(I,J)=0.0
         END DO
       END DO

C     SET UP MODEL EQUATIONS
      N4=4*N+4
      N2=2*N+3
      A(1,MP+3)=1.0
      DO I=1,N1
       I2=2*I
       A(I2,I2-3+MP)=1.0
       A(I2+1,I2-3+MP)=1.0
      END DO
      DO J=1,M
       HJ=TB(J+1)-TB(J)
       CALL BSWTS(0,HJ,VJ1)
       CALL BSWTS(1,HJ,VJ2)
       CALL BSWTS(2,HJ,VJ3)
       DO I=1,N
        HI=YB(I+1)-YB(I)
        CALL BSWTS(0,HI,VI1)
        CALL BSWTS(1,HI,VI2)
        CALL BSWTS(2,HI,VI3)
        CALL PDWTS(VI2,VJ1,VY)
        CALL PDWTS(VI3,VJ1,VYY)
        CALL PDWTS(VI1,VJ2,VT)
        CALL PDWTS(VI1,VJ3,VTT)
```

```
      IR=N2+(J-1)*N4+4*(I-1)
      DO K=1,2
       TJV=TB(J)+HJ*G(K)
       TJVF=(1.0-TJV**2)/SCALE
       DO L=1,2
        KK=2*(K-1)+L
        IV=2*(I-1)+L
        YIU=YB(I)+HI*G(L)
        ALPHA=RE*PR*DTDP/2.0
        CALL EPS(YIU,E,DEDY)
        BETA=E+(1-E)*KSKF
        GAMMA=(1-KSKF)*DEDY
        DELTA=KAKF*TJVF
        IR=IR+1
        IC=4*(I-1)+(J-1)*N4
        DO LL=1,2
         IC=IC+(LL-1)*(4*N-4)
         DO LC=1,8
          IC=IC+1
          L1=LC+8*(LL-1)
          ICOL=IC-IR+MP
          A1=ALPHA*UR(YIU,TJV)*VY(KK,L1)
          A2=ALPHA*UZ(YIU)*TJVF*VT(KK,L1)
          A3=BETA*(VYY(KK,L1)+VY(KK,L1)/YIU)
          A4=GAMMA*VY(KK,L1)
          A5=DELTA*(TJVF*VTT(KK,L1)-2.0*TJV/SCALE*VT(KK,L1))
          A(IR,ICOL)=A1+A2-A3-A4-A5
           END DO
          END DO
         END DO
        END DO
      END DO
      DO K=1,2
       IR=IR+1
       TJV=TB(J)+HJ*G(K)
       IF (TJV.GT.0.0) B(IR)=BIOT
       IF (ABS(TJV).LT.1.0E-9) B(IR)=0.5*BIOT
       DO KK=1,2
        IC=(J+KK-1)*N4-4-IR+MP
        L=2*(KK-1)+1
        A(IR,IC+1)=VJ1(K,L)*BIOT
```

```
          A(IR,IC+2)=0.0
          A(IR,IC+4)=0.0
          A(IR,IC+3)=VJ1(K,L+1)*BIOT
            END DO
          END DO
        IF (J.LT.M) THEN
          A(IR+1,7)=1.0
          A(IR+2,8)=1.0
           END IF
      END DO
      A(NT+1-N2,9)=1.0
      DO I=1,N1
       I2=NT-N2+2+2*(I-1)
       J2=NT-N4+1+4*(I-1)
       A(I2,J2-I2+MP)=1.0
       B(I2)=1.0
       A(I2+1,J2-I2+MP)=1.0
        END DO

C     SOLVE MODEL EQUATIONS
      CALL BNDLU(ND,NT,MD,MT,M1D,M1,A,XM,IP,IV,IFAIL)
      IF (IFAIL.EQ.1) GOTO 200
      CALL BNDSO(ND,NT,MD,MT,M1D,M1,A,XM,IP,B)

C     INTERPOLATE FOR SOLUTION
      DO I=1,NTT
       DO J=1,M
        IF (T(I).GE.TB(J) .AND. T(I).LE.TB(J+1)) KT=J
       END DO
       CALL INWTS(0,T(I),TB(KT),TB(KT+1),VB)
       DO J=1,NY
        DO K=1,N
         IF (Y(J).GE.YB(K).AND.Y(J).LE.YB(K+1)) KR=K
           END DO
        CALL INWTS(0,Y(J),YB(KR),YB(KR+1),VA)
        CALL OPROD(VA,VB,VC)
        U(J,I)=0.0
        IC=(KT-1)*N4+4*(KR-1)
        DO L=1,2
         IC=IC+(L-1)*(4*N-4)
         DO LL=1,8
```

```
            IC=IC+1
            L1=LL+8*(L-1)
            U(J,I)=U(J,I)+VC(L1)*B(IC)
              END DO
             END DO
           END DO
         END DO
      RETURN
200   WRITE(6,104) IV
104   FORMAT(' IFAIL EQUALS ONE',I6)

999   STOP
      END



C     ****************************************************************
C     ************* VOID FRACTION MODEL ******************************
C     ****************************************************************
      SUBROUTINE EPS(Y,E,DEDY)
      COMMON/DAT/NYDAT,NTDAT,YDAT(30),TDAT(30),ECOEFF(30),VTCOEFF(30),
     1         VYCOEFF(900),YKNOT(35),TKNOT(35)

         E=BSVAL(Y,3,YKNOT,NYDAT,ECOEFF)
      DEDY=BSDER(1,Y,3,YKNOT,NYDAT,ECOEFF)

         RETURN
      END

C     ****************************************************************
C     *********** VELOCITY PROFILE SUBROUTINES ***********************
C     ****************************************************************
      REAL FUNCTION UZ(Y)
      COMMON/DAT/NYDAT,NTDAT,YDAT(30),TDAT(30),ECOEFF(30),VTCOEFF(30),
     1         VYCOEFF(900),YKNOT(35),TKNOT(35)

         U=BSVAL(Y,3,YKNOT,NYDAT,VTCOEFF)
      UZ=U

         RETURN
      END
```

```
C     ************************************************************
      REAL FUNCTION UR(Y,T)
      COMMON/DAT/NYDAT,NTDAT,YDAT(30),TDAT(30),ECOEFF(30),VTCOEFF(30),
     1         VYCOEFF(900),YKNOT(35),TKNOT(35)

         TINT=T

      DO WHILE (TINT .GT. TDAT(NTDAT))
       TINT=TINT-TDAT(NTDAT)
      END DO
      DO WHILE (TINT .LT. TDAT(1))
       TINT=TINT+TDAT(NTDAT)
      END DO

      U=BS2VL(Y,TINT,3,3,YKNOT,TKNOT,NYDAT,NTDAT,VYCOEFF)
      UR=U

         RETURN
      END

**********************************************************************
****************************** BSWTS *********************************
**********************************************************************
      SUBROUTINE BSWTS(ID,H,V)
      DIMENSION V(2,4)
      S3=SQRT(3.0)
      IF (ID-1) 1,2,3
1     V(1,1)=0.5+2.0/(3.0*S3)
      V(1,3)=1.0-V(1,1)
      V(1,2)=(1.0+1.0/S3)/12*H
      V(1,4)=(1.0/S3-1.0)/12*H
      GOTO 4
2     V(1,1)=-1.0/H
      V(1,3)=-V(1,1)
      V(1,2)=0.5/S3
      V(1,4)=-V(1,2)
      GOTO 4
3     V(1,1)=-2.0*S3/(H**2)
      V(1,3)=-V(1,1)
      V(1,2)=-(1.0+S3)/H
      V(1,4)=(1.0-S3)/H
```

```
4     J=(-1)**(ID+1)
      V(2,2)=J*V(1,4)
      V(2,4)=J*V(1,2)
      V(2,3)=-J*V(1,1)
      V(2,1)=-J*V(1,3)
      RETURN
      END
```

```
**********************************************************************
****************************** INWTS *********************************
**********************************************************************
      SUBROUTINE INWTS(ID,X,XI,XJ,VECT)
      DIMENSION VECT(4)
      H=XJ-XI
      Z=(X-XI)/H
      Y=(X-XJ)/H
      IF (ID-1) 1,2,3
1     VECT(3)=(3-2*Z)*Z**2
      VECT(1)=1-VECT(3)
      VECT(4)=H*Y*Z**2
      VECT(2)=H*Z*Y**2
      GO TO 5
2     VECT(1)=6/H*(Z**2-Z)
      VECT(3)=-VECT(1)
      VECT(4)=Z**2+2*Z*Y
      VECT(2)=2*Z*Y+Y**2
      GOTO 5
3     VECT(1)=6/H**2*(2*Z-1)
      VECT(3)=-VECT(1)
      VECT(2)=(2*Z+4*Y)/H
      VECT(4)=(4*Z+2*Y)/H
5     RETURN
      END
```

```
**********************************************************************
****************************** OPROD *********************************
**********************************************************************
      SUBROUTINE OPROD(VA,VB,V)
      DIMENSION VA(4),VB(4),V(16)
```

```
      JJ=1
      DO 10 J=1,2
      DO 10 I=1,2
      K=2*(I-1)+1
      L=2*(J-1)+1
      V(JJ)=VA(K)*VB(L)
      V(JJ+1)=VA(K+1)*VB(L)
      V(JJ+2)=VA(K)*VB(L+1)
      V(JJ+3)=VA(K+1)*VB(L+1)
10    JJ=JJ+4
      RETURN
      END



**********************************************************************
****************************** PDWTS *********************************
**********************************************************************
      SUBROUTINE PDWTS(V1,V2,V)
      DIMENSION V1(2,4),V2(2,4),V(4,16),VA(4),VB(4),VV(16)
      IPT=0
      DO 10 J=1,2
      DO 10 I=1,2
      IPT=IPT+1
      DO 15 K=1,4
      VA(K)=V1(I,K)
15    VB(K)=V2(J,K)
      CALL OPROD(VA,VB,VV)
      DO 10 K=1,16
10    V(IPT,K)=VV(K)
      RETURN
      END



**********************************************************************
****************************** BNDLU *********************************
**********************************************************************
      SUBROUTINE BNDLU(ND,N,MTD,MT,M1D,M1,A,XM,IP,IV,IFAIL)
      DIMENSION IP(ND),A(ND,MTD),XM(ND,M1D)
      IFAIL=0
      L=M1
      DO 30 I=1,M1
```

```
      IJ=M1+2-I
      DO 25 J=IJ,MT
25    A(I,J-L)=A(I,J)
      L=L-1
      JL=MT-L
      DO 30 J=JL,MT
30    A(I,J)=0
      L=M1
      DO 100 K=1,N
      X=A(K,1)
      I=K
      IF (L.LT.N) L=L+1
      IF (K+1.GT.L) GO TO 40
      IK=K+1
      DO 35 J=IK,L
      IF (ABS(A(J,1)).LE.ABS(X)) GO TO 35
      X=A(J,1)
      I=J
35    CONTINUE
40    IP(K)=I
      IF (X.NE.0) GO TO 50
      IFAIL=1
      IV=K
      RETURN
50    IF (I.EQ.K) GO TO 70
      DO 65 J=1,MT
      X=A(K,J)
      A(K,J)=A(I,J)
65    A(I,J)=X
70    IF (K+1.GT.L) GO TO 100
      IK=K+1
      DO 90 I=IK,L
      XM(K,I-K)=A(I,1)/A(K,1)
      X=XM(K,I-K)
      DO 80 J=2,MT
80    A(I,J-1)=A(I,J)-X*A(K,J)
90    A(I,MT)=0
100   CONTINUE
      RETURN
      END
```

```
**********************************************************************
******************************** BNDSO ********************************
**********************************************************************
      SUBROUTINE BNDSO(ND,N,MTD,MT,M1D,M1,A,XM,IP,B)
      DIMENSION A(ND,MTD),XM(ND,M1D),IP(ND),B(ND)
      L=M1
      DO 40 K=1,N
      I=IP(K)
      IF (I.EQ.K) GO TO 10
      X=B(K)
      B(K)=B(I)
      B(I)=X
10    IF (L.LT.N) L=L+1
      IF (K+1.GT.L) GO TO 40
      IK=K+1
      DO 20 I=IK,L
      X=XM(K,I-K)
20    B(I)=B(I)-X*B(K)
40    CONTINUE
      L=1
      DO 70 I1=1,N
      I=N+1-I1
      X=B(I)
      IW=I-1
      IF (L.EQ.1) GO TO 65
      DO 60 K=2,L
60    X=X-A(I,K)*B(IW+K)
65    B(I)=X/A(I,1)
      IF (L.LT.MT) L=L+1
70    CONTINUE
      RETURN
      END
```

APPENDIX E

SURFER PROCEDURE TO EXTRACT MAPS FROM FLUENT DATA

Velocities are given for each cell. Each cell is defined by their X, Y, Z position.

To plot it in an exploitable way, we have to create a map from these data. These data are extracted from a cylinder of constant radius along the fixed bed. Cells are extracted in a random manner in a large chart. We have to sort them to get exploitable data. The simple calculations below explain how I plotted maps:

$$\begin{aligned} X &= r\cos\theta \\ Y &= r\sin\theta \end{aligned} \tag{57}$$

with $r = \sqrt{X^2 + Y^2}$

$$\begin{aligned} \theta &= \cos^{-1}\left(\frac{X}{r}\right), \quad \theta \in [0, 2\pi] \\ \theta &= \sin^{-1}\left(\frac{Y}{r}\right), \quad \theta \in [-\pi, \pi] \end{aligned} \tag{58}$$

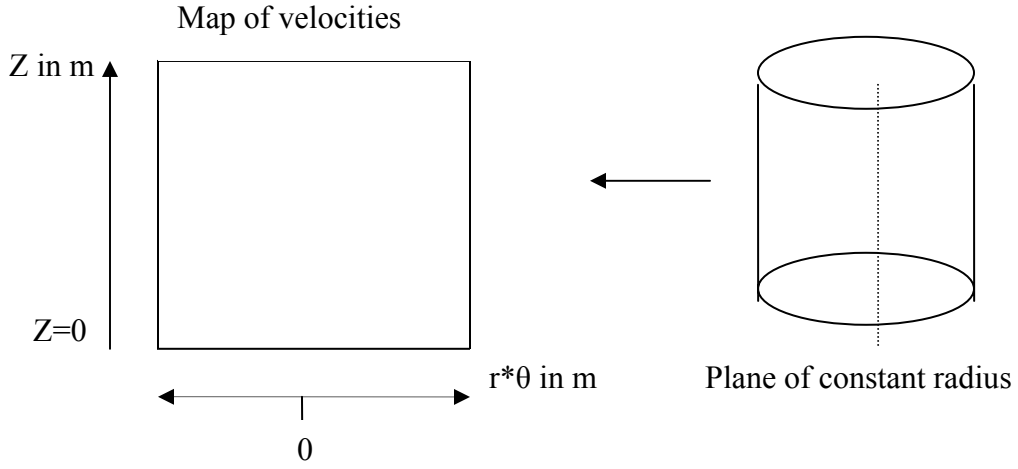

Figure E.1: velocities map creation

So in SURFER (software used) terms:

- Data / Transform

  E = pow(pow(B,2)+pow(C,2),1/2)

  F = asin(C/E)

  G = r*F

Remark: one has to be careful with the number of rows involved.

Now data are ready to be exploited. Here is the procedure to plot:

- File / New / Plot Document
- Grid / Data
  - Select X,Y,Z (Map coordinates + value to map in Z)
  - Select number of lines
- Map / Contour Map / New
  - Select level lines
- Grid / Extract
  - Select grid
  - Select size of extract
  - Save under new name
- Redo this procedure until getting a correct size
- If correct, Grid Extract
  - Select grid

- Save in ASCII XYZ for excel table

Planes obtained using the method above.

All radial velocities planes are available below, from r = 25e-4 m plane to r = 503e-4 m. There are exactly 13 maps. As explained in the chapter 4.2, only the middle section of the complete plane has been extracted (second map). Then, the number of point is reduced to give a coarser map (third map). The number of points is indicated on each set of maps, same for cutoff numbers in the axial direction (corresponding to the Y axis so to speak on the map).

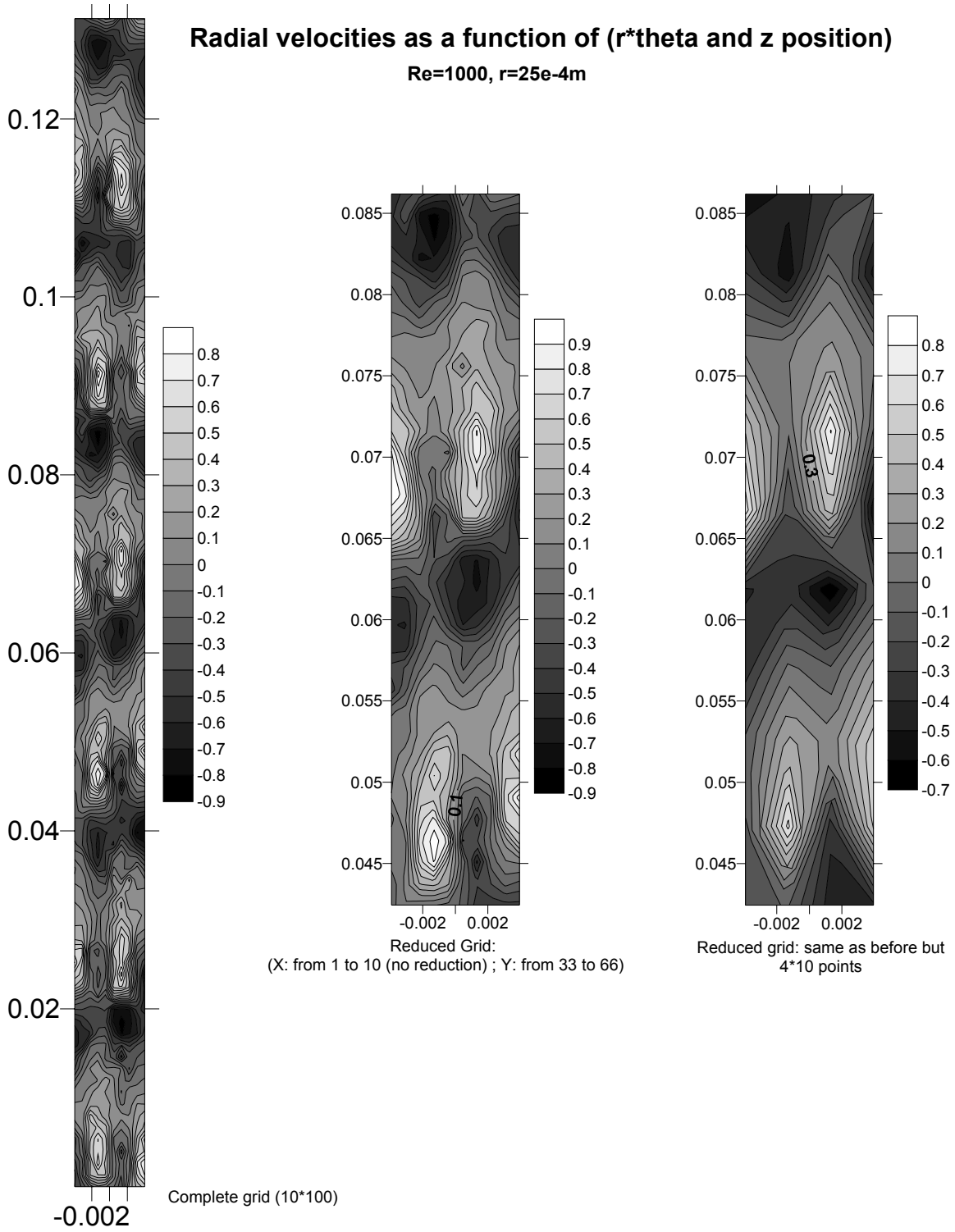

Figure E.2: Radial velocities map for constant r=25e-4m plane

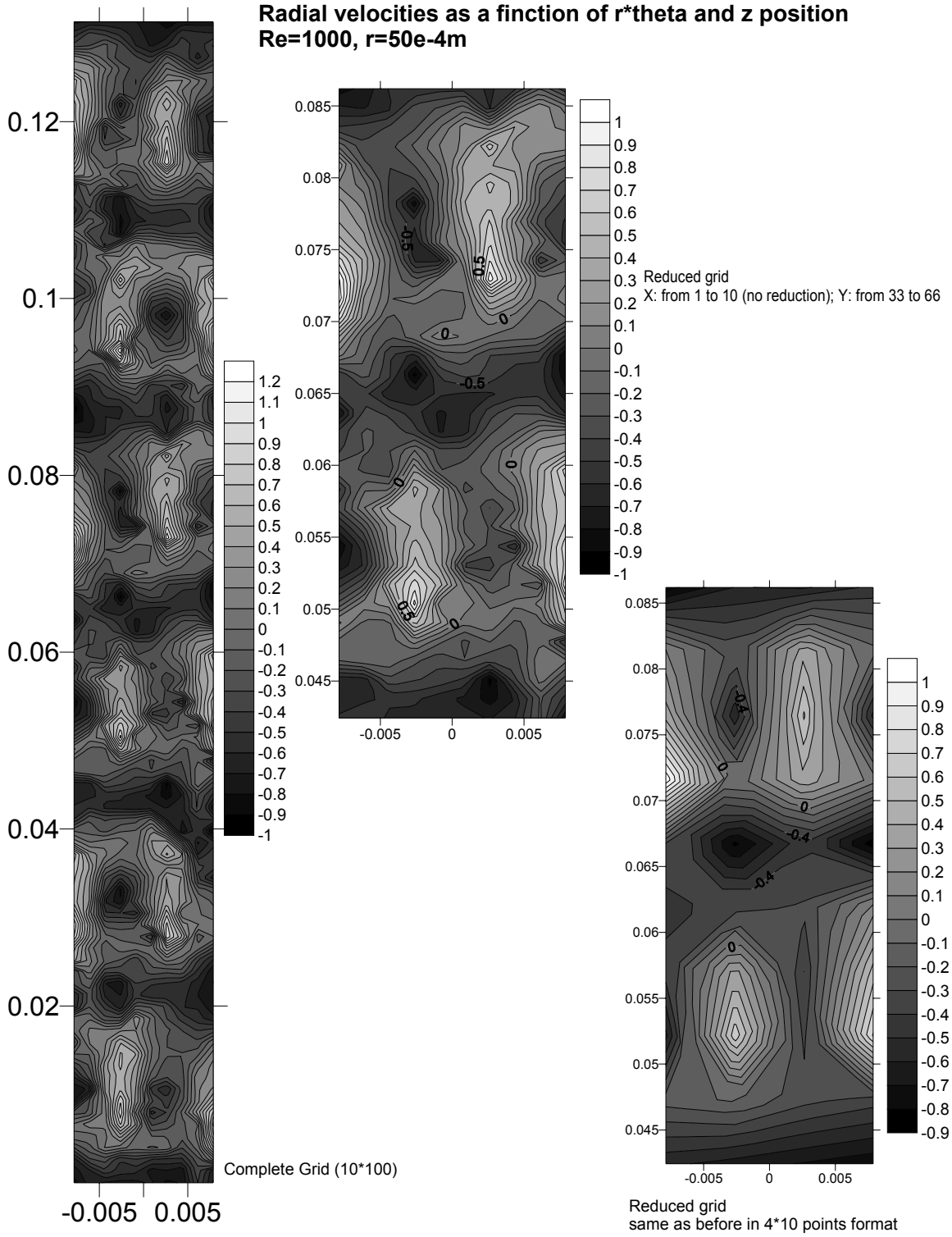

Figure E.3: Radial velocities map for constant r=50e-4m plane

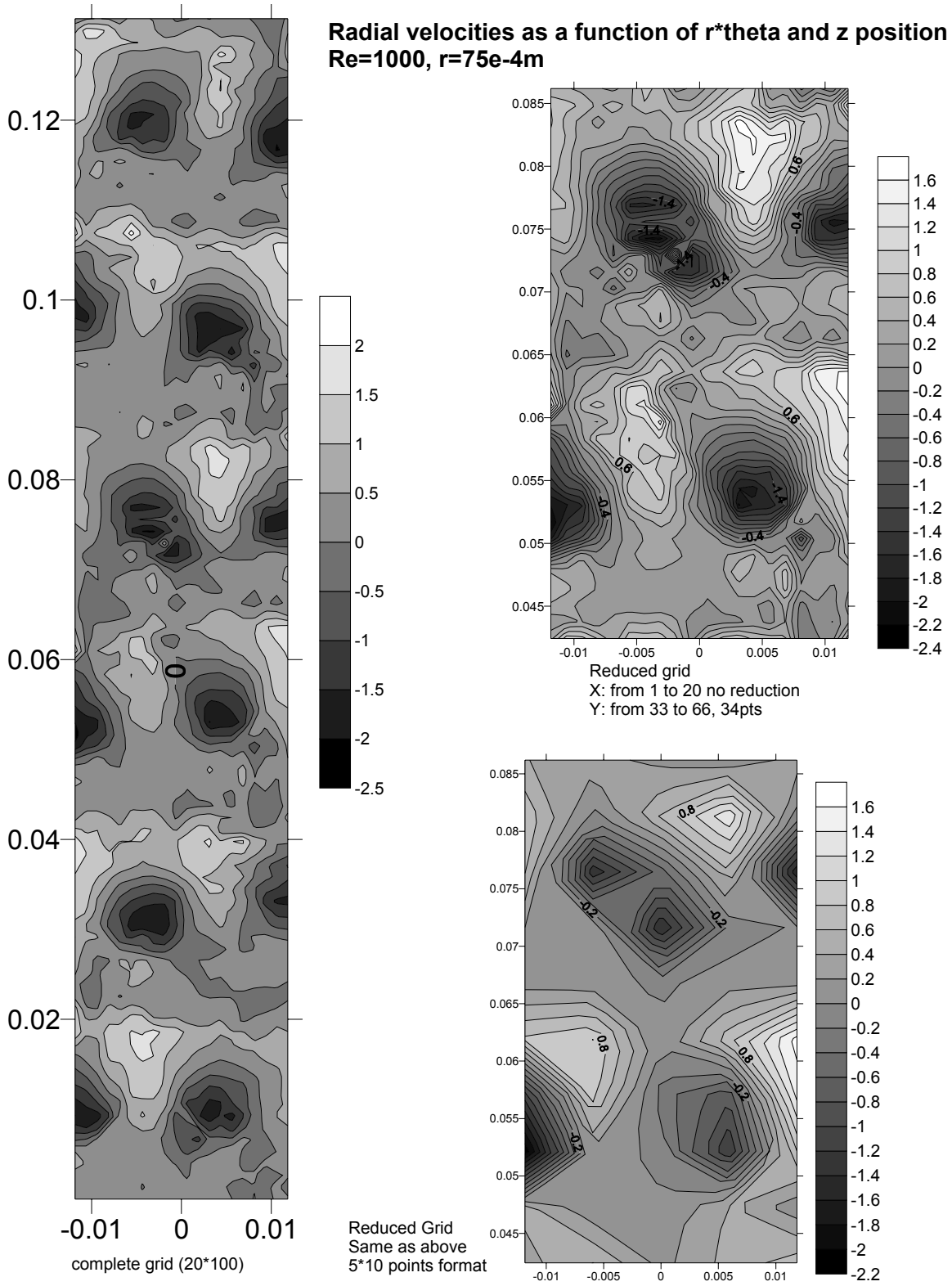

Figure E.4: Radial velocities map for constant r=75e-4m plane

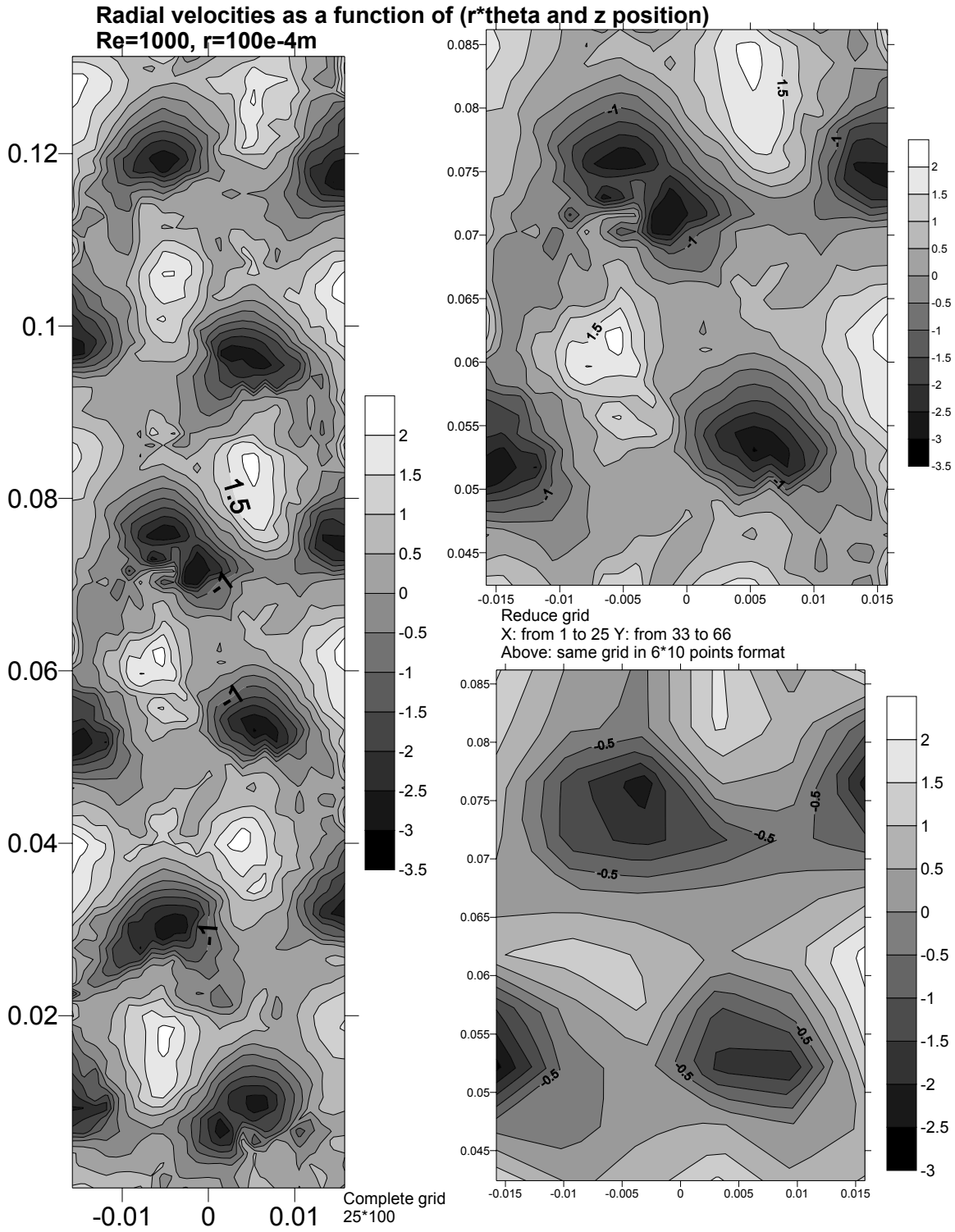

Figure E.5: Radial velocities map for constant r=100e-4m plane

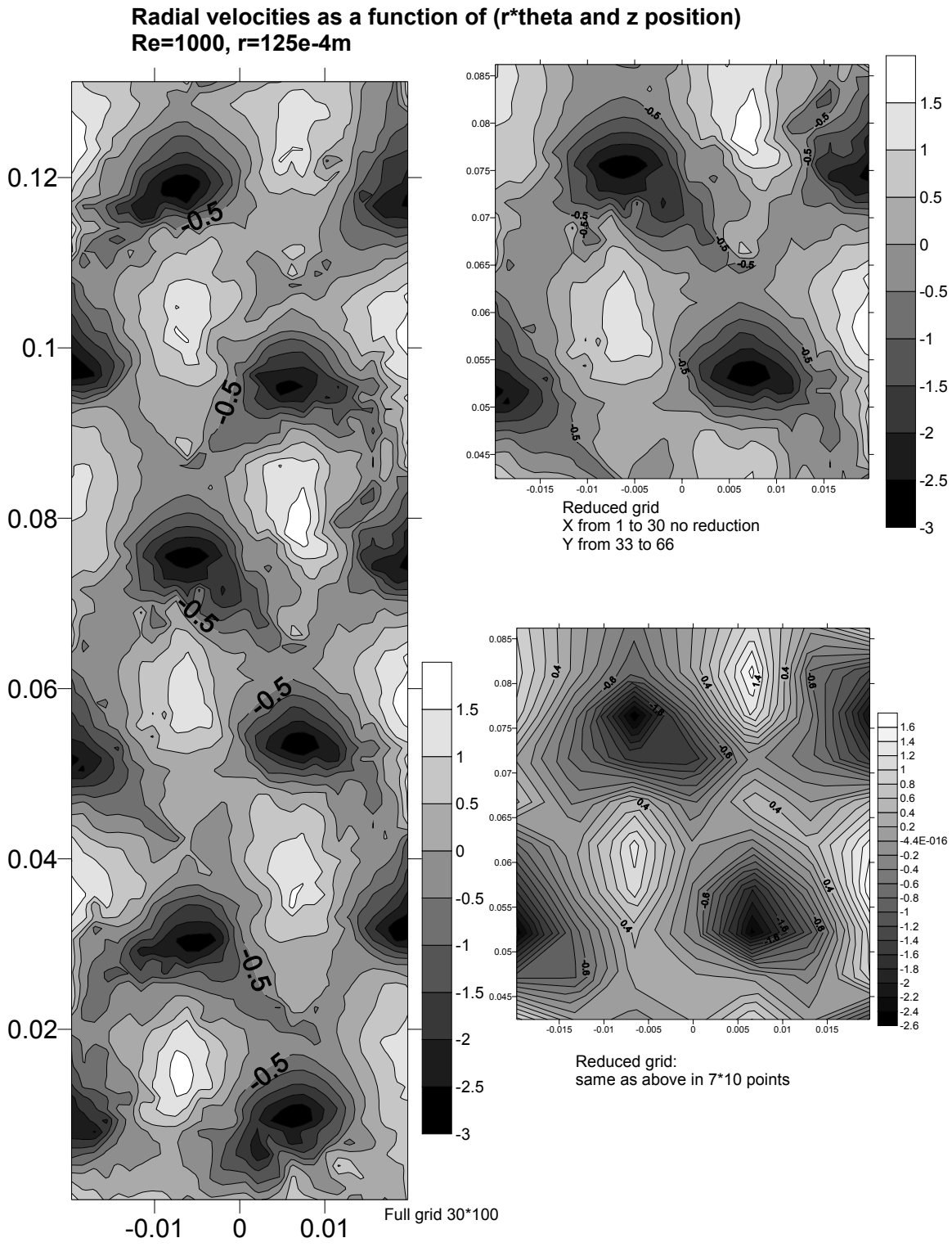

Figure E.6: Radial velocities map for constant r=125e-4m plane

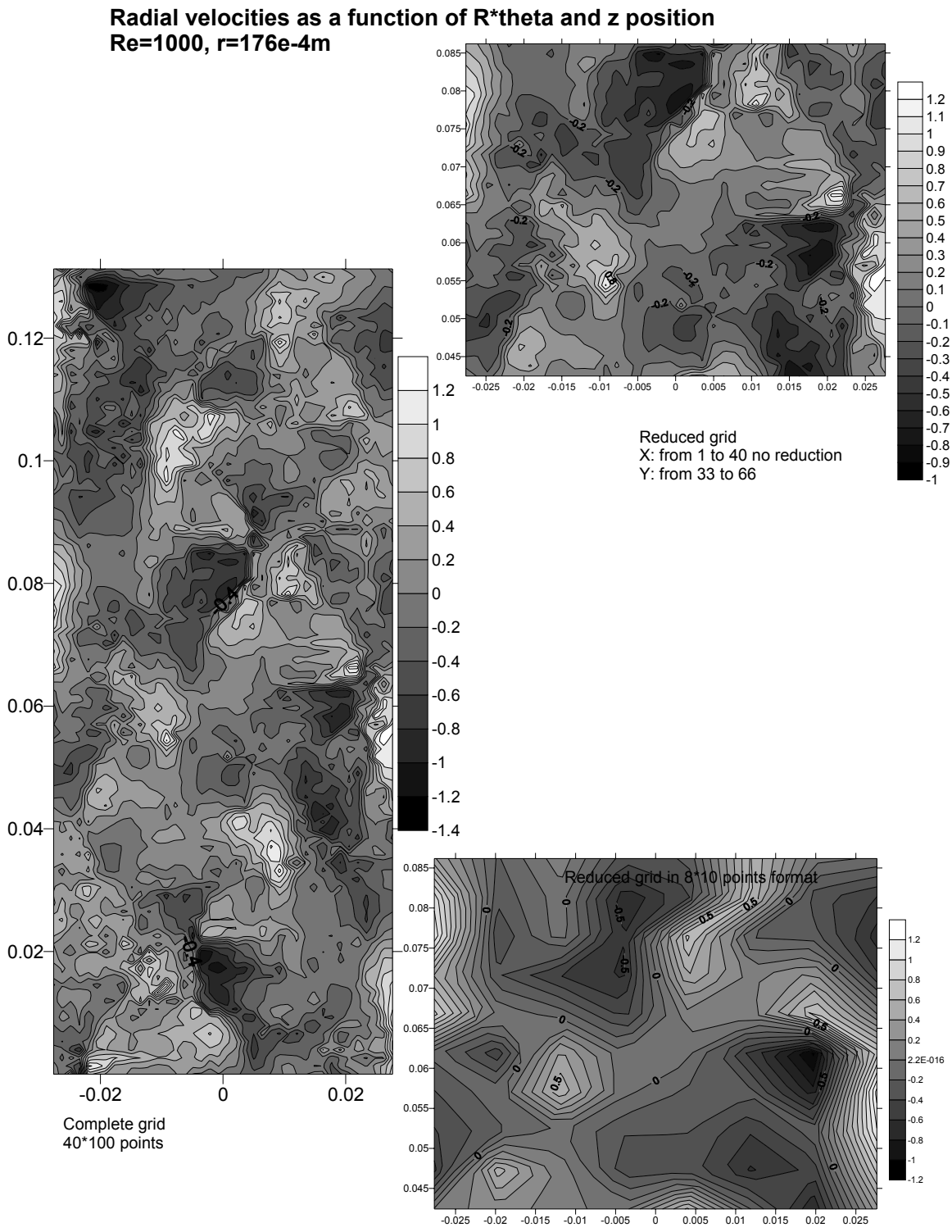

Figure E.7: Radial velocities map for constant r=176e-4m plane

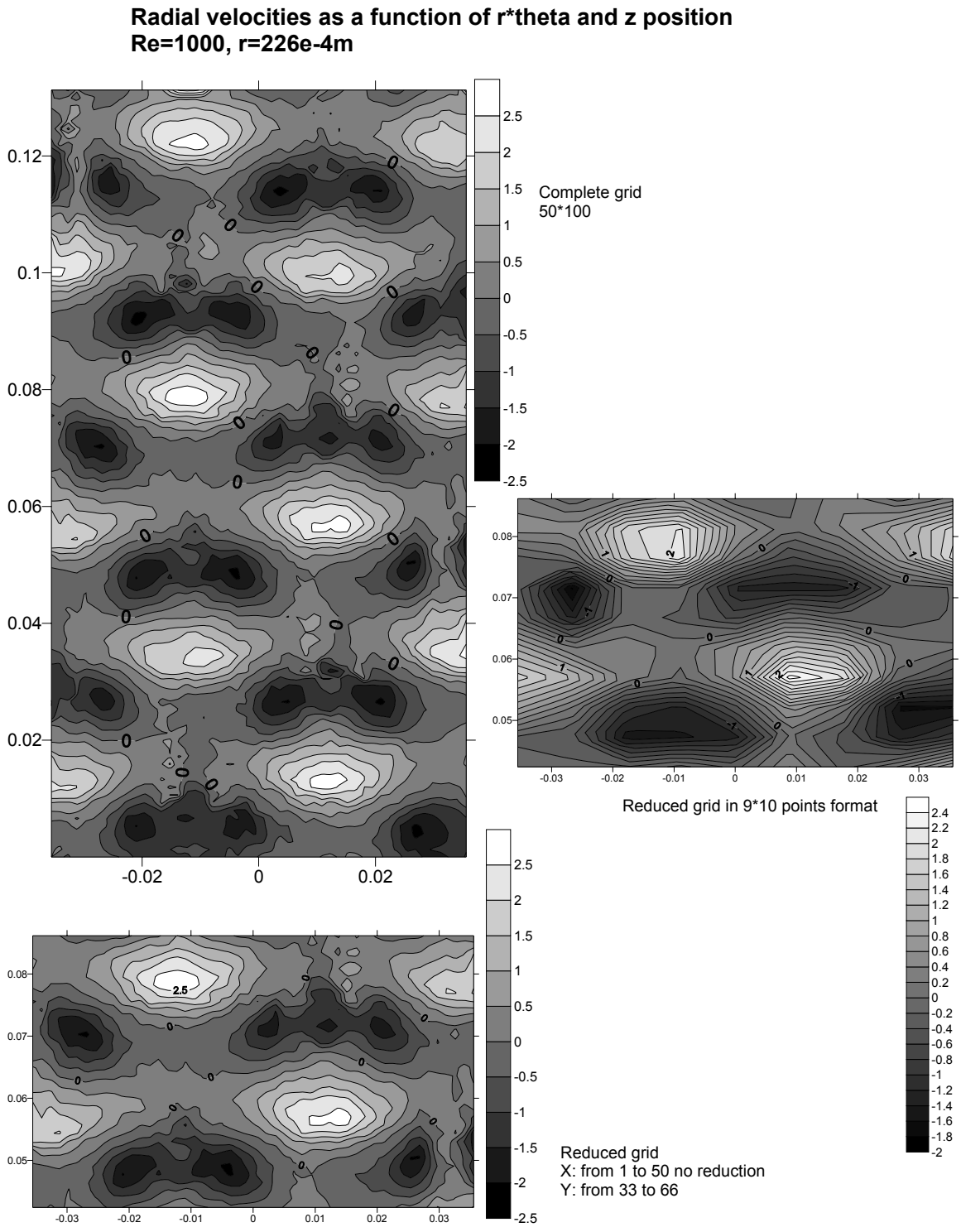

Figure E.8: Radial velocities map for constant r=226e-4m plane

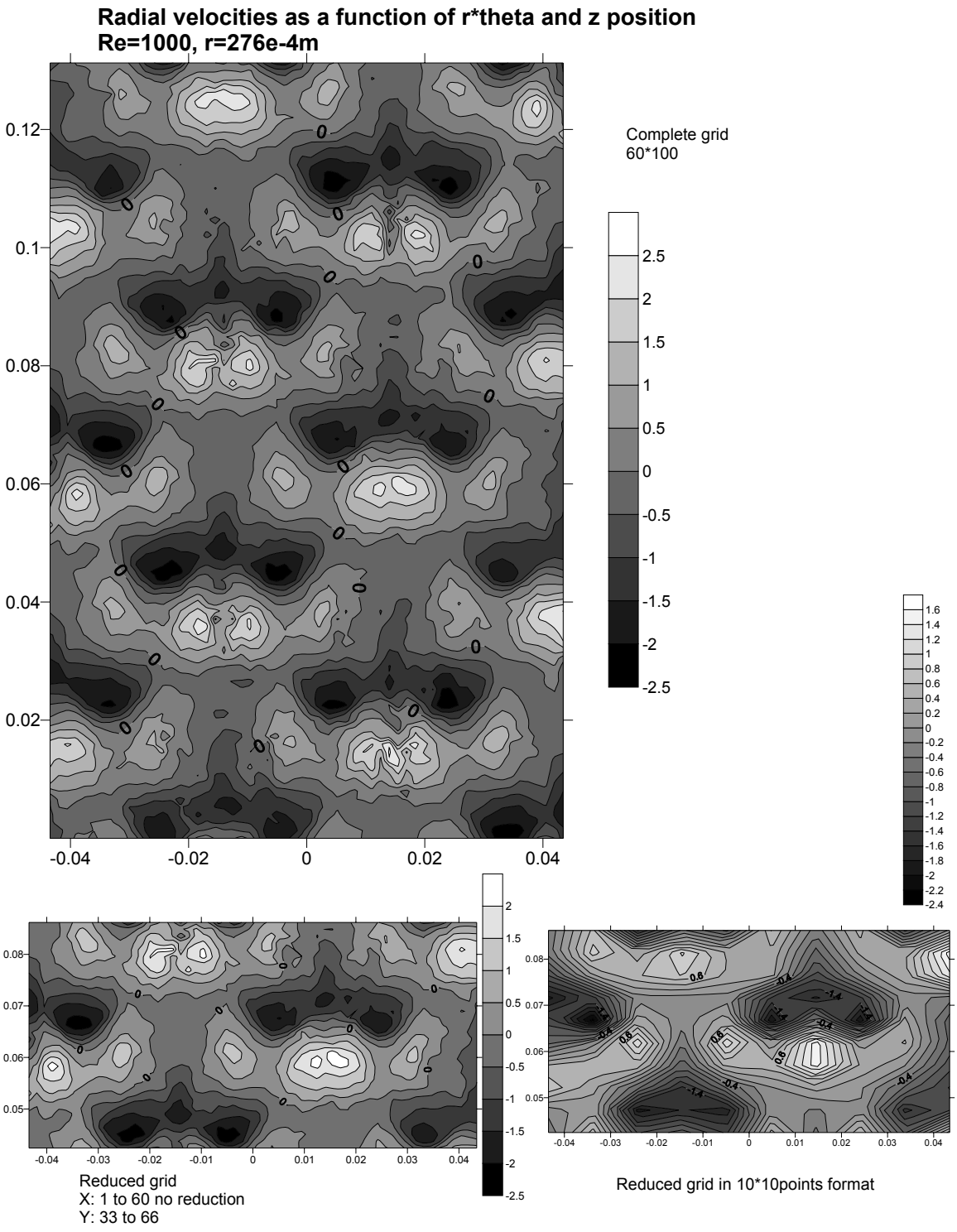

Figure E.9: Radial velocities map for constant r=276e-4m plane

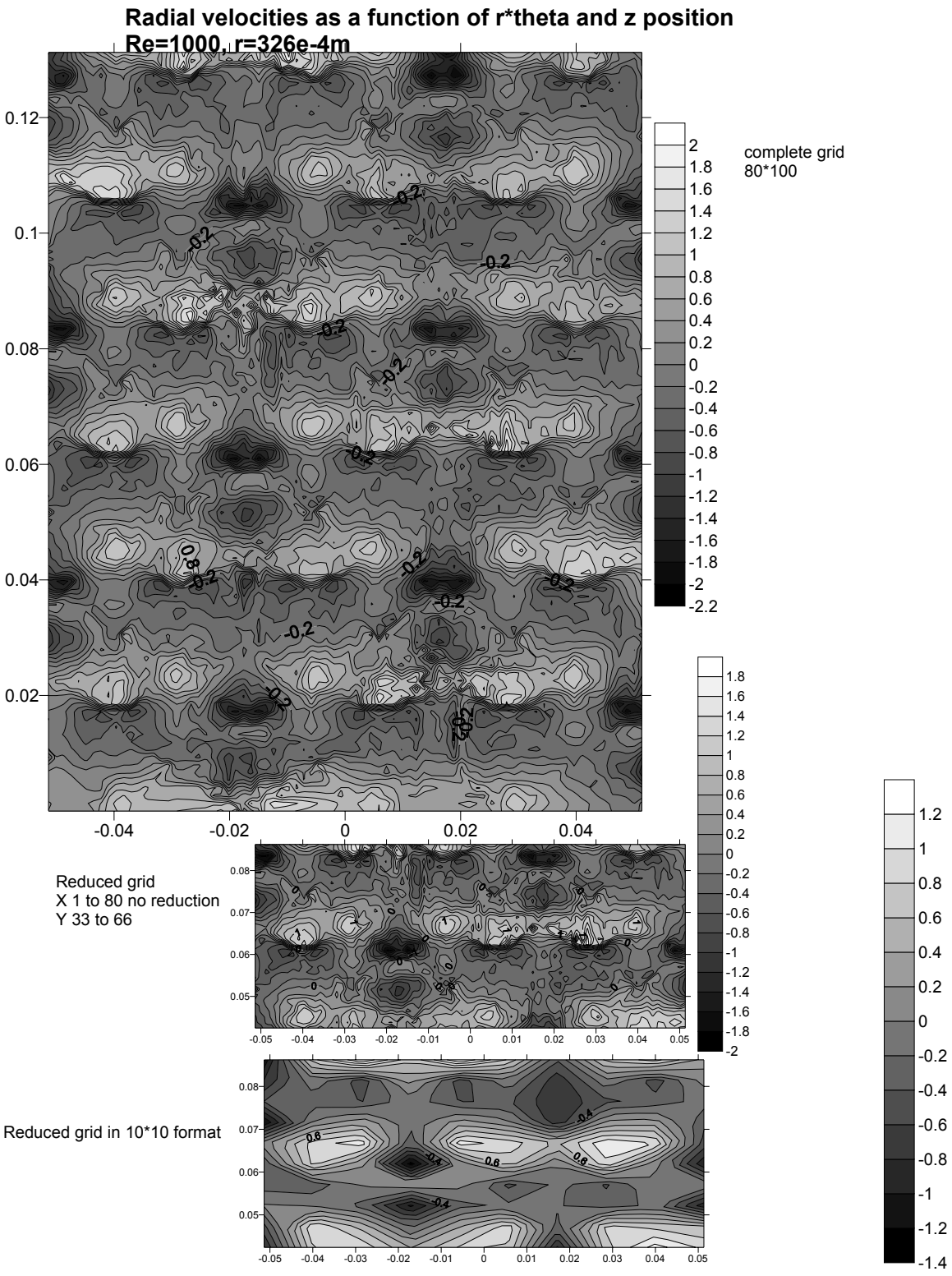

Figure E.10: Radial velocities map for constant r=326e-4m plane

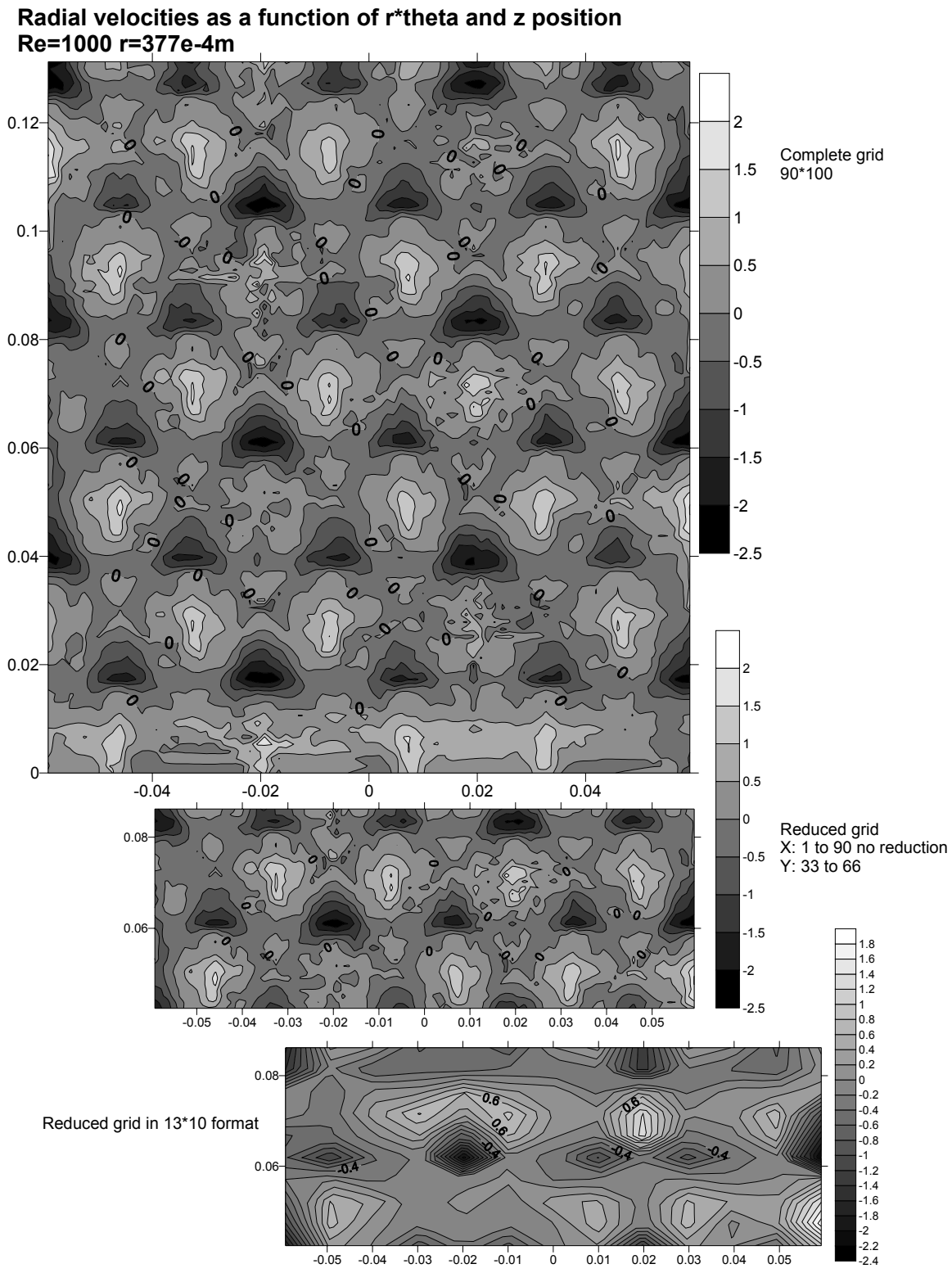

Figure E.11: Radial velocities map for constant r=377e-4m plane

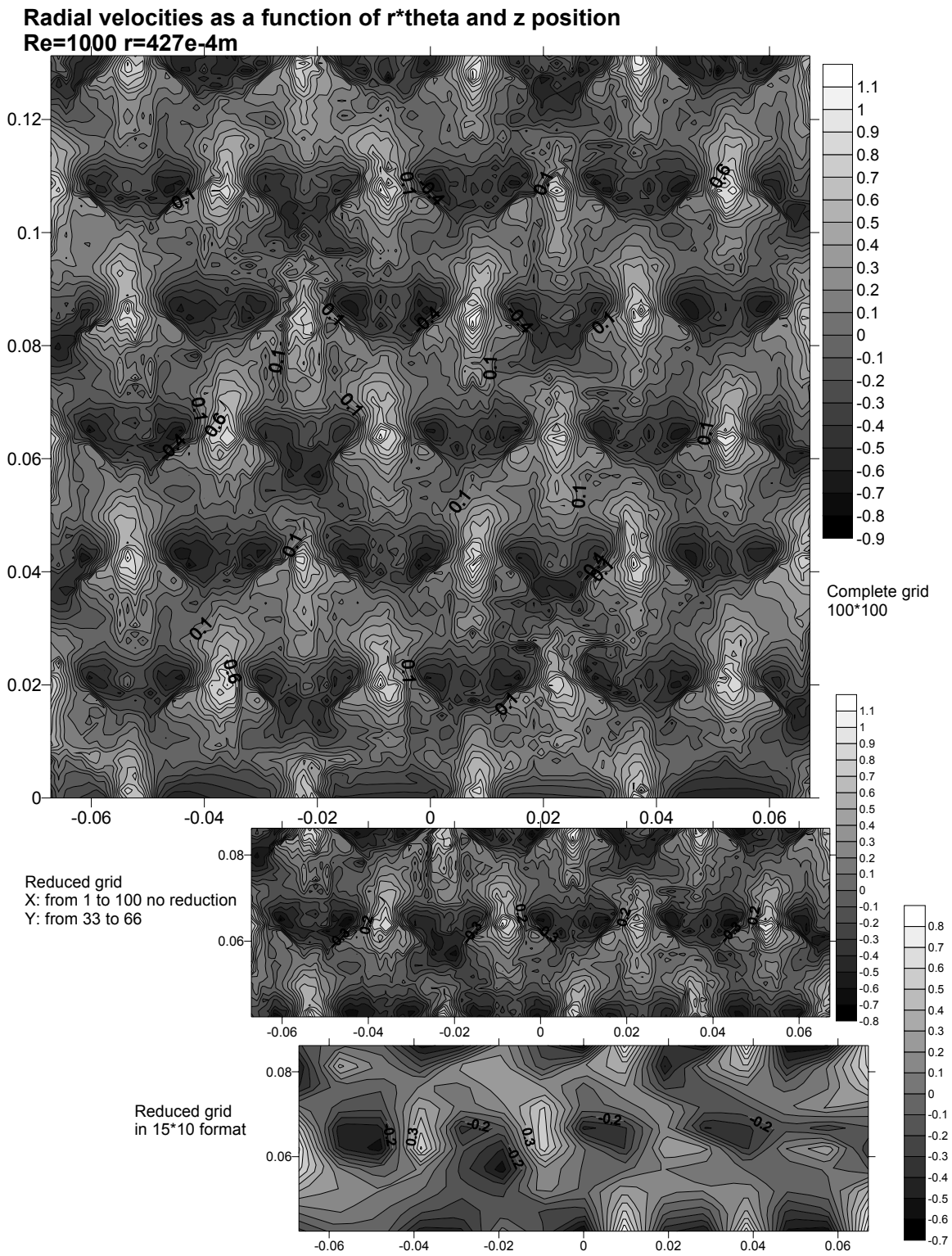

Figure E.12: Radial velocities map for constant r=427e-4m plane

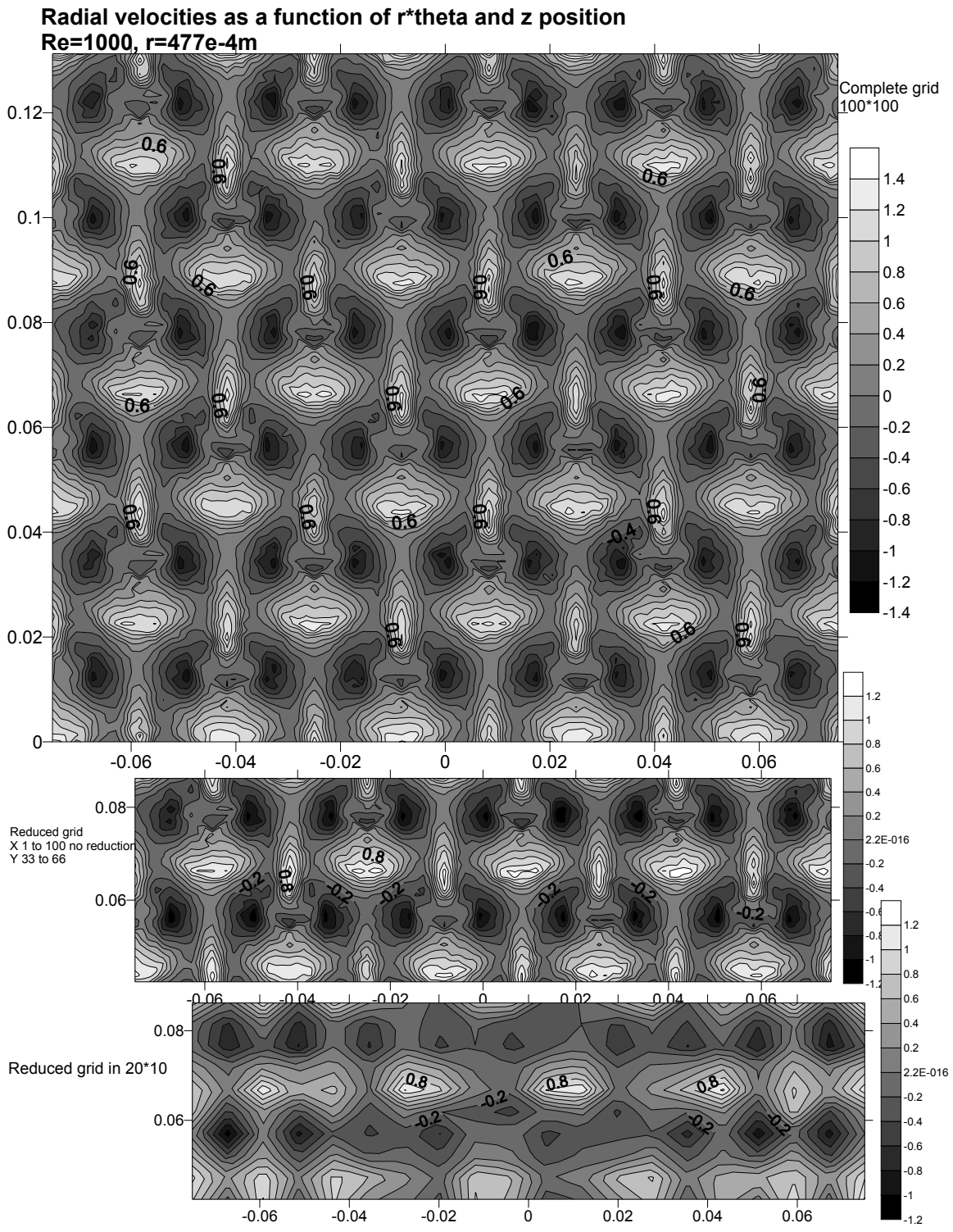

Figure E.13: Radial velocities map for constant r=477e-4m plane

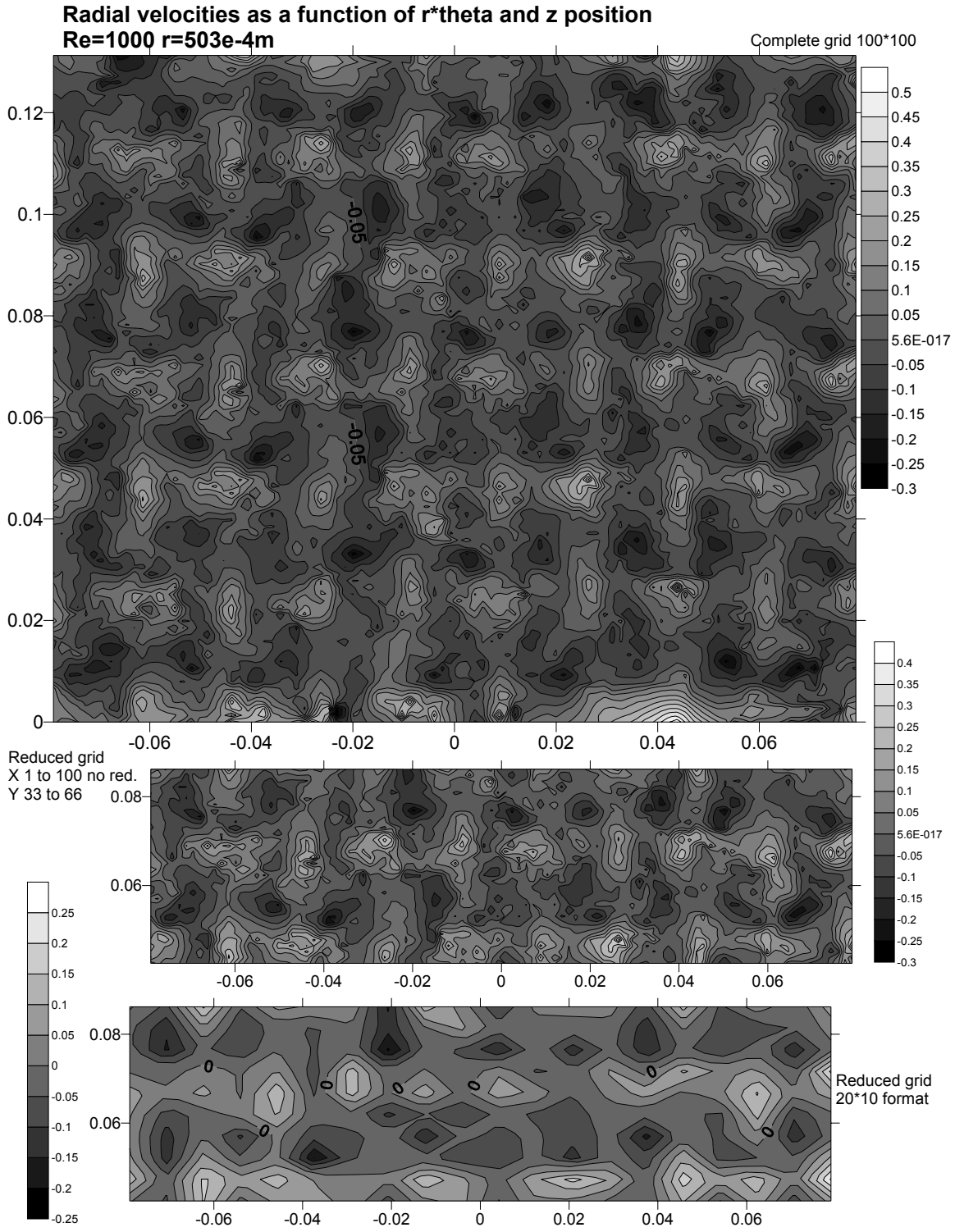

Figure E.14: Radial velocities map for constant r=503e-4m plane